

# Mobilization and isotope fractionation of uranium, copper and iron in the environment - implications for (bio)remediation of contaminated sites and mine tailings

Von der Naturwissenschaftlichen Fakultät der  
Gottfried Wilhelm Leibniz Universität Hannover

zur Erlangung des Grades

Doktorin der Naturwissenschaften (Dr. rer. nat.)

genehmigte Dissertation

von

Yvonne Röbbert, M. Sc.

[2021]

Referent: Prof. Dr. Stefan Weyer

Korreferent: apl. Prof. Dr. habil. Axel Schippers

Tag der Promotion: 16.07.2021

## **Acknowledgements**

I would not have written this thesis without the support and assistance of many people whom I wish to thank at the beginning.

First of all, I would like to thank Prof. Dr. Stefan Weyer, Prof. Dr. Rizlan Bernier-Latmani and Prof. Dr. Stephan Kraemer for initiating this project and giving me the opportunity to be a part of it. I thank you for your support during my PhD years.

I especially thank Stefan for being my supervisor, for all constructive discussions, answering my questions, and sharing his knowledge and supporting my work in all the years.

Furthermore, I am grateful for all the support and the possibilities offered from Prof. Dr. Axel Schippers in the Federal Institute for Geosciences and Natural Resources (BGR). Without him, it would not have been possible to complete this doctoral thesis to this extent, I am thankful for his support, all valuable discussions and reviews of my work.

I thank my colleagues at the Leibniz University of Hannover who have supported me with their help and guidance through this time. My special thanks go to Dr. Nadia Pierau who taught me the method of measuring isotopes and introduced me to the world of uranium. I thank Dr. Marina Lazarov who taught me measuring Cu isotopes and supported me with the second chapter. I thank Dr. Stephan Schuth who helped a lot in the lab, at the machines and with helpful guidance through all questions. I would like to thank PD Dr. Ingo for supporting me in any trouble shooting on the machines. Special thanks go to Chris Rosendahl, being a great student helper, bachelor and master student and a friend! I also thank Dr. Annika Neddermeyer with a lot of helpful chemical, machine, lab and all other knowledge and being a good friend.

I thank all the others from our working group, who have been great colleagues and supported me during my PhD: Alexandra Tangen, Dr. Martin Oeser-Rabe, Dr. Mona Weyrauch, Dr. Lena Steinmann, Lili Meier, Dr. Maria Kirchenbaur, Dr. Ashley Martin, Andreas Kaufmann, Dr. Sebastian Kommescher and Benedict Hagel. I especially thank Lena, Annika, Lili, Chris, Andreas and Sebastian for sharing the office and the common experience of all highs and lows, for every mental support, every friendly encouragement and every great laugh together. I also thank Teresa Zahoransky, Insa Cassens and Philipp Beckmann for their help and support. Of course, I am also thankful to all colleagues from the Institute of Mineralogy in Hannover who have shared my PhD time with me and who have become very good friends.

I thank all my collaboration partners at the EPFL in Lausanne. I especially thank Prof. Rizlan Bernier-Latmani for her support, for her amazing talk in Hannover in the Colloquium, which I

was so enthusiastic about, that I approached her and Stefan to write my exciting master's thesis, from which the great doctoral period later emerged. I am grateful for the opportunity to conduct experiments in Lausanne at any time and for all her support. I thank Dr. Luca Lorregian for teaching me all methods and his support. Especially, I thank Dr. Ashley Brown for his support, knowledge and time for me. I am grateful for all people in the working group of Prof. Dr. Rizlan Bernier-Latmani, who supported me during my stays and always welcomed me warmly.

I thank the BGR for the possibility to perform all my experiments. I am very thankful for the working group, who patiently taught me all microbial tools and supported me in every way. I would especially like to thank Isabell and Sabrina, who always took a lot of time for me.

I am thankful to the Deutsche Forschungsgemeinschaft (DFG), Swiss National Science Foundation (SNSF) and the European Research Council (ERC) for funding this project.

Mein ganz besonderer Dank gilt meiner Familie, die mich immer unterstützt hat, finanziell und emotional, meine Neugier und meinen Wissensdurst gestillt hat und mich immer mit Liebe umgeben hat. Ich danke besonders Lukas, der immer für mich da war und mich immer unterstützt hat.

## Abstract

The change of the oxidation state of redox-sensitive elements is frequently associated with a change in solubility and mobility. Understanding these mobilization processes and developing monitoring tools is crucial to limit environmental pollution in the future and may even support the identification of prospection-worth mineralization. Specifically, this thesis explores the use of the isotope systems of copper (Cu), iron (Fe), and uranium (U) as potential tools for tracing environmental processes related to the impact of mine tailings and (bio)remediated sites.

In the first part, sulfidic mine tailings were investigated since they have a high potential for contamination of the environment by releasing acid mine drainage. An optimized and tested sequential extraction method of Cu and Fe isotopes was applied to samples from two depth profiles of porphyry copper mine tailings from the Atacama Desert (Chile). Iron isotope fractionation was traced to oxidative sulfide weathering and secondary enrichment like (re-) precipitation. The Cu isotope signature was interpreted to result from capillary Cu rising due to arid climate conditions, and/or, by the preferential adsorption of heavy Cu isotopes to the surface of Fe(hydr-)oxides. These findings showed that the composition of Cu and Fe isotopes can be used to trace mobilization processes and secondary element enrichment.

In the second part, U isotope fractionation as a monitoring tool for the long-term stability of non-crystalline U(IV) - an important U host in sedimentary U deposits and the dominant product of (bio)remediation - was examined. Laboratory anoxic complexation experiments were performed in which the ligands EDTA, citrate, and bicarbonate were found to preferentially mobilize heavy  $^{238}\text{U}$ . These findings demonstrated that heavy U isotope signatures are not necessarily the result of U reduction but may also be generated during U mobilization. They may potentially be used to distinguish between anoxic ligand complexation and oxidative U mobilization or U adsorption to oxides.

In the last part, oxidative mobilization (biotic and abiotic) of non-crystalline U(IV) was explored, which might also affect the U isotope composition. No significant U isotope fractionation was observed during oxidation with both Fe(III) or *Acidithiobacillus ferrooxidans*. Isotope fractionation during all involved reactions was thus either very small or different isotope effects cancelled each other out, implying that oxidative mobilization can be neglected in the interpretation of natural and anthropogenic U isotopic signatures.

In conclusion, the main findings of this thesis are (1) sequential extraction in combination with Cu and Fe isotope analysis can trace mobilization and enrichment processes in mine tailings and (2) a differentiation between oxic mobilization and abiotic complexation in the subsurface is trackable using U isotope systematics, which helps to assess the long-term stability of non-crystalline U(IV) after *in-situ* leaching or (bio)remediation.

## Zusammenfassung

Die Änderung des Oxidationszustandes von redox-sensitiven Elementen ist häufig mit einer Änderung ihrer Löslichkeit und Mobilität verbunden. Die Erforschung dieser Mobilisierungsprozesse und die Entwicklung von Überwachungstechniken ist essentiell, um Umweltverschmutzung in Zukunft zu verringern und vermag sogar die Exploration von prospektionswürdigen Mineralisierungen unterstützen. Diese Arbeit untersucht dafür die Verwendung der Isotopensysteme von Kupfer (Cu), Eisen (Fe) und Uran (U) zur Verfolgung von Umweltprozessen im Zusammenhang mit Abraumhalden und mit (Bio-) Sanierung.

Im ersten Teil wurden sulfidische Abraumhalden untersucht, welche durch die Freisetzung von saurem Grubenwasser die Umwelt kontaminieren können. Eine optimierte und getestete sequentielle Extraktionsmethode von Cu- und Fe-Isotopen wurde an Proben aus zwei Tiefenprofilen porphyrischer Kupferminen-Abraumhalden aus der Atacama-Wüste (Chile) angewandt. Die Fe-Isotopenfraktionierung wurde dabei auf oxidative Sulfidverwitterung und sekundäre Anreicherung durch z. B. (Wieder-)Ausfällung zurückgeführt. Die Cu-Isotopensignatur wurde als Ergebnis des kapillaren Cu-Aufstiegs durch aride Klimabedingungen oder durch die bevorzugte Adsorption schwerer Cu-Isotope an die Oberfläche von Fe(hydr-)oxiden interpretiert. Es wurde folglich gezeigt, dass sich Cu- und Fe-Isotope gut dafür eignen, Mobilisierungen und sekundäre Elementanreicherungen zu verfolgen.

Im zweiten Teil wurde die U-Isotopenfraktionierung als Überwachungsinstrument für die Langzeitstabilität von nicht-kristallinem U(IV) – ein wichtiger Bestandteil von sedimentären Uranvorkommen und das Hauptprodukt von (Bio)Sanierung - untersucht. Dafür wurden anoxische Komplexierungs-Experimente im Labor durchgeführt. Dabei stellte sich heraus, dass die Liganden EDTA, Citrat und Na-Hydrogencarbonat bevorzugt schweres <sup>238</sup>U mobilisieren. Diese Ergebnisse haben aufgezeigt, dass schwere U-Isotopensignaturen nicht nur durch Uran-Reduktion entstehen können, sondern auch durch U-Mobilisierung generiert werden können.

Im letzten Teil wurde die oxidative Mobilisierung (biotisch und abiotisch) von nicht-kristallinem U(IV) untersucht, da sie ebenfalls die U-Isotopenzusammensetzung beeinflussen könnte. Dabei wurde keine signifikante U-Isotopenfraktionierung bei der Oxidation mit Fe(III) oder *Acidithiobacillus ferrooxidans* beobachtet. Daher kann die oxidative Mobilisierung bei der Interpretation von natürlichen/anthropogenen U-Isotopensignaturen vernachlässigt werden.

Zusammenfassend sind die wichtigsten Ergebnisse dieser Arbeit: (1) mit Hilfe der sequenziellen Extraktion in Verbindung mit der Analyse von Cu- und Fe-Isotopen lassen sich die Mobilisierungs- und Anreicherungsprozesse in Abraumhalden nachverfolgen und (2) eine Unterscheidung zwischen oxidativer Mobilisierung und abiotischer Komplexierung kann mit Hilfe der U-Isotopensystematik erfolgen, was eine bessere Abschätzung der Langzeitstabilität von nicht-kristallinem U(IV) nach *in-situ*-Laugung oder (Bio)Sanierung ermöglicht.

**Key words:** Uranium, copper, iron, (bio)remediation, mine tailings, sequential extraction, *Shewanella oneidensis* MR-1, *Acidithiobacillus ferrooxidans*, stable isotope fractionation

**Schlüsselwörter:** Uran, Kupfer, Eisen, (biologische) Sanierung, Bergbaurückstände, Sequentielle Extraktion, *Shewanella oneidensis* MR-1, *Acidithiobacillus ferrooxidans*, stabile Isotopenfraktionierung

## Table of contents

Acknowledgements .....	3
Abstract .....	5
Zusammenfassung .....	6
Key words .....	7
Table of contents .....	8

### **Chapter I: Objectives and background..... 11**

1 Metal stable isotope fractionation – U, Cu and Fe.....	12
1.1 Uranium .....	13
1.2 Copper .....	14
1.3 Iron.....	15
2 Mining – impacts, consequences and mine tailings.....	16
3 (Bio)remediation and non-crystalline U(IV).....	19
4 Bacteria ( <i>Shewanella oneidensis</i> MR-1; <i>Acidithiobacillus ferrooxidans</i> ).....	20
5 Objectives .....	22

### **Chapter II: Fractionation of Fe and Cu isotopes in acid mine tailings: modification and application of a sequential extraction method ..... 24**

1 Introduction.....	27
2 Material and methods.....	30
2.1 Sample material .....	30
2.1.1 Sequential extraction test samples.....	30
2.1.2 Samples from the Chañaral bay mine tailings.....	31
2.2 Sequential extraction .....	33
2.3 Cu and Fe chromatographic separation .....	35
2.4 Concentration measurements.....	35



2.5	Isotope measurement: MC-ICP-MS .....	36
3	Results and discussion .....	37
3.1	Testing of the sequential extraction method.....	37
3.1.1	Iron .....	37
3.1.2	Copper .....	40
4	Application to mine tailings samples .....	42
4.1	Iron.....	42
4.1.1	Mass balance calculations .....	45
4.2	Copper .....	47
4.2.1	Concentration .....	47
4.2.2	Isotope composition .....	49
4.2.3	Mass balance calculations .....	52
5	Conclusions.....	53
6	Acknowledgments.....	54

**Chapter III: Uranium isotope fractionation during anoxic mobilization of non-crystalline U(IV) by ligand complexation .....** **55**

1	Introduction.....	57
2	Materials and methods .....	59
2.1	Preparation of non-crystalline U(IV).....	59
2.2	Ligand mobilization experiment.....	61
2.3	Anion exchange resin separation of U(IV) and U(VI) .....	61
2.4	Uranium concentration and isotope analyses .....	61
3	Results and discussion .....	63
4	Implications for the use of the U isotope proxy.....	71

<b>Chapter IV: Abiotic and biotic U oxidation processes and associated U isotope fractionation.....</b>	<b>75</b>
1 Introduction.....	77
2 Methods.....	80
2.1 Experiment (1) – Fe(III) .....	81
2.2 Experiment (2) – Sulfur & <i>At. ferrooxidans</i> .....	81
2.3 Experiment (3) – Tetrathionate & <i>At. ferrooxidans</i> .....	82
2.3.1 High-performance liquid chromatography .....	83
2.4 Concentration and isotope measurements .....	83
3 Results and discussion .....	84
3.1 Experiment (1) – Fe(III) .....	84
3.2 Experiment (2) – Sulfur & <i>At. ferrooxidans</i> .....	84
3.3 Experiment (3) – Tetrathionate & <i>At. ferrooxidans</i> .....	88
Conclusions and Perspectives .....	100
Supporting Information .....	101
Supporting Information for Chapter II .....	101
Supporting Information for Chapter III.....	102
Supporting Information for Chapter IV.....	116
References .....	119
Curriculum Vitae.....	140
Publications .....	142

**Chapter I:**

**Objectives and background**

## **1 Metal stable isotope fractionation – U, Cu and Fe**

Metal stable isotopes are a powerful tool for elucidating processes on Earth in recent and ancient times, numerous applications have been developed during the last years. Isotopes can help to understand processes on the early Earth and throughout the Earth's history. With isotope fractionation the reconstruction of redox conditions on the early Earth like the oxygenation of the oceans and atmosphere is possible (Wasylenki, 2012), e.g., uranium isotope fractionation can be applied to indicate oxidative U mobilization in the Archean (Brüske et al., 2020a; Kendall et al., 2013; Wang et al., 2018) or molybdenum isotopes to show anoxia in Mid-Proterozoic Oceans (Arnold et al., 2004). Isotope fractionation can be employed to understand the formation of profitable metal ores, e.g. iron and copper isotope fractionation are used to understand hydrothermal ore deposition and alteration (Markl et al., 2006b, 2006a) or U formation processes (Brennecka et al., 2010; Uvarova et al., 2014). Moreover, isotopes are helpful to understand anthropogenic pollution. Zinc has a relatively low boiling point, during Zn ore smelting, light Zn isotopes preferentially evaporated in the atmosphere, resulting also in fractionated industrial tailings (Bigalke et al., 2010a; Mattielli et al., 2009; Sivry et al., 2008; Thapalia et al., 2010). Mercury isotopes are also a suggested tracer for different industrial pollution in sediments (Wiederhold et al., 2013). Copper isotopes are applied to identify contaminations in soils, streams or acid mine drainage (Bigalke et al., 2010a; Kimball et al., 2009; Song et al., 2016). Biological processes can also result in isotope fractionation, e.g. microorganisms preferentially reduce heavy U isotopes (e.g., Stirling et al., 2015; Stylo et al., 2015b, 2015a), microbial Fe oxidation results in an enrichment of the heavier isotope in the product (Balci et al., 2006a; Croal et al., 2004). Isotopes may be a tool to trace remediation processes and the evolution of mine waste and tailings (Basu et al., 2015; Bopp et al., 2010; Herbert and Schippers, 2008; Smuda et al., 2008).

Obviously, the application of isotope fractionation to numerous natural and anthropogenic systems is very versatile. This thesis focuses on the three isotope systems uranium, copper and iron, as all three elements are redox-sensitive elements and the redox-reaction of these elements produces a specific isotope fractionation which may be used as a fingerprint for such processes. However, several other processes, including non-redox reactions, such as adsorption onto mineral surfaces or organic substances, or complexation by ligands, also result in isotope fractionation which is in many cases not yet well characterized and understood. All three elements have in common that a change in their redox state, is associated with a change their solubility and environmental mobility. Mobilization of these elements may generate

environmental pollution on the one hand or enriches the elements for economical extraction on the other hand. Consequently, it is crucial to understand and trace these processes. In this thesis, mobilization and enrichment of Fe and Cu by redox change in mine tailings and related isotope fractionation will be exemplified. In addition, the mobilization of uranium by complexation and oxidation and the resulting U isotope fractionation will be investigated. In addition, the application at contamination sites and the effects of the mobilization processes on the environment are discussed in this thesis.

In general, stable isotope fractionation is related to the different partitioning of the isotopes of an element between two substances or two coexisting phases, resulting in variations in the abundance ratios in products and reactants. These processes arise mainly from differences in the mass and relative mass differences of the isotopes and are produced by isotope exchange reactions (equilibrium isotope fractionation) and kinetic processes (Hoefs, 2018; Wiederhold, 2015). Equilibrium isotope fractionation occurs if a reaction occurs in both directions in an exchange reaction, the heavy isotopes prefer stronger bonds (e.g. higher redox state or lower coordination number) and fractionation arises from small differences in zero-point vibrational energy (Wiederhold, 2015).

In the case of kinetic fractionation, the different isotope ratios result from varying reaction rates of light and heavy isotopes and occur mostly in fast and unidirectional (irreversible) processes like dissociation, evaporation, diffusion or enzymatically mediated biogeochemical processes. In addition to the mass-dependent isotope fractionation described above, some elements also exhibit mass-independent fractionation (e.g. Thiemens, 2006), which is caused, for example, by photochemical processes or, in the case of very heavy elements ( $Z > 80$ ) by the nuclear field shift effect which is related to the nuclear volume (Bigeleisen, 1996; Moynier et al., 2013).

## 1.1 Uranium

Uranium (U) is the chemical element with the atomic number 92, it is a radioactive metal and all its isotopes are unstable. However, the two isotopes  $^{238}\text{U}$  and  $^{235}\text{U}$  have long half-lives ( $4.468 \cdot 10^9$  years and  $0.7038 \cdot 10^9$  years; Villa et al., 2016) and only formed primordial. Accordingly, their present-day isotope ratio is independent of radioactive decay. Uranium is a lithophile element with a high affinity to oxygen, it is enriched in the crust compared to the upper mantle and has an average abundance of  $\sim 1.3$  ppm U (Rudnick and Gao., 2003).

Several parameters determine the solubility of U in aqueous solutions. In general, the solubility depends on pH and Eh. Furthermore, U has the tendency to form complexes with numerous anions like carbonate and phosphate (Langmuir, 1978). As a result, minerals can precipitate or

the oxidized form of the element can be reduced. Additionally, many organic and inorganic substances, such as clay, organic matter and humic substances and also some hydroxides, adsorb U (Dahlkamp, 2013).

Uranium occurs naturally in two oxidation states, the oxidized form U(VI) is mobile and the reduced U(IV) is poorly soluble and immobile. The intermediate U(V) is considered to be unstable and disproportionates easily (Borch et al., 2010; Langmuir, 1978; Ulrich et al., 2008).  $^{235}\text{U}$  is used in nuclear power plants for energy production and for nuclear weapons, and for this it is concentrated by enrichment from natural uranium. Major uranium mining countries are Kazakhstan, Australia, Canada, Russia, Niger, Namibia, Russia, China, Uzbekistan and the USA (International Atomic Energy Agency, 2018; Zammit et al., 2014).

Considering the very heavy weight of the uranium isotopes and the resulting small relative mass difference, a small mass-dependent fractionation would be expected, but nevertheless large isotope effects can be seen due to the nuclear field shift (NFS). It is caused by a combination of differences in nuclear size and shape and electron densities at the nucleus (Bigeleisen, 1996; Moynier et al., 2013). This competes and overwhelms the mass-dependent effect as conventional mass-dependent isotopic fractionation and the NFS effect work in opposition (Moynier et al., 2013). Uranium reduction enriches the heavy  $^{238}\text{U}$  isotope in solid U(IV), either by biotic reduction (Dang et al., 2016; Stirling et al., 2015; Stylo et al., 2015a, 2015b) or at high Ca concentration also during abiotic reduction (Brown et al., 2018). Uranium oxidation with dissolved oxygen results in initial mobilization of U(VI) which is depleted in  $^{238}\text{U}$ , but with ongoing reaction  $\delta^{238}\text{U}$  increase towards values of  $\sim 0\text{‰}$  (Wang et al., 2015a). Equilibrium isotope fractionation occurs between dissolved U(IV) and U(VI) with U(IV) enriched in  $^{238}\text{U}$  ( $1.64 \pm 0.16\text{‰}$ , Wang et al., 2015b). Only little U isotope fractionation is observed during adsorption, adsorbed U is  $\sim 0.2\text{‰}$  lighter than dissolved U (Brennecke et al., 2011b; Jemison et al., 2016a).

## 1.2 Copper

Copper (Cu) is the chemical element with the atomic number 29, the metal has very high thermal and electrical conductivity. With these properties, Cu is a valuable economic metal and used in various applications today: e.g., building construction, power generation and transmission, electronic products, wiring, heating and cooling systems, telecommunications links and motor vehicles (Mathur and Fantle, 2015; United States Geological Survey (USGS), 2020). Copper has three oxidation states  $\text{Cu}^0$ ,  $\text{Cu}^+$  and  $\text{Cu}^{2+}$ . The cuprous ion ( $\text{Cu}^+$ ) is colorless, the cupric ion ( $\text{Cu}^{2+}$ ) is blue in aqueous solution. The  $\text{Cu}^+$  ion is unstable, and tends to

disproportionate to  $\text{Cu}^0$  and  $\text{Cu}^{2+}$ , but it can form compounds like  $\text{Cu}_2\text{O}$  (Moynier et al., 2017). For living organisms Cu is an essential micronutrient, but in high concentrations it can also be toxic. It has a strong redox sensitivity, it is strongly affected by processes like flooding or water saturation (Mathur and Fantle, 2015).

Copper has two stable isotopes,  $^{63}\text{Cu}$  (69.2%) and  $^{65}\text{Cu}$  (30.8%) (Shields et al., 1964). Copper isotopic variations are caused by numerous processes like biotic reactions by plants and microorganisms, liquid-vapor separation, equilibrium processes, elemental exchange between dissolved, adsorption on minerals surfaces and organic matter and solid phases and by redox reactions (e.g., Balistrieri et al., 2008; Ehrlich et al., 2004; Hoefs, 2018; Markl et al., 2006a; Mathur et al., 2005; Pokrovsky et al., 2008; Sherman, 2013; Weinstein et al., 2011). The Cu isotope composition in most primary magmatic Cu-sulfides exhibit only minor isotope variations (Markl et al., 2006a; Mathur et al., 2009) but secondary alteration and low temperature redox processes are the main reason for isotope variations (e.g. Bigalke et al., 2013; Moynier et al., 2017; Wiederhold, 2015). In general, the reduced Cu species prefers the lighter Cu isotopes, Cu oxidation lead to an enrichment of the heavy  $^{65}\text{Cu}$  (e.g., Ehrlich et al., 2004; Mathur et al., 2005; Zhu et al., 2002).

### 1.3 Iron

Iron (Fe) ( $Z = 26$ ) is a transition metal and it is the fourth most abundant element in the earth's crust. Most of the iron produced is used to make steel and cast iron. It is also used for electromagnets in generators, transformers and electric motors due to its ferromagnetic properties.

Iron has four stable isotopes,  $^{54}\text{Fe}$  (5.85 %),  $^{56}\text{Fe}$  (91.75 %),  $^{57}\text{Fe}$  (2.12 %) and  $^{58}\text{Fe}$  (0.29 %) and is one of the most studied isotope systems (Berglund and Wieser, 2011; Johnson, 2020). For low temperature environments detailed reviews show numerous applications like tracing reactions and understanding (im)mobilization processes of iron (Dauphas et al., 2017; Johnson, 2020; Johnson et al., 2008; Wiederhold, 2015). Redox reactions fractionate Fe isotopes, e.g., the heavier Fe isotopes are preferentially enriched in the oxidized reaction products by aerobic and anaerobic microorganisms (e.g. Balci et al., 2006; Croal et al., 2004; Crosby et al., 2007; Johnson et al., 2004; Kappler et al., 2010). But also abiotic processes result in Fe isotope fractionation: Fe(II) oxidation produces for example an isotopically heavier isotope composition of ferrihydrite compared to  $\text{Fe(II)}_{\text{aq}}$  (Bullen et al., 2001). Fe(III) precipitation results in isotopically lighter remaining solutions and heavier precipitates (e.g. Balci et al., 2006; Beard and Johnson, 2004; Bullen et al., 2001). Igneous rocks in contrast display only

limited variations in their Fe isotope composition (e.g. Johnson et al., 2004; Weyer et al., 2005). Heavier Fe isotope are preferentially adsorb on oxide surfaces, producing isotopically lighter solutions, but also on microbial cells (Icopini et al., 2004; Kimball et al., 2009; Mathur et al., 2005; Teutsch et al., 2005).

## **2 Mining – impacts, consequences and mine tailings**

Since the earliest times of the earth's history, people have used stones, ceramics and later metals, to build and develop civilization. Initially, only metals from the earth's surface were mined, but as time went by, more and more complex methods were developed to extract products such as metal and coal even deeper in the earth. However, this technological progress was also accompanied by increased environmental impacts as mining affects nature to a certain extent and causes damage.

The impacts of mining are manifold, they can be caused for instance through erosion (Zhang et al., 2015), sinkholes (Singh and Dhar, 1997), water pollution (acid rock drainage (ARD)/ acid mine drainage (AMD)) and it can have effects on the biodiversity (Sonter et al., 2018). Moreover, mining changes and disturbs the landscape, the existing vegetation and fauna, it causes changes in the topography and hydrology (Lottermoser, 2010). In addition, huge amounts of solid and liquid heterogeneous mine wastes are stored in piles and tailings (Hudson-Edwards et al., 2011; Kossoff et al., 2014).

Tailings are generated after mining and extraction and consist of crushed rocks and solutions that have been used for extracting metals and minerals, e.g., in mills, washeries or concentrators (Hudson-Edwards et al., 2011; Kossoff et al., 2014; Lottermoser, 2010). Tailings can be found as riverine or submarine disposal, wetland retention, backfilling, dry stacking and storage behind dammed impoundments, increasing environmental hazards (e.g., Dold, 2006; Hayes et al., 2009; Hudson-Edwards et al., 2011; Kelm et al., 2009; Kossoff et al., 2014; Lottermoser, 2010; Wang et al., 2014). Mine waste must be properly disposed of or treated for sufficient period of time to prevent oxidation, the release of toxic substances, erosion, and other uses of the waste. If the mining wastes are dumped without control, there can be large-scale release of harmful elements and radioactivity, which can have very serious consequences in the long term for the pedosphere, biosphere, atmosphere, and hydrosphere (Lottermoser, 2010).

By anthropogenic treatments, but also by natural processes, sulfide-rich rocks (e.g. in mine tailings) are exposed to the atmosphere and water. As a consequence, sulfide minerals are oxidized and thereby mobilizing various, partly toxic elements in high concentrations and sulfuric acid as acid mine drainage (AMD). If released uncontrolled, e.g. in abandoned mines,



the surrounding waters may be contaminated or secondary minerals may form, depending on conditions like pH, climate or redox state (Akcil and Koldas, 2006; Dold, 2017; Kefeni et al., 2017; Kossoff et al., 2014; Lottermoser, 2010; Simate and Ndlovu, 2014). An example for typical processes in mine tailings and how isotopes can be applied to track them, will be presented in Chapter II of this thesis. A sequential extraction method in combination with Cu and Fe isotope analysis is used to understand processes occurring in porphyry copper mine tailings in the Atacama Desert in Chile.

Copper is mainly mined from porphyry copper deposits, located at plate boundaries. They have a large volume, but contain Cu only with low grade. The metal is mostly extracted by open-pit mining followed by crushing, grinding, milling, flotation and pyrometallurgy (Sillitoe, 2010). But supergene processes like weathering oxidize primary Cu-rich sulfide minerals and dissolved Cu migrates downward until secondary minerals precipitate at redox boundaries like the water table, resulting in mining regions with higher copper content (Mathur and Fantle, 2015).

Biomining is used for the extraction of Cu, gold (Au), cobalt (Co), nickel (Ni), zinc (Zn) and U from ores stored as dumps or heaps. The metals Cu, Ni, Co, lead (Pb) and Zn exist in nature mostly as sulfides which are insoluble at neutral and slightly acidic conditions. In biomining operations, low grade ores containing metal sulfides are oxidized by aerobic, acidophilic Fe(II)- and/or sulfur compound oxidizing bacteria or archaea in acidic solution to metal ions and sulfate (Brierley, 2008; Hedrich and Schippers, 2017; Johnson, 2014; Schippers et al., 2014). The material is fractured, stored in huge dumps and sprinkled with acidified water. The solution migrates through the dump and dissolves the metals, addition of bacteria further accelerates the process. Heap bioleaching is mostly used for extraction of Cu from secondary Cu ores (Brierley, 2008). The microorganisms oxidize the metal sulfides, Fe(II) and sulfur compounds, producing continuously Fe(III) and protons for the sulfide oxidation, guaranteeing low pH conditions which keeps the Fe ions in solution (Schippers et al., 2014).

Uranium is conventionally recovered by open pit (13 %) or underground mining (31 %), *in situ* or *in place* leaching (*in situ* recovery (ISR), 50 %), co-product and by-product recovery from copper and gold operations (6 %) and heap leaching (<1 %) (Abdelouas, 2006; Campbell et al., 2015; International Atomic Energy Agency, 2018; Zammit et al., 2014). Nowadays, U is mostly mined via ISR by which U is extracted through wells via oxidative dissolution in the subsurface (Figure I.1) (Zammit et al., 2014). It is a specialized form of U production, and is commonly suitable for sandstone type deposits only where U is deposited in an U roll-front and fluids can

migrate through the porous subsurface (Borch et al., 2012). Alkaline or acidic leaching solutions are pumped down into boreholes, the solution migrates through the ore deposit and dissolves the ore. Finally, it is pumped to the surface in a plant where the U is extracted from the leaching solution (Zammit et al., 2014).

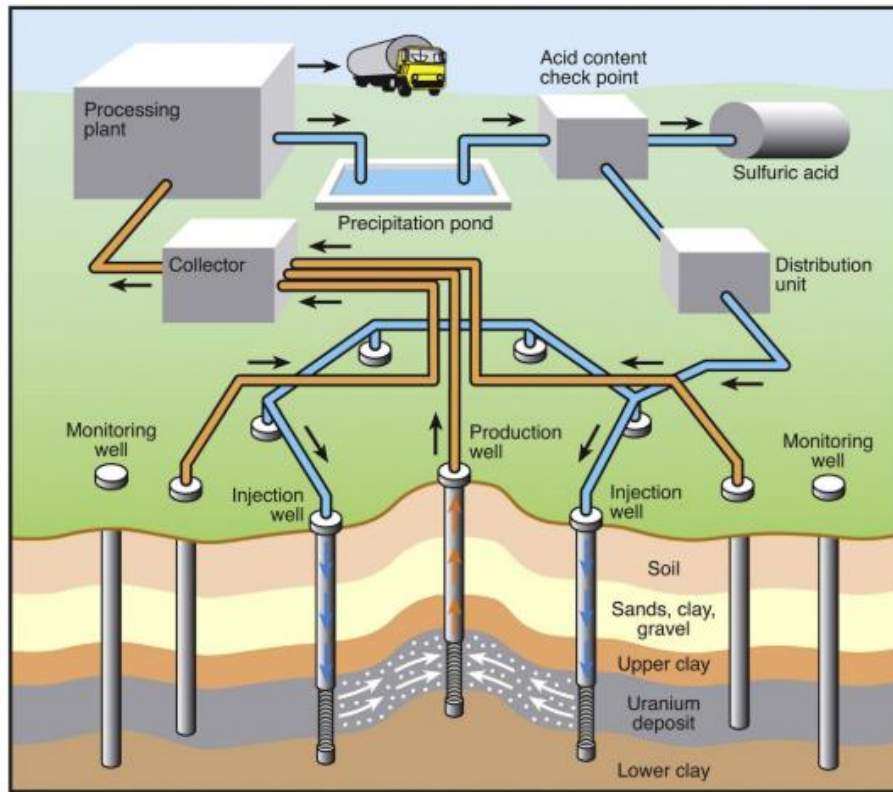


**Figure I.1.** In situ recovery site (after Zammit et al. (2014)).

On the one hand ISR has the advantages that it is an economic recovery for low-grade ores without mining and a big environmental impact (Zammit et al., 2014). Furthermore, it does not generate tailings (and has less safety hazards) and has a relatively low carbon footprint (Basu et al., 2015; Zammit et al., 2014). It is also less expensive, produces less solid mine wastes, has a smaller footprint than conventional U mining (Campbell et al., 2015). On the other hand, there are numerous environmental concerns and dangers from ISR as groundwater with mobilized U can be transported out of the mining area and may contaminate water resources downgradient. This could lead to direct consumption of poisonous water by animals or humans but also to U migration through the soil and the uptake by plants with the possible consequence of entering the human food chain (Borch et al., 2012; Davis and Curtis, 2007; Taylor et al., 2004). It is problematic that the ore dissolution is not well understood and heterogenous materials further complicate the understanding. After mining, the U concentration is increased in the groundwater, significantly above the permitted values. Consequently, ISR restoration is a

crucial and essential concern and generally based on a return of the site to baseline conditions (Campbell et al., 2015; Jemison et al., 2020).

### **3 (Bio)remediation and non-crystalline U(IV)**

The industrial demands for uranium increased during the last decades because of its numerous applications for nuclear energy and nuclear weapon productions and resulted in widespread U mining and ore processing which leaves a legacy of U contamination of aqueous systems, soils and sediments all over the world (National Research Council, 2000; Riley and Zachara, 1992). There are several remediation options including abiotic and biotic processes: For abiotic processes, zero-valent iron ( $\text{Fe}^0$ ), can be evaluated as a permeable reactive barrier material (Cantrell et al., 1995) or U(VI) can be reduced with redox-active minerals in the soil like pyrite, mackinawite or magnetite and via indirect reduction by biologically formed minerals like biogenic mackinawite (e.g., Veeramani et al., 2013). Recently, groundwater sweep is mostly used in combination with reverse osmosis to remove U (and also other elevated contaminant concentrations) from the groundwater (Borch et al., 2012; Gallegos et al., 2015; Jemison et al., 2020; WoldeGabriel et al., 2014).

However, there are several promising biotic possibilities, which have the advantage of reducing uranium much faster. For U bioreduction, indigenous bacteria are stimulated by adding an electron donor to promote enzymatic reduction of aqueous U(VI) to insoluble U(IV) (e.g., Anderson et al., 2003; Bargar et al., 2013; Newsome et al., 2014; Williams et al., 2013).

The advantage is that the remediation can be carried out without further major intervention in nature and it is economically advantageous. However, non-crystalline U(IV) is often formed under these conditions where the long-term stability cannot yet be properly estimated. U reduction by bacteria, by biogenic Fe(II)-bearing minerals or in reduced sediments can result in the formation of non-crystalline U(IV) (e. g. Alessi et al., 2014; Bernier-Latmani, 2010; Boyanov et al., 2011; Campbell et al., 2011; Fletcher et al., 2010; Latta et al., 2012; Sharp et al., 2011; Veeramani et al., 2011). It is usually associated with microbial biomass (Bernier-Latmani et al., 2010) and the production of  $\text{UO}_2$  vs. non-crystalline U(IV) appears to be correlated with the chemical speciation of the medium in which the reduction takes place (Bernier-Latmani et al., 2010; Boyanov et al., 2011).

Non-crystalline U(IV) is defined by the lack of the 3.85 Å U–U pair correlation characteristic of  $\text{UO}_{2(s)}$  observed using EXAFS (extended X-ray absorption fine structure) Fourier transform spectrum and without evidence of a crystalline lattice (Bernier-Latmani et al., 2010; Boyanov et al., 2011; Schofield et al., 2008). Apparently, U(IV) is bound in biological systems to

phosphate groups (Alessi et al., 2014). However, due to the absence of the crystalline structure, non-crystalline U(IV) easily reoxidized and therefore more labile compared to its crystalline species (Alessi et al., 2014, 2013, 2012; Cerrato et al., 2013). This remobilization may be caused by oxidants such as dissolved oxygen, Fe(III) and nitrate or through complexation by organic ligands such as bicarbonate, siderophores, citrate and humic substances or by bacteria (Alessi et al., 2012; Finneran et al., 2002; Frazier et al., 2005; Ginder-Vogel et al., 2010, 2006; Gu et al., 2005; Luo and Gu, 2011, 2009; Sani et al., 2005; Wan et al., 2005).

Therefore, several methods were developed for monitoring the remediation of U contaminated sites and U ore mines, including the application of U isotope signatures (Abdelouas, 2006; Andersen et al., 2017; Basu et al., 2015; Bhattacharyya et al., 2017; Bopp et al., 2010; Dang et al., 2016). Uranium reduction produces distinct isotopic signatures, with the solid U(IV) enriched in  $^{238}\text{U}$  (Basu et al., 2014; Brown et al., 2018; Stylo et al., 2015b, 2015a), isotopically light groundwaters may therefore indicate successful remediation. However, it is also important to monitor the long-term stability of the reduced U(IV). Methods that are only based on concentration measurements have limitations because common transport processes such as dilution or adsorption could change the U concentration in the groundwater significantly without any long-term immobilization (Bopp et al., 2010). Groundwater dilution does not induce U isotope fractionation and during adsorption  $^{235}\text{U}$  is slightly preferentially adsorbed, but the fractionation is smaller than that generated by U(VI) reduction (Brennecka et al., 2011a; Jemison et al., 2016b). Oxidation of solid U(IV) produces only minor U isotope fractionation due to a layer effect (Wang et al., 2015a). The reoxidation at remediation sites and consequent mobilization of U(IV) may also be indicated by U isotope fractionation (Jemison et al., 2018). The study consisted of oxidation experiments at a formerly bioremediated site and reported the accumulation of  $^{238}\text{U}$  in the groundwater upon oxidation: former reduction of U(VI) produces  $^{238}\text{U}$ -enriched U(IV) which is then reoxidized without any further U isotope fractionation. To enhance the understanding of natural U isotope signatures, Chapter III of this thesis examines anoxic U mobilization with ligands and associated U isotope fractionation. In Chapter IV abiotic and biotic oxidations processes and related U isotope fractionation was investigated.

#### **4 Bacteria (*Shewanella oneidensis* MR-1; *Acidithiobacillus ferrooxidans*)**

Two bacteria were mainly used for the experimental work of this thesis: *Shewanella oneidensis* MR-1 is used for the production of non-crystalline U(IV) as it is commonly found after U reduction in natural and anthropogenic environments and the best studied bioleaching bacterium *Acidithiobacillus ferrooxidans* for biotic U oxidation experiments.

*Shewanella oneidensis* MR-1 is a gram-negative bacterium which is facultative anaerobe, it can survive in both aerobic and anaerobic conditions. If there are no other terminal electron acceptors, *S. oneidensis* can couple oxidation of organic matter to reduction of oxidized metals (like  $\text{Fe}^{3+}$  or  $\text{Mn}^{4+}$ ), via a biological process called dissimilatory metal reduction (DMR) that can be coupled to energy conservation (Shi et al., 2009). If there is no iron or manganese present, these bacteria are even able to reduce metals like uranium (Lovley et al., 1991; Wall and Krumholz, 2006).

For extracellular reduction, *S. oneidensis* forms first biofilms on the metal oxides to facilitate close contact between the metal oxide and the bacteria (Thormann et al., 2004). Extracellular polymeric substances (EPS) are made of polysaccharides, proteins and lipids and contain several functional groups like carboxyl, phosphoryl, amide and hydroxyl, with them, EPS complexes metals (Baker et al., 2010). After formation of the biofilm, for respiration the bacteria have to transfer electrons from their cells to the metal. *Shewanella oneidensis* uses electron transport proteins called cytochromes for reversible energy transition. The product of U reduction, a mixture of non-crystalline U(IV) and  $\text{nanoUO}_2$ , depends on the geochemical conditions: groundwater solutes (sulfate, silicate, and phosphate) results in increased bacterial viability and more EPS. With less EPS, U is associated with the cell walls of bare cells, whereas U is associated directly with the EPS in EPS-rich environments (Stylo et al., 2013a). Multihaem c-type cytochromes are the major electron carrier proteins in the cells of *S. oneidensis* (Shi et al., 2009; Wall and Krumholz, 2006). *Shewanella oneidensis* is one of numerous microorganisms applied at contamination sites for bioremediation (Bargar et al., 2013; Sharp et al., 2011; Williams et al., 2013).

On the other side there are also bacteria that can gain energy from the oxidation of insoluble metal sulfide. In natural environments, but also in mine tailings and waste rocks from sulfide processing plants, acidophilic Fe(II)- and sulfur-oxidizing bacteria have a significant impact in producing sulfuric acid and dissolving metals (bioleaching and acid mine drainage; Hedrich and Schippers, 2020; Korehi et al., 2013). *Acidithiobacillus ferrooxidans* (*At. ferrooxidans*) is widely distributed in natural environments, such as hydrothermal sites, acid sulfate soils and acidic fens, naturally exposed ore deposits (gossans) as well as in man-made acidic environments such as mine sites including mine waste dumps and tailings, acid mine drainage and biomining operations (Hedrich et al., 2011; Hedrich and Schippers, 2020; Schrenk et al., 1998; Zhang et al., 2018). It lives in extremely acidic conditions by fixing  $\text{CO}_2$  and dinitrogen (Zhang et al., 2018). It is a Gram-negative, chemolithoautotrophic, acidophilic microorganism.

It obtains energy by oxidizing  $\text{Fe}^{2+}$ ,  $\text{S}^0$  or other reduced sulfur compounds and uses molecular oxygen (aerobic) or  $\text{Fe}^{3+}$  as electron acceptor as a facultative anaerobic bacterium (Kelly and Wood, 2000; Schippers et al., 2014; Temple and Colmer, 1951; Valdés et al., 2008; Zhang et al., 2018).

## 5 Objectives

This thesis is separated into three main chapters that aim at answering different objectives by using Fe, Cu and U isotope analyses. Mine tailings, metal contaminations and (bio)remediation sites are complex and heterogenous areas with high potential for environmental damage and many knowledge gaps regarding the involved processes still exist. Laboratory batch experiments and analyses of environmental samples are a promising way to better understand and unravel these processes. This thesis aims to use metal isotope fractionation to explore processes at mining settings which may be useful in the development of strategies to reduce environmental risks.

**Chapter II** aimed to develop a modified sequential extraction method and to investigate the potential application for acidic mine tailings. Iron and copper isotopes are suggested as a monitor tool for metal sulfide oxidation processes, as resulting acid mine drainage causes large environmental damage and releases toxic elements. Sequential extractions help to identify metal distributions among different components of sediments and soils and thus contributes to a better understanding of processes in mine tailings consisting of heterogenous materials. After the performance (including accuracy and precision) of the sequential extraction method for metal isotope analysis was tested, it was applied to samples from two sites of porphyry copper mine tailings in the Atacama Desert in Chile (Chañaral bay). The isotopic signatures of the sediment components revealed important processes regarding the mobility of Fe and Cu at those sites.

**Chapter III** examines the anoxic mobilization and U isotope fractionation of non-crystalline U(IV) with the ligands EDTA, citrate and bicarbonate in laboratory batch experiments to better predict the long-term stability of reduced U in the subsurface and to further specify the application of U isotopes as a monitoring tool for remediation. Non-crystalline U(IV) is the major product of bioreduction and is significantly more labile than uraninite and thus faster remobilized. The objective of this chapter was the investigation of U mobilization and U isotope fractionation of laboratory produced non-crystalline U(IV). Isotope fractionation was modeled and discussed and implications for the use of U isotope as a proxy in mining environments were derived. Additionally, the findings of these investigations will also advance the interpretation of U isotope signatures of ancient sediments which are investigated as archives for the rise of

atmospheric oxygen in the Archean and early Proterozoic which, however, cannot be simply explained by redox reactions alone.

**Chapter IV** deals with U isotope fractionation caused by U oxidation with Fe(III), the biomass of *Acidithiobacillus ferrooxidans* or molecular oxygen. Apart from anoxic U mobilization by ligands at remediation and contamination sites discussed in Chapter III, abiotic or biotic oxidation reactions also cause U mobilization and may result in additional and variable U isotope fractionation which may further complicate the interpretation of natural U isotope signatures. Uranium oxidation is examined with living and dead cells. Corresponding abiotic experiments without biomass were conducted to study the influence of molecular oxygen on the biotic results. In this chapter, observed U mobilization and associated isotope fractionation was fitted with Rayleigh distillation and equilibrium models in order to discuss the implications for natural and anthropogenic environments.

## Chapter II:

# **Fractionation of Fe and Cu isotopes in acid mine tailings: modification and application of a sequential extraction method**

Published in *Chemical Geology* 493 (2018): 67-79  
[doi.org/10.1016/j.chemgeo.2018.05.026](https://doi.org/10.1016/j.chemgeo.2018.05.026)

Y. Roebbert<sup>1</sup>, K. Rabe<sup>1</sup>, M. Lazarov<sup>1</sup>, S. Schuth<sup>1</sup>, A. Schippers<sup>2</sup>, B. Dold<sup>3</sup>, S. Weyer<sup>1</sup>

<sup>1</sup> Leibniz Universität Hannover, Institut für Mineralogie, Callinstr. 3, 30167 Hannover, Deutschland ([y.roebbert@mineralogie.uni-hannover.de](mailto:y.roebbert@mineralogie.uni-hannover.de))

<sup>2</sup> Bundesanstalt für Geowissenschaften und Rohstoffe, Stilleweg 2, 30655 Hannover, Deutschland

<sup>3</sup> Luleå University of Technology, Department of Civil, Environmental and Natural Resources Engineering, F861 Luleå, Sweden

Some data have been analyzed and processed by Katharina Rabe. Pre-work (development of the sequential extraction method) was done as the bachelor thesis of Yvonne Röbbert. All data processing, interpretation and writing of the manuscript was done by Yvonne Röbbert, but all co-authors contributed with comments.



## Abstract

Sulfidic mine tailings have a high potential for contamination of the environment by triggering acid mine drainage. Hence, it is crucial to understand metal mobilization processes and to develop monitoring tools. Metal isotope fingerprinting as a potential monitoring tool for metal sulfide oxidation processes was in the focus of this study by using stable isotope signatures of Cu and Fe. For Fe, a six-step sequential extraction method was applied, in order to separate potential Fe-bearing minerals (water-soluble, exchangeable fraction, Fe(III)(oxyhydr)oxides, Fe-oxides, sulfides and organic compounds and residual/silicates). For Cu, this method was modified into a four step extraction method (water-soluble, exchangeable fraction, oxalate fraction/bound to Fe-oxides and sulfides/residual). To verify accuracy and precision of the sequential extraction method for metal isotope analysis, isotope fractionation during the extraction procedure was investigated employing minerals for which the mineral composition and the isotopic composition was known. The developed procedure is suitable to separate target minerals with only a small loss in the elemental budget. No significant isotope fractionation was observed during the extraction procedure.

Application of this method on two sites of porphyry copper mine tailings in the Atacama Desert in Chile (Chañaral bay) revealed several implications about the mobilization of Fe and Cu in an environmental setting. Iron contents and Fe isotope compositions are homogeneous with depth (0-61 cm;  $\delta^{56}\text{Fe}$  ~0.2-0.3 ‰) for the bulk and the Fe(hyr)oxide fraction and only the deepest samples at ~60 cm exhibited lower  $\delta^{56}\text{Fe}$  values (~0 ‰), which are likely related to the occurrence of an alluvium at this depth. The Fe silicate fraction shows higher  $\delta^{56}\text{Fe}$  values (0.6-0.9 ‰), most likely because of preferential leaching of the light Fe isotopes. This consequently indicates a more pronounced Fe isotope fractionation with depth, as is expected from longer weathering. The Fe sulfide fraction is isotopically lighter compared to the Fe(hydr)oxide fraction, because during sulfide oxidation the heavy Fe isotopes prefer the oxidized forms and oxidative precipitation results in an enriched Fe isotopic signature for Fe(hydr)oxides. The Cu isotope compositions of all bulk samples and individual fractions (except the Cu sulfides) of one site (Ch1) exhibited a decrease of the  $\delta^{65}\text{Cu}$  values from the depth towards the surface, i.e. in agreement with the capillary water rise in the arid climate. A correlation of  $\delta^{65}\text{Cu}$  with pH indicates preferential adsorption of  $^{65}\text{Cu}$  on Fe(oxy)hydroxides at site Ch1, which is evident by a change of  $\delta^{65}\text{Cu}$  from 0.5 ‰ to -0.7 ‰ in the water-soluble fraction. At another site (Ch12), where pH at depths was potentially not high enough for the formation of Fe-minerals that could

adsorb Cu, only minor Cu isotope fractionation was observed in the water-soluble fraction. The Cu sulfide fraction at site Ch1 exhibits higher  $\delta^{65}\text{Cu}$  values with an increase from the bottom (0.42 ‰) to the surface (0.92 ‰), which might be related to preferential leaching of the light isotopes, e.g. by microorganisms.

Keywords:

- Sequential extraction
- Fe isotopes
- Cu isotopes
- mine tailings

## 1 Introduction

Mine tailings are generally stored in piles or in impoundments close to mining sites and consist of heterogeneous materials that are mostly fine grained (Hudson-Edwards et al., 2011; Kossoff et al., 2014). In the past and sometimes also nowadays tailings are deposited directly or nearby of marine environments, rivers, and lakes, and contaminate the surroundings through erosion, the dispersal of dust, or the release of acid mine drainage (AMD) (Gault et al., 2005; Hayes et al., 2009; Hudson-Edwards et al., 2011; Kelm et al., 2009; Lottermoser, 2010; Wang et al., 2014). Large environmental damage can be caused by AMD (e.g. Akcil and Koldas, 2006; Kefeni et al., 2017; Simate and Ndlovu, 2014) which is a result of sulfide minerals reacting with oxygen and water at supergene conditions, hence triggering an increase of acidity. Microorganisms may further accelerate the oxidation of sulfide minerals. Acidophilic iron(II)- and sulfur-oxidizing bacteria are able to produce sulfuric acid during mineral degradation, which in turn further enhances the dissolution of minerals, and thus may mobilize toxic elements like As, Pb, and Cd (Dold, 2017; Hedrich and Schippers, 2017; Schippers et al., 2010). Consequently, large areas may be contaminated, resulting in a degraded water quality and a high risk for life (Akcil and Koldas, 2006; Dold, 2010; Korehi et al., 2013).

Moreover, mine tailings may function as sinks for many elements. Trace metals are accumulated in the material via e.g. adsorption or precipitation, and these may be released due to changes of pH or redox potential (Hindersmann and Mansfeldt, 2014; Kossoff et al., 2014; Ramirez et al., 2005). Even more significant is metal association with different mineralogical fractions, here the metal availability strongly depends on chemical binding partners and speciation (Mansfeldt and Overesch, 2013; Ramirez et al., 2005; Sparks, 2005).

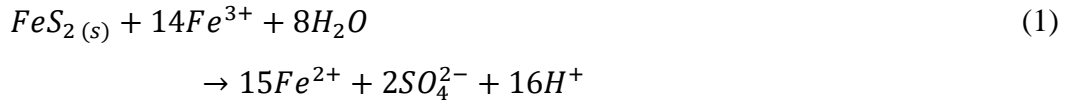
Consequently, the knowledge about metal concentration is not sufficient to delineate mobilization, bioavailability and environmental consequences of mine tailings. Sequential extractions enable to investigate metal distributions in different sediment or soil fractions and can be furthermore applied for exploration purposes or to gain knowledge about biogeochemical element cycling in natural and in mine waste environments (Dold, 2003; Gleyzes et al., 2002; Silveira et al., 2006). They provide a powerful tool to identify the potential mobility and consequently the toxicity and bioavailability of certain elements like As, Hg, and Se (Bacon and Davidson, 2008). The general principle is based on the treatment of sample material with different selective reagents to dissolve discrete mineral fractions without attacking other phases (Gleyzes et al., 2002).

Sequential extractions have already been combined with stable isotope analysis for several elements, e.g. for Fe (Guelke et al., 2010; Mansfeldt et al., 2012; Wiederhold et al., 2007a), Se (Schilling et al., 2014), Zn (Thapalia et al., 2010), Mo (Siebert et al., 2015), and Hg (Wiederhold et al., 2015, 2013). In previous studies, the combination of a sequential extraction method with Cu isotopes (Kusonwiriawong et al., 2016) and Fe isotopes, respectively, was used to determine the response of Cu release in a soil during a flooding event the role of colloidal Fe (Kusonwiriawong et al., 2017). For Fe, isotope fractionation during pedogenic Fe transformation and translocation processes were examined under oxic conditions by Wiederhold et al. (2007b) and the same was done to analyze the relationships between pedogenic Fe transformation and redistribution processes (Wiederhold et al., 2007a).

Numerous studies determined the variation of the Fe isotope composition in low temperature environments which are caused by diverse fractionation mechanisms (e.g. Johnson et al., 2008; Wiederhold, 2015), hence demonstrating that Fe isotope fractionation is a powerful tool to trace reactions and understand mechanisms that are mobilizing or immobilizing Fe (e.g. Akerman et al., 2014; Fekiacova et al., 2013; Mansfeldt et al., 2012; Opfergelt et al., 2017; Schuth and Mansfeldt, 2016; Yesavage et al., 2012). Oxidation and reduction of Fe by various microorganisms (aerobic and anaerobic) results in Fe isotopic fractionation, the heavier Fe isotopes are preferentially enriched in the oxidized form (e.g. Balci et al., 2006; Croal et al., 2004; Crosby et al., 2007; Johnson et al., 2004; Kappler et al., 2010). Furthermore, Fe isotope fractionation has also been observed during diverse abiotic processes: Fe(II) oxidation produces for example an isotopically heavier isotope composition of ferrihydrite compared to Fe(II)<sub>aq</sub> (Bullen et al., 2001). Iron isotope fractionation was moreover investigated during Fe(III) precipitation, with isotopically lighter remaining solutions and heavier precipitates (e.g. Balci et al., 2006; Beard and Johnson, 2004; Bullen et al., 2001). Igneous rocks in contrast display only limited variations in their Fe isotope composition (e.g. Johnson et al., 2004; Weyer et al., 2005).

In addition to the above mentioned need to identify chemical forms and the speciation of the contaminants, sequential extractions may reveal more details about microbial processes in tailings. Herbert and Schippers (2008) already examined Fe isotope fractionation in mine tailings at the interface between the oxidized and non-oxidized zone. Iron isotope fractionation in these environments is mostly controlled by redox reactions, precipitation, and adsorption processes yielding isotopic variations within the different Fe pools. At the redox interface in mine tailings microorganisms catalyze sulfide oxidation. Ferric iron (FeIII) oxidizes metal

sulfides like pyrite, thereby forming sulfuric acid, and Fe(III) is regenerated from ferrous Fe (Fe(II)) by iron-oxidizing microorganisms (Herbert and Schippers, 2008; Nordstrom, 2011):



Consequently, the resulting AMD is rich in dissolved metals, which may have a severe effect on the environment. Herbert and Schippers (2008) ascertain that pyrite oxidation (eqn. 1) was mediated by microorganisms and Fe was precipitated abiotically (eqn. 2), which both had effects on the Fe isotope composition of the pore water and the solid phase. The Fe isotope fractionation between the pore water and secondary ferric oxyhydroxides produces  $\delta^{56}Fe$  values of -1.4 to -2.4 ‰ with a light Fe isotope composition in the dissolved Fe pool and heavier  $\delta^{56}Fe$  values for the solid phase (Herbert and Schippers, 2008). Similar results were also obtained experimentally by Schuth et al. (2015) for variable redox conditions and reductive Fe mobilization.

Copper isotope fractionation is mostly based on redox chemistry and on elemental exchange between dissolved and solid phases. The Cu isotope composition in most primary magmatic Cu-sulfides exhibit only minor isotope variations (e.g. chalcopyrite average  $\delta^{65}Cu$ : 0.12 ‰,  $1\sigma = 0.33$  ‰; Markl et al., 2006; primary ores  $\delta^{65}Cu$ :  $0 \pm 0.5$  ‰, 2.s.d.; Mathur et al., 2009) but secondary alteration and low temperature redox processes are the main reason for isotope variations (e.g. Bigalke et al., 2013; Moynier et al., 2017; Wiederhold, 2015).

In several earlier studies, experiments indicated that redox reactions between Cu(I) and Cu(II) are the most important processes that fractionate Cu in natural settings. For instance, reduction of  $Cu(II)_{aq}$  (to Cu(I)) results in the preferential reduction of the lighter Cu isotope (Ehrlich et al., 2004; Zhu et al., 2002). Mathur et al. (2005) explored biotic and abiotic Cu oxidation with contrasting results: Abiotic oxidation entails an enrichment of the heavy Cu isotope in solution whereas the contribution of microorganisms leads to a Cu pool depleted in  $^{65}Cu$  because the heavy Cu isotope is incorporated in metal oxides on the external membranes of the cells of Fe-oxidizing bacteria. This was further demonstrated by Balistrieri et al. (2008) and Pokrovsky et al. (2008). Adsorption onto amorphous ferric oxyhydroxides during the mixture of metal-rich acid rock drainage and river water resulted in lower  $^{65}Cu$  values of the water (Balistrieri et al., 2008). Similarly, during adsorption experiments on Fe-oxy(hydr)oxide surfaces and ascorbic

acid, preferential adsorption of  $^{65}\text{Cu}$  was observed (Pokrovsky et al., 2008; Bigalke et al., 2011), while on biological cell surfaces  $^{65}\text{Cu}$  was depleted (Kimball et al., 2009; Navarrete et al., 2011; Pokrovsky et al., 2008). Song et al. (2016) used Cu isotope fractionation in streams near a porphyry copper mine in China (Dexing Mine) to identify the source of contaminants. As a result, they identified mine tailings as source for the contamination, because of a heavier Cu isotope composition compared to average Cu isotope values from rivers and oceans. Kimball et al. (2009) examined Cu isotope fractionation in acid mine drainage (San Juan Mountains, Colorado, USA) and they determined higher  $\delta^{65}\text{Cu}$  values for the stream waters compared to mineral samples ( $1.38\text{‰} \leq \delta^{65}\text{Cu} \leq 1.69\text{‰}$ , 2 s.d.  $0.10\text{‰}$ ). Borrok et al. (2007) measured various stream waters affected by acid mine drainage and they got heterogeneous results varying between  $-0.7\text{‰}$  to  $+1.4\text{‰} \pm 0.3\text{‰}$ , 2 s.d.. Those samples did not reflect a single averaged isotopic composition within the continental crust.

Metal isotope fingerprinting as a potential monitoring tool for metal sulfide oxidation processes was in the focus of our study. It comprises an experimental part with the aim to examine and modify a sequential extraction method (after Dold, 2003, and Mehra & Jackson (1958)) for Fe and Cu separation from sediments and mine tailings. The developed procedures were tested with regard to their ability to quantitatively separate the Cu and Fe fractions that are incorporated in different minerals without generating an unwanted artificial isotope fractionation. To verify the precision of the sequential extraction procedure employed for Cu and Fe isotope analysis, potential isotope fractionation during the extraction was investigated by using minerals with a known chemical and Fe-Cu isotopic composition. In the second part of the study, the developed extraction methods were applied to samples from Cu mine tailings in Chile for which the mineralogy, geochemistry and microbiology was already described (Dold, 2006; Korehi et al., 2013).

## **2 Material and methods**

### **2.1 Sample material**

#### **2.1.1 Sequential extraction test samples**

The sequential extraction scheme was developed (for Cu) and tested for its suitability for isotopic investigations (for Fe) using individual minerals and composite samples that were prepared from individual minerals (see Table II.1) of known isotopic composition. Test minerals were selected, in order to represent typical target minerals (1) to be separated by the

sequential extraction and (2) that were also observed in the tailing samples of our case study below (Dold, 2006). For Fe, test sample 1 & 2 include iron oxide (magnetite -  $\text{Fe}_3\text{O}_4$ ), iron oxy-hydroxide (ferrihydrite -  $5\text{Fe}_2\text{O}_3 \cdot 9\text{H}_2\text{O}$ , Dold, 2010), iron sulfide (pyrite -  $\text{FeS}_2$ ) and iron silicate (biotite -  $\text{K}(\text{Mg},\text{Fe})_3[(\text{OH})_2\text{AlSi}_3\text{O}_{10}]$ ). Furthermore, the sequential extraction was tested with only magnetite and with Bayferrox 920 Z (a synthetic goethite,  $\alpha\text{-FeOOH}$ ; see Mansfeldt et al., 2012).

For copper, different minerals (hand-picked from natural samples) were used and examined individually. As water-soluble mineral, the copper sulfate (chalcantite -  $\text{Cu}[\text{SO}_4] \cdot 5\text{H}_2\text{O}$ ) was used. Copper carbonate (malachite -  $\text{Cu}_2[(\text{OH})/\text{CO}_3]_2$ ) and a synthetic Cu hydroxide ( $\text{CuOOH}$ ) were used as test minerals for the “exchangeable” and “Cu oxide” fraction, respectively, while Covellite ( $\text{CuS}$ ) and chalcopyrite ( $\text{CuFeS}_2$ ) represented the sulfide fraction.

The minerals were mostly hand-picked from natural samples under a microscope and then ground to powder (agate mortar). A small amount of the powdered samples was used for bulk digestion (for concentration and isotope measurements) and another aliquot was subjected in parallel to the sequential extraction.

**Table II.1.** Mineralogical composition of the test samples.

	sample	magnetite [g]	ferrihydrite [g]	pyrite [g]	biotite [g]	[g]
<b>Fe</b>	test sample 1	0.0134	0.0251	0.0126	0.0264	-
	test sample 2	0.0115	0.0259	0.0130	0.0273	-
	magnetite	0.0430	-	-	-	-
	Bayferrox 920 Z	-	-	-	-	0.02919
	chalcantite	-	-	-	-	0.00317
<b>Cu</b>	malachite	-	-	-	-	0.00296
	Cu hydroxide	-	-	-	-	0.02766
	covellite	-	-	-	-	0.01653
	chalcopyrite	-	-	-	-	0.02556

### 2.1.2 Samples from the Chañaral bay mine tailings

Decades of sulfidic mine waste deposition in the Chañaral bay in the Atacama Desert in Chile left an environment characterized by extreme acidic (pH 2-4), metal-rich (pore water concentrations of up to more than 6000 mg/L sulfate, 2265 mg/L copper, 20 mg/L zinc, and 18 mg/L nickel), and high-saline conditions (NaCl concentrations of up to more than 1 M in the pore water) at the tailings surface (Korehi et al., 2013). Between 1938 and 1975 mine tailings from the Potrerillos and El Salvador mines were dumped without any treatment into the bay through the river Salado resulting in a polluted environment and strongly affected marine life

(Castilla, 1983; Dold, 2006; Ramirez et al., 2005). The Potrerillos deposit comprised  $1.8 \cdot 10^6$  t Cu and the El Salvador porphyry copper deposit  $5.7 \cdot 10^6$  t Cu. The mine tailings consist of over 220 Mt of tailings material. For the gangue mineralogy Dold (2006) identified quartz, feldspar (albite-anorthite), muscovite-biotite, kaolinite, magnetite, and rutile ( $\text{TiO}_2$ ). The main sulfide minerals were mostly pyrite and in smaller quantities chalcopyrite and chalcocite ( $\text{Cu}_2\text{S}$ ). The pyrite content, which determined mostly the quantity of AMD, was  $0.8 \pm 0.25$  wt.% in the tailings (Dold, 2006).

Regarding metal mobility in this specific mine tailings, the climate has to be considered. Between 1962 and 1984, the precipitation was approx. 20 mm/a, hence indicating hyper-arid conditions. This resulted in very high annual evaporation rates (Dold and Fontboté, 2001). The dissolution of the primary mineral phases still being present after ore processing in the mine tailings led to metal enrichment by an upward transport via capillary ascending water because of the high evaporation rate. This resulted in a precipitation of secondary minerals at the surface of the mine tailings, mostly the water-soluble halite ( $\text{NaCl}$ ) and eriochalcite ( $\text{CuCl}_2 \cdot 2\text{H}_2\text{O}$ ) (e.g. up to 2.4% Cu) (Dold, 2006; Korehi et al., 2013). The oxidation zone in the tailings contained secondary ferric minerals with mainly jarosite ( $\text{KFe}_3(\text{SO}_4)_2(\text{OH})_6$ ) and Fe(III) hydroxides. Moreover, gypsum ( $\text{CaSO}_4 \cdot 2\text{H}_2\text{O}$ ), clay minerals like illite, kaolinite, and a vermiculite-type mixed-layer mineral were present in the oxidation zone (Dold, 2006).

The samples originated from outcrop profiles at two different sites of the tailings. They were taken in November 2008 in 3 cm depth intervals, including the oxidation zone to a maximum depth of 105 cm (see SI, Figure S II.1, Korehi et al., 2013). Site Ch1 was located in the southern part near the city of Chañaral and was analyzed for its Fe and Cu concentrations and isotopes. Site Ch12 was in the central part of the mine tailings near the actual shore line (~30 m from the sea), and was analyzed only for Cu (concentrations and isotopes).

In the acidic mine tailings, metals (including Cu) may frequently be liberated by microbial oxidation. Korehi et al. (2013) used these samples for a study of the microbial communities under extreme conditions (low pH, high salinity, almost organic-carbon free) in these mine tailings. They found the acidophilic iron(II)- and sulfur-oxidizing and iron(III)-reducing genera *Acidithiobacillus*, *Alicyclobacillus* and *Sulfobacillus* among other bacteria and also archaea. The horizons with the highest pyrite oxidation rate exhibited also the highest cell numbers and the highest proportion of biotic pyrite oxidation. This was seen as an indicator for the fact that the pyrite oxidation was mostly controlled by microorganisms.



For site Ch1, Korehi et al. (2013) observed a strong correlation of pH with depth with values of 2 at the surface and of 7 at ~60 cm depth. For site Ch12, a more constant pH with values mostly between 2 and 3 was observed at a similar depth, which was increasing, however, within the uppermost 20 cm towards a value of ~5 at the surface.

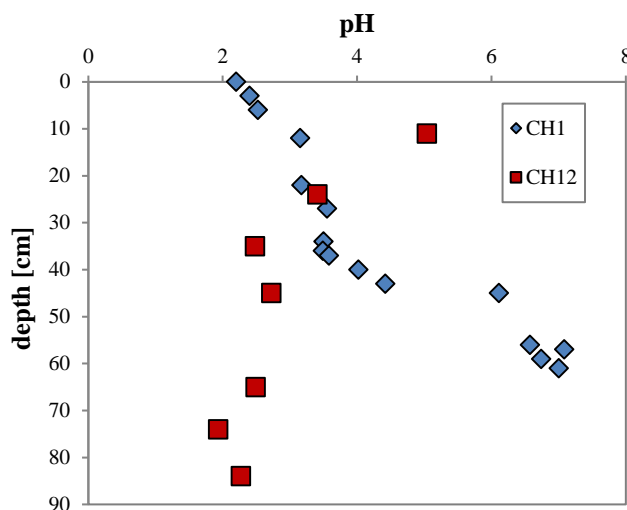


**Figure II.1.** Depth profiles of pH at sites Ch1 and Ch12 of the Chañaral bay mine tailings (modified after Korehi et al., 2013).

In this study, the tailings were analyzed at different depths by employing the established sequential extraction procedures of this study for their Fe and Cu concentration and isotopic signatures. Analyses were performed on both, bulk samples and on individual fractions, employing below described sequential extraction procedures modified after Dold (2003) and Mehra and Jackson (1958).

## 2.2 Sequential extraction

For this study, sequential extraction of Fe and Cu is evaluated on the basis of the modified methods of Dold (2003) and Mehra & Jackson (1958).

Approximately 100 mg of each sample was used and submitted to the six steps sequential extraction procedure (see Table II.2) for Fe separation. The *water-soluble fraction* (1) was extracted with 50 ml water (Millipore MQ system, 18.2 MΩ grade) and shaken for 1h at room temperature (RT). The *exchangeable fraction* (2) was mobilized with 1 M NH<sub>4</sub>-acetate (Sigma Aldrich, ≥ 98 %) at pH = 4.5 (ca. 30 ml 1 M NH<sub>4</sub>-acetate and 2 ml 25 % acetic acid (Merck)), shaken for 2 h at RT. The *Fe(III)(oxyhydr)oxides* (3) were extracted employing Na dithionite as described by Mehra & Jackson (1958) (1 g Na<sub>2</sub>S<sub>2</sub>O<sub>4</sub> at 80°C). The next step, (4) the *oxalate-fraction*, attacked magnetite (after Dold, 2003). To the residue of step (3), 35 ml of a 0.2 M NH<sub>4</sub>-oxalate (Merck, 99.5-101.0 %) solution were added and brought to pH 3 with oxalic acid

(Merck,  $\geq 99.5\%$ ), shaken for 2 h and heated to  $80^\circ\text{C}$  to dissolve the oxalate-fraction. The *sulfides and organic compounds* (5) (Dold, 2003; Hall et al., 1996) were dissolved by adding 750 mg  $\text{KClO}_3$  (Sigma Aldrich,  $\geq 99\%$ ) and 5 ml of 12 M HCl (Roth) to the residue of step (4). After shaking, a further 10 ml of 12 M HCl were added. After 30 min, 15 ml water (MQ) was added and shaken for 5 min. The remaining residue was treated with 10 ml 4 M  $\text{HNO}_3$  (Roth) in a water-bath at  $90^\circ\text{C}$  for 20 min. All leachates of this step (5) were collected in a centrifuge tube. In order to dissolve the *residual* (6) fraction a mixture of 5 ml 24M HF (Merck) and 3 ml 15M  $\text{HNO}_3$  (5:3) was used. The mixture was heated for 24 h at  $140^\circ\text{C}$  in closed teflon beakers. After evaporation at  $110^\circ\text{C}$ , the samples of step (6) were treated with aqua regia (1 ml 15 M  $\text{HNO}_3$  and 3 ml 11 M HCl) and heated for 1 h at  $120^\circ\text{C}$ . Table II.2 shows an overview about the target minerals expected to be dissolved in each step.

After each step, the sample solutions were centrifuged and the dissolved supernatant was taken up with a pipette. Furthermore, the remaining residue was stirred in 1 ml water (MQ), centrifuged again, and the supernatant was added to the initial supernatant.

Applying this 6-step sequential extraction procedure, as listed in Table II.1, to separate the Cu-bearing minerals of the investigated tailings revealed that extraction steps (3) and (4) targeted similar minerals and step 3 does not result in a quantitative mobilization of Cu in Cu-oxides. Therefore, only step (4) employing  $\text{NH}_4$ -oxalate was used for extraction of Cu in Cu- and Fe-oxides. The extraction of the sulfide fraction with  $\text{KClO}_3$  was not applied to the Cu minerals. As Cu in the silicate fraction is negligible and  $\text{HNO}_3/\text{HF}$  quantitatively dissolves both sulfides and silicates, the original sulfide step (5) was omitted and only the residual step (6) was performed. Copper silicates are scarce and only form at temperatures above  $100^\circ\text{C}$  (Ilton and Veblen, 1988; Otto, 2000). Thus, potential Cu silicates must be of detrital origin from the mine. Furthermore, the residual material (after applying a sulfide leaching step) of some samples have been optically examined and no Cu-silicates have been observed. Thus, we assumed that no Cu-silicates are present in the investigated samples and only step 6 (residual) was performed by assuming that it targets only Cu sulfides. As a result of these modifications, only four extraction steps for Cu were used (water-soluble, exchangeable, oxides and residual/sulfides, i.e. steps 1, 2, 4 and 6 of Table II.2 below).

**Table II.2.** The different steps of the sequential extraction.

Step	Chemical	Target minerals	Example
1	MQ-water	sulfates, salts	gypsum, metal salts, chalcantite, secondary sulfates
2	NH <sub>4</sub> -acetate	adsorbed & exchangeable ions, carbonates	calcite, malachite, azurite
(3)*	(Na-dithionite)	(amorphous & crystalline Fe-oxides)	(ferrihydrite, goethite, hematite)
4	NH <sub>4</sub> -oxalate	Fe-oxides	magnetite (ferrihydrite, goethite, hematite)
(5)*	(KClO <sub>3</sub> & HCl)	(sulfides)	(pyrite, chalcocite, chalcopyrite)
6	HF & HNO <sub>3</sub>	residual (silicates)	biotite, phlogopite

\* step only used for Fe sequential extraction

### 2.3 Cu and Fe chromatographic separation

Copper and Fe from the bulk samples and each fraction of the sequential extraction were purified by ion-exchange chromatography following a modified method described by Borrok et al. (2007) (see also Table S II.1 in SI). Afterwards, the recovery for Fe and Cu was tested (see below).

The digested samples were taken up in 1 ml 9 M HCl, and purified Fe and Cu fractions were obtained by passing the solution through Bio-Rad® AG MP-1 (100-200 mesh) anion resin in 2 ml Bio-Rad® columns. Prior loading of the sample, the resin was cleaned with 10 ml 7 M HCl, water (MQ), 5 % HNO<sub>3</sub>, and again water. Subsequently, 12 ml 9 M HCl was added to condition the resin. The samples were then loaded and the matrix was removed with 7 ml 9 M HCl. The Cu fraction was eluted from the columns with 18 ml 5 M HCl and subsequently, the Fe fraction with 12 ml 1 M HCl. After purification, all fractions were dried and treated with a mixture of concentrated HNO<sub>3</sub> and H<sub>2</sub>O<sub>2</sub> (30 %) in order to remove any potential resin contribution. The fractions were finally dissolved in 3 % HNO<sub>3</sub>, and diluted to a final concentration of approximately 500 ppb Cu and 8 ppm Fe, respectively, for ICP analyses.

### 2.4 Concentration measurements

The bulk concentrations and any potential loss of Fe and Cu during the sequential extraction were determined for each sample. A small aliquot of the bulk samples and each fraction from

the sequential extraction was taken after sample dissolution, prior to the chromatographic purification, for Fe and Cu concentration measurements.

For these measurements, a Thermo-Scientific (Bremen, Germany) Element-XR inductively coupled plasma source mass spectrometer (ICP-MS), and an optical emission spectrometer (ICP-OES, Varian Vista AX) at University Hannover, Germany, were employed. For calibration of the instruments and standardization for the concentration measurements, multi-element standard solutions have been prepared gravimetrically. For the measurements employing the Element XR, an Indium solution (Alfa-Aesar, Germany) was added as an internal standard to all samples, yielding a final concentration of 1 ppb In. The precision was typically below 5 % (2 s.d.) for the ElementXR and below 10 % (2 s.d.) for the ICP-OES analyses.

## 2.5 Isotope measurement: MC-ICP-MS

Iron and Cu isotope measurements were performed at the Leibniz Universität Hannover using a Thermo-Finnigan Neptune multi-collector ICP-MS (MC-ICP-MS). For sample introduction, a quartz spray chamber (double pass, Scott design) and a nebulizer made of perfluoroalkoxy alkane (PFA) with an uptake rate of ~100  $\mu\text{l}/\text{min}$  (Elemental Scientific) were used. During analyses the standard sample bracketing method was applied, i.e. two sample measurements were bracketed by two standard measurements.

The analytical procedures for *Fe isotope* measurements in our laboratory have been previously described in detail by Oeser et al. (2014). Briefly, for Fe isotope analysis, H-type Ni sampler and Ni skimmer cones were employed. Masses  $^{53}\text{Cr}$ ,  $^{54}\text{Fe}$ ,  $^{56}\text{Fe}$ ,  $^{57}\text{Fe}$ ,  $^{58}\text{Ni}$  and  $^{60}\text{Ni}$  were detected simultaneously.

Iron was measured in high mass resolution, in order to separate mass interferences of polyatomic argide ions ( $^{40}\text{Ar}^{14}\text{N}^+$ ,  $^{40}\text{Ar}^{16}\text{O}^+$ ,  $^{40}\text{Ar}^{16}\text{OH}^+$ , and  $^{40}\text{Ar}^{18}\text{O}^+$ ) from the Fe isotopes  $^{54}\text{Fe}^+$ ,  $^{56}\text{Fe}^+$ ,  $^{57}\text{Fe}$ , and  $^{58}\text{Fe}^+$ , respectively (Weyer and Schwieters, 2003). In addition,  $^{54}\text{Cr}$  adds as an isobaric interference on the signal of  $^{54}\text{Fe}$ , hence  $^{54}\text{Cr}$  was monitored by analysis of  $^{53}\text{Cr}$  and applying the natural  $^{53}\text{Cr}/^{54}\text{Cr}$  of 4.0173 (Rosman and Taylor, 1998) for correction of  $^{54}\text{Fe}$ . Instrumental mass bias of all measured ratios was corrected via the exponential law and simultaneous determination of Ni isotope signals (Poitrasson and Freydier, 2005; Oeser et al., 2014) of a 4 ppm Ni reference solution (NIST SRM 986) which was doped to all samples and standards to yield similar Ni concentrations. The reproducibility of different aliquots of the same sample, including separate dissolutions and chemical purifications, was better than  $\pm 0.05\%$  (2s; n = 8) for  $\delta^{56}\text{Fe}$ . The in-house standard ETH Fe salt (from Eidgenössische

Technische Hochschule (ETH), Zürich, Switzerland; courtesy J. Wiederhold) was analyzed repeatedly (n=11) during sample measurements. The resulting  $\delta^{56}\text{Fe}$  values ( $-0.74\text{‰} \pm 0.03\text{‰}$ , 2 s.d.) are in good agreement with those given elsewhere (e.g. Schuth et al., 2015; Schuth and Mansfeldt, 2016).

All results are given relative to the Fe standard IRMM-014 in the  $\delta^{56}\text{Fe}$  notation:

$$\delta^{56}\text{Fe} (\text{‰}) = [((^{56}\text{Fe}/^{54}\text{Fe})_{\text{sample}} / (^{56}\text{Fe}/^{54}\text{Fe})_{\text{IRMM-014}}) - 1] * 1000 \quad (3)$$

All samples have been analyzed for their *Cu isotope compositions* in low resolution mode following the procedure reported by Bigalke et al. (2010b) and Kusonwiriawong et al. (2016). For instrumental mass bias correction the same certified NIST SRM 986 as used for Fe isotope measurements was added to each sample and standard before analysis, yielding 1 ppm Ni. The certified ratios  $^{62}\text{Ni}/^{60}\text{Ni}$  ( $0.138600 \pm 0.000045$ ) and  $^{61}\text{Ni}/^{60}\text{Ni}$  ( $0.043469 \pm 0.00015$ ) were used for mass bias correction applying the exponential law (Ehrlich et al., 2004).

The results for all sample analyses are reported in the delta notation relative to the Cu isotopic standard NIST 976:

$$\delta^{65}\text{Cu} (\text{‰}) = [((^{65}\text{Cu}/^{63}\text{Cu})_{\text{sample}} / (^{65}\text{Cu}/^{63}\text{Cu})_{\text{NIST 976}}) - 1] * 1000 \quad (4)$$

Each sample was analyzed three times and the precision is reported as two standard deviations (2 S.D.) of the replicate analyses for each sample (typically  $\leq 0.05\text{‰}$ ).

Additionally, to monitor analytical quality, reproducible analyses of two in-house standards (C125-1 and C125-2) relative to NIST 976 were conducted for each analysis session. The measured  $\delta^{65}\text{Cu}$  of these standards was reproducible ( $\delta^{65}\text{Cu} = 0.30 \pm 0.03\text{‰}$  and  $\delta^{65}\text{Cu} = 0.34 \pm 0.03\text{‰}$ , respectively; see also Kusonwiriawong et al., 2016; 2017).

### 3 Results and discussion

#### 3.1 Testing of the sequential extraction method

##### 3.1.1 Iron

The suitability of the sequential extraction procedure, consisting of six steps (Dold (2003) and Mehra & Jackson (1958), see Table II.2), was investigated using the test samples for Fe (see Table II.2) and the results for the recovery of Fe are shown in Figure II.2. A small amount of

the powdered samples was used for a bulk digestion and analysis and another aliquot was subjected to the sequential extraction.

Ferric iron is only sparingly water-soluble (only under very acidic conditions, e.g. Kappler and Straub, 2005), therefore none of the Fe minerals dissolved in the first two steps from the sequential extraction (neutral pH for water in step (1) and pH 4.5 in step (2)).

The results for two test samples with known initial weights of the minerals (test samples 1 & 2), one sample made of pure goethite (Bayferrox 920 Z), and one sample, which consisted only of magnetite are displayed in Figure II.2. For the bulk Fe content, deviations from 1 to 7 % between the calculated (measured mineral composition of an aliquot of the powdered sample using ICP-MS or ICP-OES, see chapter 2.4) and the measured Fe content were determined. Concerning the steps 3 and 4, for which break-down of Fe-oxides and magnetite was expected, respectively, divergent results were observed. For the test samples 1 and 2 approximately 15 % less Fe than expected was measured in the dithionite step (3). For the synthetic goethite, the measured Fe concentration was in agreement with a full recovery as expected for the dithionite extraction step (see also Mansfeldt et al., 2012). With regard to the magnetite fraction (step 4,  $\text{NH}_4$ -oxalate) both test samples did not deviate significantly between the expected and measured Fe contents but the magnetite sample showed an excess of Fe by 14 %. The sulfide extraction by  $\text{KClO}_3$  (step 5) of test sample 1 revealed a full Fe recovery of 99 %. Finally, the residual fraction represented by biotite (step 6) showed differences between the two test samples, i.e. in one sample 22 % less and in the other one 28 % more Fe than expected. One reason for the differences between the measured and the expected concentration could be that the minerals were mostly hand-picked under a microscope. As these samples are of natural origin, heterogeneities offer one explanation for the variable Fe recoveries. Moreover, during the treatment of the minerals with different reagents, the powdered material was very adhesive to the centrifuge tubes and pipette tips, which may furthermore have resulted in a Fe concentration loss during the procedure.

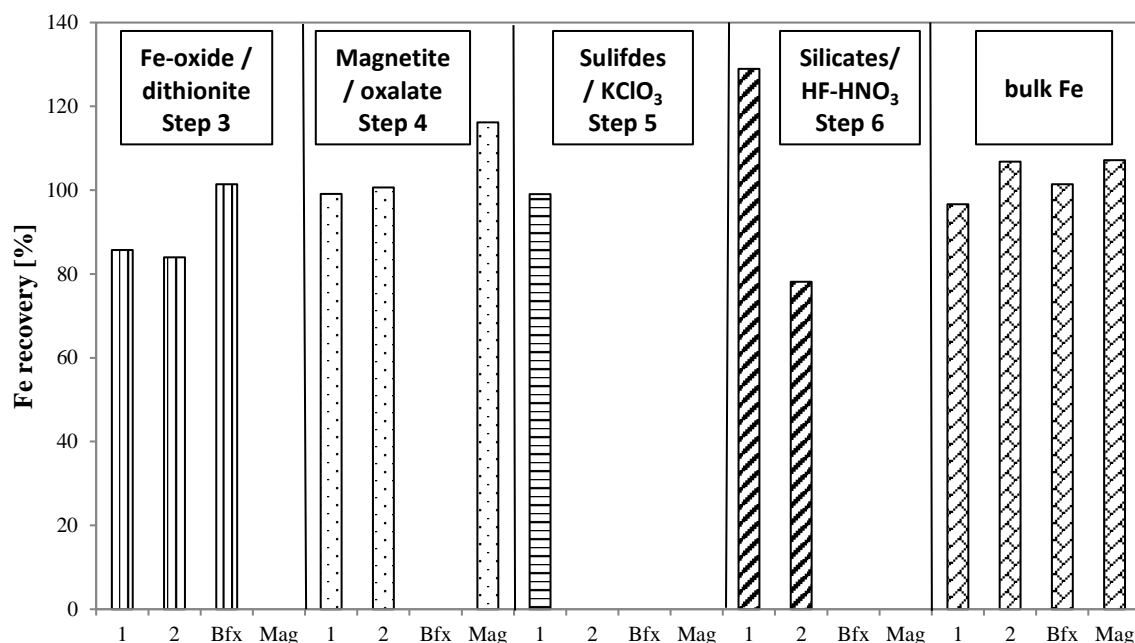


**Figure II.2.** Test for the selectivity of the Fe sequential extraction for the different steps. The Fe recovery (in %) is shown for test samples 1 & 2, Bfx (Bayferrox 920 Z), and Mag (magnetite).

It was furthermore evaluated if the sequential extraction resulted in Fe isotope fractionation. The results in Figure II.2 show significant Fe concentration variations between the different test minerals. Nevertheless, the Fe isotope compositions before and after the sequential extraction of the targeted fraction are in good agreement, indicating that no detectable isotope fractionation occurs during the extraction steps applied in our study.

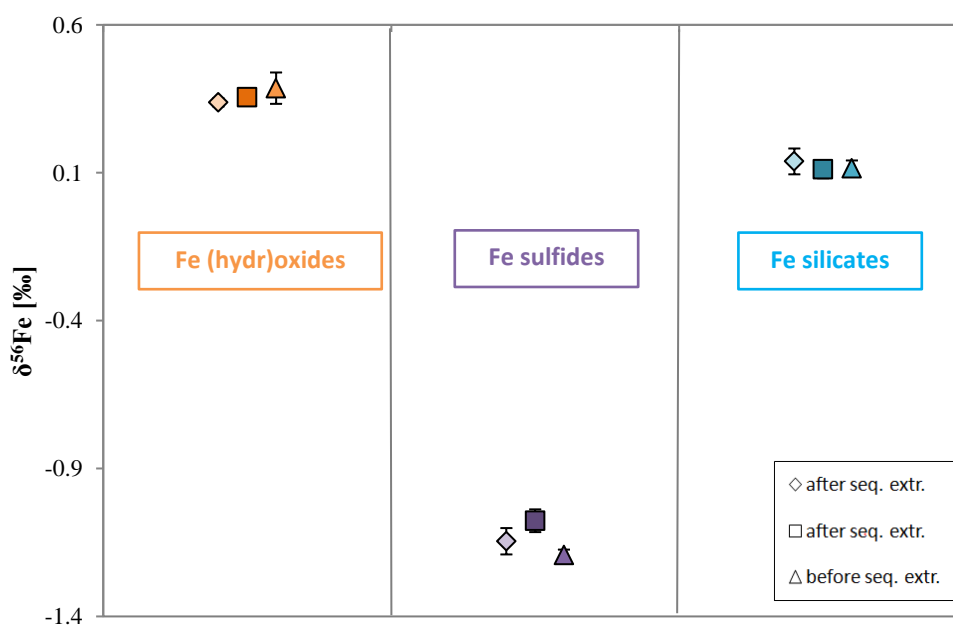


**Figure II.3.** Results of the sequential extraction test showing no significant fractionation between  $\delta^{56}\text{Fe}$  of the test minerals before (triangles) and after the sequential extraction (squares & diamonds). Error bars 2 s.d.

Accordingly, the test of the applied extraction scheme revealed that although some differences between the expected and the measured Fe concentration within each step were found, this did not affect the Fe isotope compositions of the respective extracts, which are the focus of this study. Potentially, the deviations in the Fe concentrations observed in some cases are related to the testing procedure rather than evidence for incomplete phase separation. In either case, they do not affect the interpretation of our case study, as discussed below.

### **3.1.2 Copper**

The test minerals used for the Cu sequential extraction are 1) the water-soluble mineral chalcantite, 2) malachite as a Cu-carbonate, 3) a synthetic Cu hydroxide, and 4) the Cu sulfides covellite and chalcopyrite. The results are presented in Figure II.3: the water-soluble mineral chalcantite was leached in the first extraction step by water (MQ), with a recovery of 89% of the total Cu amount expected for this mineral as determined from another aliquot of this powdered sample. Malachite dissolved in the second extraction step for exchangeable elements with a recovery rate of 126 %. In this extraction step, also some of the Cu hydroxide dissolved. The remaining Cu hydroxide (and no additional minerals) dissolved in step 4 with oxalate, but we had problems to quantitatively re-dissolve precipitates. Accordingly, the recovery rate for Cu hydroxide was only 75 %. We have not observed dissolution of the Cu hydroxide in the water-soluble fraction (step 1). As expected, covellite dissolved in the final extraction step, but only 60 % of the estimated Cu could be recovered. Chalcopyrite was also extracted in the residual/sulfide step, with a 116 % Cu recovery. The reason for the differences between recovered and expected Cu concentration are presumably the same as for Fe: potential chemical or mineralogical heterogeneity, impurities of the natural minerals and an adhesive behavior of solutions with regard to beakers and pipette tips.



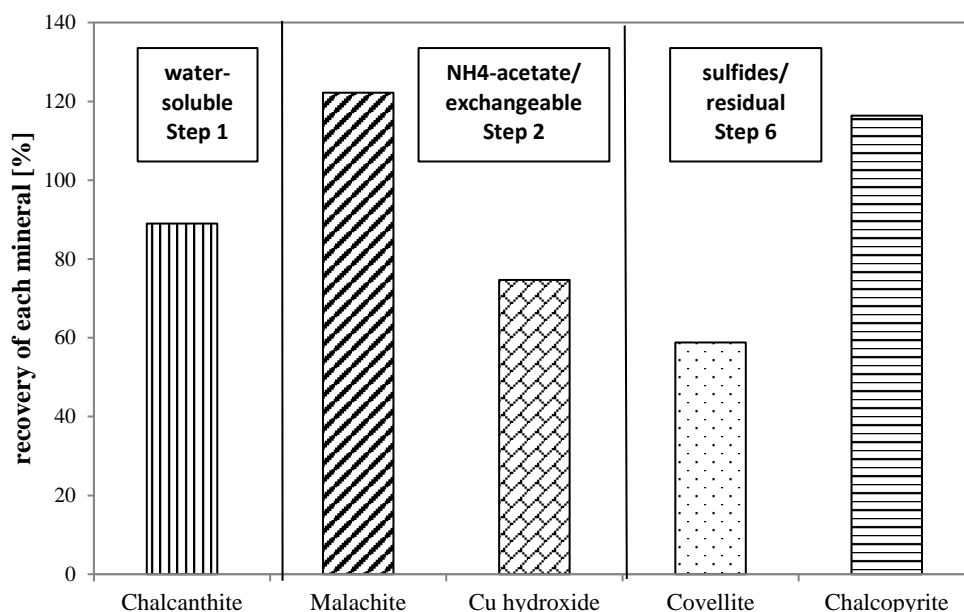


**Figure II.4.** Test for the selectivity of the Cu sequential extraction for the different steps.

Despite some inconsistency in the Cu recovery tests, the Cu isotope analysis (Figure II.5) of the different extraction steps reveal, within uncertainties, identical  $\delta^{65}\text{Cu}$  values for the test minerals analytical uncertainty before and after extraction, demonstrating that no Cu isotope fractionation occurs during the extraction procedure. For example, a presumable loss of ~40 % in the Cu recovery of the Cu sulfides (covellite in Figure II.4) in the step 6, still yielded  $\delta^{65}\text{Cu}$  values of the sulfide with and without the sequential extraction being in good agreement. Thus, covellite is likely quantitatively dissolved during step 6.

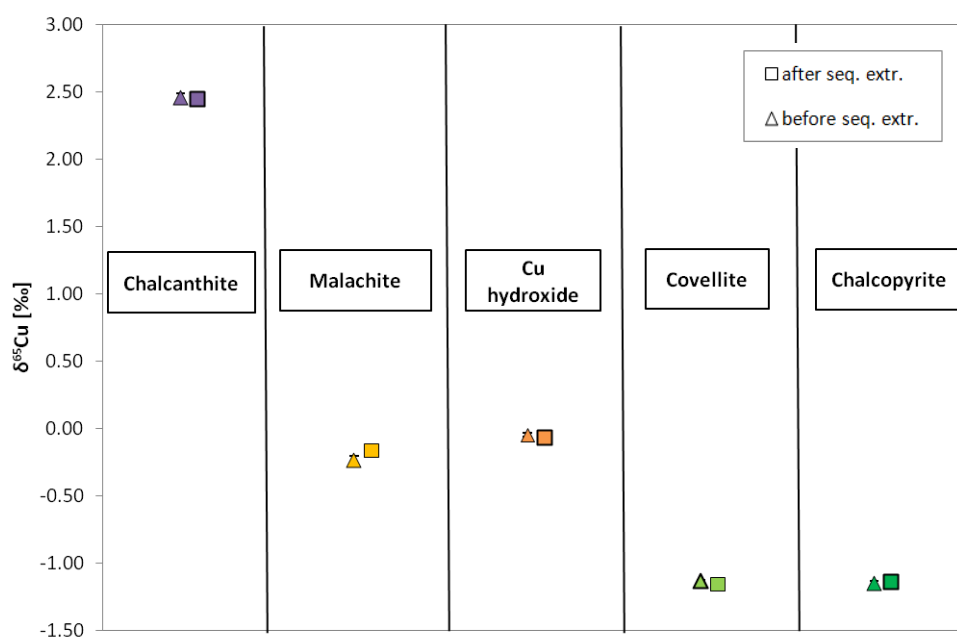


**Figure II.5.** Results of the sequential extraction test showing no significant fractionation between  $\delta^{65}\text{Cu}$  of the test minerals before (triangles) and after the sequential extraction (squares).

In summary, the achieved results show that the sequential extraction method for Fe and Cu leached the targeted mineral phases with some concentration differences between (calculated) original- and the recovered Fe and Cu concentrations. However, if this was related to a real Cu and Fe loss, due to incomplete dissolution of the target minerals in respective extraction steps, this process did not generate discernible isotope fractionation. Hence, the here presented extraction methods may be used as a potential tool to determine the isotope composition of secondary Fe and Cu minerals, discuss their formation conditions and the mobility of Fe and Cu in the environment, e.g. for Fe and Cu-rich mine tailings.

## **4 Application to mine tailings samples**

### **4.1 Iron**

With regard to the mine tailings samples from site Ch1, a very low fraction of the total Fe was stored in the water-soluble, the exchangeable, and the oxalate fractions (water-soluble: 0.0008 wt.%; exchangeable: 0.0027 wt.%; Fe(hydr)oxides within the oxalate step: 0.038 wt.%), thus their contribution to the overall Fe isotope budget is negligible. Not much Fe was determined in the oxalate step, because all Fe(hydr)oxides were probably dissolved in the dithionite-step. The bulk Fe content increased with depth from 1.1 wt.% at the surface to 4.2 wt.% at a depth of 59 cm (Figure II.6 A). The Fe concentrations in the fractions (besides the silicate fraction) in the first 36 cm of the profile were homogenous and most of the Fe was stored in (hydr)oxides (~0.7 wt.% Fe). In the uppermost samples Fe in sulfides was higher (~0.5 wt.%) than in the sulfide samples below (~ 0.1 wt.%). At 36 cm a sudden increase of sulfide-bound Fe to 1.4 wt.% was observed. This is related to an increase of the pyrite content at this depth, and was also measured by Korehi et al., (2013). At the same depth, the (hydr)oxide Fe content also increased to 1.2 wt.%. From 36 to 61 cm the Fe concentration in the sulfide fraction decreased again to values <0.5 wt.%. The concentration in the silicate Fe fraction was constantly low (mostly ~0.3 wt.% Fe) until a depth of 59 cm where it sharply increased to ~ 1.1 wt.% Fe. At this depth a buried alluvium occurs, underlying the mine tailings (Korehi et al., 2013).

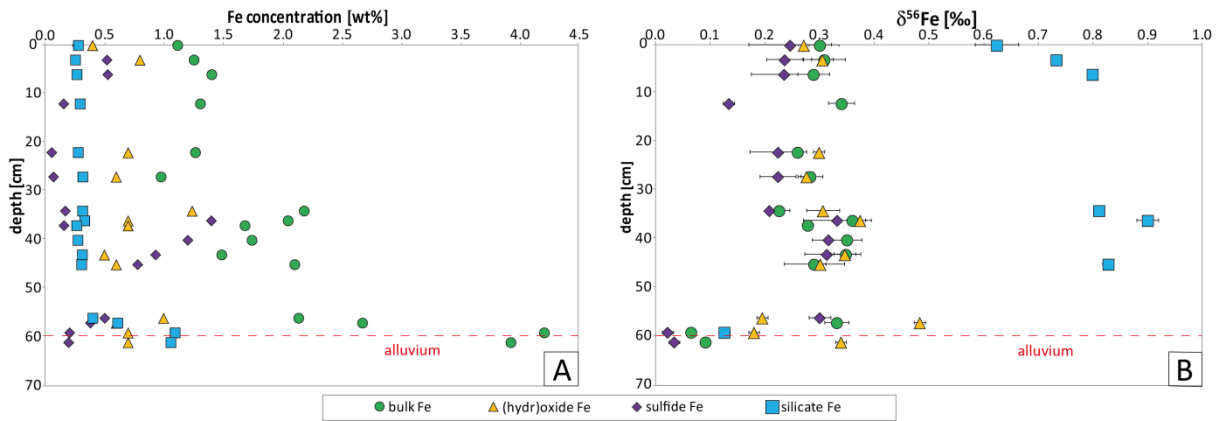


**Figure II.6.** Site Ch1; A: Fe concentration data (in wt.%) plotted against the depth for all significant fractions of the sequential extraction for Fe. B:  $\delta^{56}\text{Fe}$  data (in ‰) for (hydr)oxide, sulfide and bulk fraction show very little variations. Higher  $\delta^{56}\text{Fe}$  values were found for the silicate fraction.

All samples investigated in this study originated from the oxidation zone of the tailings, i.e., the redox front was below the sampling area and no redox transformation was observed (Dold, 2006). Moreover, due to the fact that the study area is located in an arid climate, prolonged Fe reducing conditions due to a high groundwater level are unlikely.

Similarly, to Fe concentrations, the Fe isotope depth profile of Ch1 given as bulk  $\delta^{56}\text{Fe}$  as well as that of hydroxides and sulfides was essentially homogeneous within the first 36 cm from the surface (see Figure II.6 B). Beneath, only a small change in the sulfide and bulk  $\delta^{56}\text{Fe}$  from  $\sim 0.2$  to  $\sim 0.3$  ‰ was observed. Otherwise, the bulk samples are overall isotopically similar to the Fe(hydr)oxides until a depth of  $\sim 60$  cm.

The Fe(hydr)oxides exhibit mostly  $\delta^{56}\text{Fe}$  values around  $+0.3$  ‰ above the alluvium at  $\sim 60$  cm, hence being isotopically slightly heavier than primary magmatic material (Beard and Johnson, 2004, 1999; Fantle and DePaolo, 2004; Skulan et al., 2002). In general, (re-) precipitation of Fe-oxides causes the preferential removal (from solution) and precipitation of the heavy Fe isotopes resulting in positive  $\delta^{56}\text{Fe}$  values (Bullen et al., 2001; Jang et al., 2008; Mansfeldt et al., 2012; Schuth and Mansfeldt, 2016). This enrichment in  $^{56}\text{Fe}$  was also observed by (Herbert and Schippers, 2008) in sulfidic mine tailings in Sweden. They measured an enrichment of  $^{56}\text{Fe}$  in secondary Fe(III)oxyhydroxides ( $\delta^{56}\text{Fe} = +0.03$  ‰ to  $+0.31$  ‰) compared to materials from below the oxidation front which is not oxidized yet ( $\delta^{56}\text{Fe} = -0.31$  ‰ to  $+0.06$  ‰). These effects were also observed by Bullen et al. (2001) in laboratory studies, where ferrihydrite, formed from abiotic Fe(II) oxidation was also enriched in the heavy Fe isotopes, and the light isotopes remained in the coexisting aqueous phase. Moreover, heavy Fe isotopes are preferentially adsorbed on already existing Fe oxides during a capillary rise of Fe-rich water like it is the case in Chañaral, because of the high evaporation rates (Beard et al., 2010; Icopini et al., 2004; Jang

et al., 2008; Mikutta et al., 2009; Schuth and Mansfeldt, 2016; Teutsch et al., 2005). Eventually, the positive  $\delta^{56}\text{Fe}$  values of the Fe(hydr)oxide fraction are presumably due to oxidative Fe (re)precipitation.

The sulfide fraction shows in general the lowest  $\delta^{56}\text{Fe}$  values (~0.1 to 0.3 ‰). The idea that the sulfides are enriched in the light Fe isotopes during oxidation was supported by Rodríguez et al. (2015). They performed bioleaching experiments and found a depletion of the heavy Fe isotope in the sulfide-rich starting material. Moreover, the heavier Fe isotopes are preferentially enriched in the oxidized form as seen in the Fe(hydr)oxides fraction and observed e.g. by Balci et al. (2006), Bullen et al. (2001), Jang et al. (2008) and Mansfeldt et al. (2012)). In particular, an increase of  $\delta^{56}\text{Fe}$  values with depth was observed from 35 to 40 cm in the bulk sample and mostly pronounced in the sulfide fraction. At this depth, Korehi et al. (2013) found the highest cell concentration and the highest proportion of biotic pyrite oxidation. Potentially, the isotopic shift was generated by microbial activity by preferential leaching/oxidation of the heavy isotopes, with the upper samples (sulfide fraction) more oxidized (and hence lighter) than the deeper samples. Another shift in the sulfide Fe fraction is observed between the tailings material and the alluvium at ~60 cm depth. Here the  $\delta^{56}\text{Fe}$  values decrease with depth from ~0.3 ‰ to ~0 ‰.

Most samples from the Fe silicate fraction exhibit a significant enrichment in heavy Fe isotopes ( $\delta^{56}\text{Fe}$  ~0.6-0.9 ‰) at a homogeneous concentration (~0.3 wt.%). Only the deepest samples beneath the alluvium at ~60 cm show a significant increase in the Fe content (1.1 wt.% Fe), combined with a prominent shift in  $\delta^{56}\text{Fe}$  (to ~0.1‰). Previous studies observed by employing scanning electron microscopy - mineral liberation analysis (SEM-MLA) (Korehi et al., 2013) a significant increase of the abundance of silicates at a depth of approximately 60 cm. This increase may explain the increase of the Fe concentration in the silicate fraction (Figure II.6 A). Also the Fe isotope signature of the silicate fraction is consistent with typical values for e.g. hornblende (e.g.  $\delta^{56}\text{Fe}$  -0.16-0.17 ‰; Brantley et al. (2004)) and magmatic rocks (Beard and Johnson, 2004). This finding is congruent with the deposition of relocated primary material (alluvium) at depth (Korehi et al., 2013).

However, the Fe isotope signature of the silicate fraction above the alluvium is significantly higher in  $\delta^{56}\text{Fe}$  than expected for such minerals. One possibility could be that the heavy Fe isotopic signature was artificially generated during the leaching process of the sequential extraction. Potentially, light Fe isotopes of other silicates (e.g. biotite) than hornblende may have been preferentially leached during earlier performed extraction steps. This would likely

result in a heavier Fe isotope signature of the residue. Our initial testing procedure of the method has, however, not shown such laboratory leaching effects, and they also have apparently not occurred for samples at deeper levels of the alluvium. Likewise, preferential leaching of light isotopes above the alluvium may have occurred in nature. This process was investigated by Liu et al. (2014) who examined Cu and Fe isotope fractionation during weathering and pedogenesis at two different sites. For Fe they found the same systematic as in our study: Light Fe isotopes were preferentially released into solution and the heavy Fe isotopes accumulated in the weathered residues. Other studies also support this observation that the heavy isotopes accumulate in the residual material during weathering (Fantle and DePaolo, 2004; Guelke et al., 2010; Mansfeldt et al., 2012; Wiederhold et al., 2007a, 2007b). Chapman et al. (2009) demonstrated experimentally, by performing leaching experiments with hydrochloric acid and oxalic acid (biotite granite and tholeiitic basalt) that in particular light Fe isotopes were released to the solution, resulting in residues featuring higher  $\delta^{56}\text{Fe}$  values. With regard to the profile in Figure II.6 B, the Fe silicate fraction exhibits  $\delta^{56}\text{Fe}$  values of 0.83 ‰ and 0.90 ‰ at 35 cm to 50 cm depth and an upwards decrease within the uppermost 10 cm to a value of 0.62 ‰. This trend can be explained by a longer weathering time of the deeper tailings material (because it was deposited earlier), hence resulting in a higher proportion of the light Fe isotopes being released from the deeper area by weathering and thus a stronger enrichment of heavy Fe isotopes in the residual silicates.

#### **4.1.1 Mass balance calculations**

In Table II.3 the measured bulk Fe content is compared to the calculated total Fe concentration by summing up the Fe concentrations of each single fraction. Most samples exhibit a loss of Fe during the procedure and only some show an increased calculated Fe content, which is probably due to analytical errors or to sample heterogeneities (see also the testing of the methods at the beginning). The median between the measured and the calculated Fe concentration is -15 %. It is not possible to unravel in which fraction most of the Fe was lost. As inferred from our experiments with minerals, some of the deviations may have been generated in the Fe silicate extraction step, which also showed an over- or underestimation of Fe in the samples. Despite some Fe loss during the procedure, the isotope measurements of our experiments showed that isotope fractionation is negligible during sequential extraction. To test for possible Fe isotope fractionation in the natural samples during the extraction procedure, an isotopic mass balance was calculated (Table II.4), including only those fractions with a sufficient Fe concentration for

isotope analyses. The measured  $\delta^{56}\text{Fe}$  values for each fraction were multiplied with their proportion in the bulk sample and summed up according to equation 5:

$$\delta^{56}\text{Fe}_{\text{bulk/calc}} = \sum x_i \delta_i \quad (5)$$

with  $x_i$  represents the mole fractions and  $\delta_i$  the isotope composition ( $\delta^{56}\text{Fe}$ ) of each extraction step. This calculated composite  $\delta^{56}\text{Fe}$  value was then compared to the measured  $\delta^{56}\text{Fe}$  of the bulk sample. An average deviation of 0.07 ‰ was found which is negligible compared to the differences observed among single fractions.

**Table II.3.** Comparison of the measured bulk Fe concentration (in wt.%) before the sequential extraction and the concentration of each fraction after the procedure and the calculated bulk Fe content with the deviation between the measured and calculated bulk Fe content.

depth [cm]	Fe bulk (measured)	Fe water-soluble	Fe exchangeable	Fe hydroxides	Fe oxides	Fe sulfides	Fe silicates	total (calculated)	deviation from bulk	in %
0	1.118	0.0008	0.0009	0.4	0.034	0.27	0.28	0.987	-0.131	-11.7
3	1.256	0.0008	0.0008	0.8	0.015	0.52	0.26	1.593	0.337	26.9
22	1.268	0.0002	0.0008	0.7	0.015	0.06	0.28	1.051	-0.217	-17.1
27	0.978	0.0002	0.0011	0.6	0.017	0.07	0.32	1.007	0.029	2.9
34	2.185	0.0003	0.0009	1.2	0.001	0.17	0.32	1.729	-0.455	-20.8
36	2.049	-	-	0.7	0.010	1.40	0.33	2.447	0.397	19.4
37	1.686	-	0.0006	0.7	0.014	0.16	0.27	1.140	-0.545	-32.3
40	1.745	-	0.0018	-	0.014	1.20	0.28	1.495	-0.249	-14.3
43	1.489	-	0.0061	0.5	0.022	0.93	0.31	1.773	0.284	19.1
45	2.105	-	-	0.6	0.023	0.78	0.31	1.711	-0.395	-18.7
56	2.138	-	0.0156	1.0	0.031	0.50	0.40	1.951	-0.188	-8.8
57	2.677	-	0.0035	0.6	0.097	0.38	0.61	1.694	-0.983	-36.7
59	4.210	0.0034	0.0012	0.7	0.001	0.21	1.10	2.008	-2.203	-52.3
61	3.929	0.0005	0.0005	0.7	0.233	0.20	1.06	2.193	-1.736	-44.2

**Table II.4:** Isotopic mass balance for the Fe isotope composition, the proportion and Fe isotope composition of each fraction are presented and used to calculate bulk  $\delta^{56}\text{Fe}$ . This is then compared to the measured bulk results which have not seen the sequential extraction. Concerning the proportion of the fractions, only the fractions with relevant Fe concentrations are shown.

	depth [cm]	0	3	34	36	59
Proportion of the fraction	Fe-Hydroxides	0.405	0.502	0.717	0.286	0.349
	Fe-Sulfides	0.274	0.327	0.098	0.573	0.103
	Fe-Silicates	0.284	0.161	0.183	0.137	0.546
Fe isotope composition [in ‰]	Hydroxides $\delta^{56}\text{Fe}$	$0.271 \pm 0.01$	$0.305 \pm 0.02$	$0.306 \pm 0.03$	$0.374 \pm 0.01$	$0.18 \pm 0.01$
	Sulfide $\delta^{56}\text{Fe}$	$0.246 \pm 0.08$	$0.236 \pm 0.03$	$0.208 \pm 0.00$	$0.332 \pm 0.06$	$0.022 \pm 0.01$
	Silicate $\delta^{56}\text{Fe}$	$0.624 \pm 0.04$	$0.733 \pm 0.01$	$0.811 \pm 0.00$	$0.9 \pm 0.02$	$0.126 \pm 0.01$
	bulk $\delta^{56}\text{Fe}$ calculated [‰]	0.355	0.348	0.388	0.420	0.134
	bulk $\delta^{56}\text{Fe}$ measured [‰]	$0.300 \pm 0.04$	$0.309 \pm 0.04$	$0.226 \pm 0.02$	$0.360 \pm 0.02$	$0.065 \pm 0.01$
	deviation	0.054	0.039	0.162	0.060	0.069

## 4.2 Copper

### 4.2.1 Concentration

The bulk Cu content at the first site (Ch1) displays an overall decrease from the top to the bottom of the profile (see Figure II.7 A). Particularly striking is the high Cu concentration in the water-soluble fraction at the top of the profile, especially at site Ch1. This fraction exhibits the same increase and nearly similar Cu concentrations to the bulk samples, hence implying that at the top of the profile most of the Cu was bound by water-soluble minerals like sulfates and/or chlorides (chalcantite and eriochalcite; Dold, 2006) (93 % and 88 % in the water-soluble fraction at 0 and 3 cm depth, respectively). Dold (2003) analyzed similar samples from the Chañaral bay with a sequential extraction method and came to the same conclusion that a large amount of copper is bound in the water-soluble fraction in samples from the evaporation zone. This matches with the appearance of efflorescent salts and the high evaporation rate in this region as described by Dold (2006). The mentioned hyper-arid climate leads to capillary ascent of the dissolved elements with subsequent precipitation of secondary minerals like halite and eriochalcite.

Two outstanding results at 45 and 56 cm depth of Ch1 profile with the highest Cu concentrations (2284 ppm and 3920 ppm Cu, respectively) were observed. This sharp increase was presumably caused by an equally pronounced increase of abundance of the exchangeable Cu fraction (e.g. carbonates) which contain 88 % of the bulk Cu at 56 cm depth.

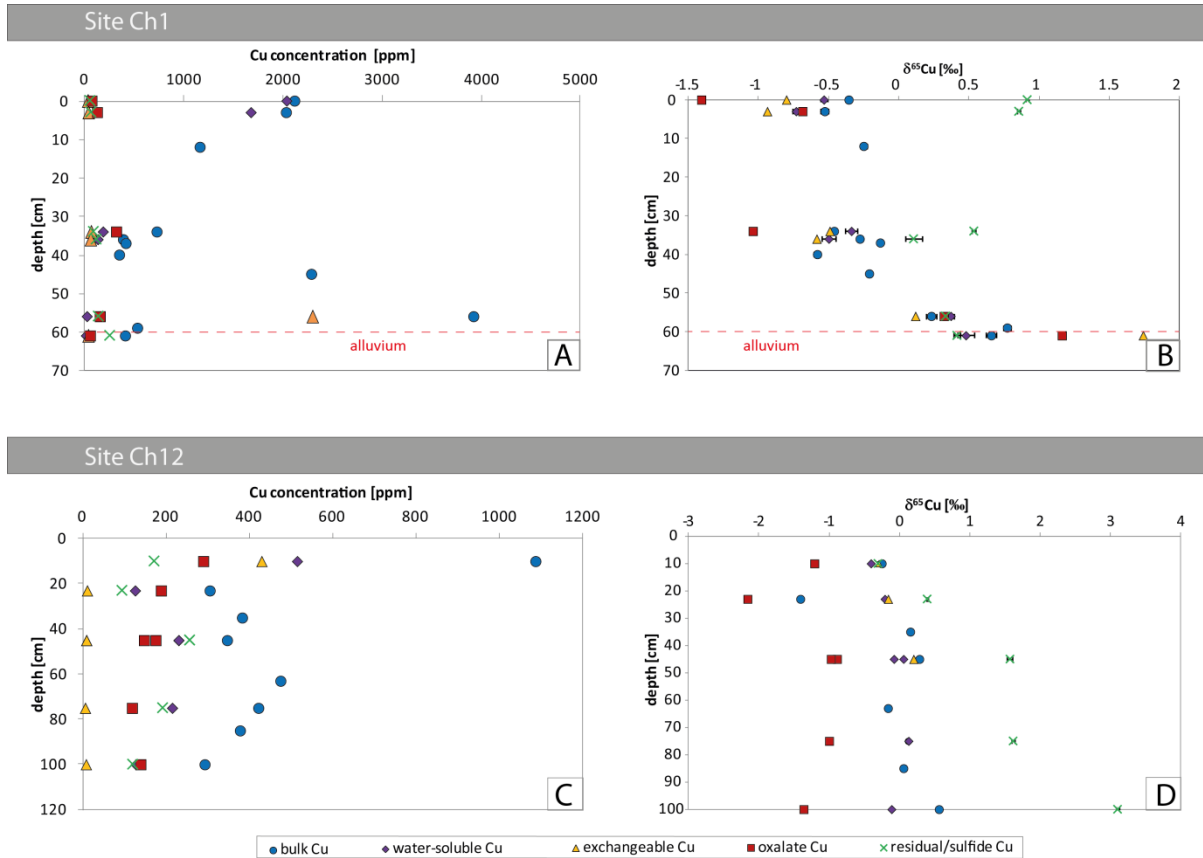


**Figure II.7.** Cu Concentration (in ppm) at sites Ch1 (A) and Ch12 (C) in bulk samples and in each fraction from the sequential extraction for different depths. Cu isotope composition at sites Ch1 (B) and Ch12 (D) in different depths of the profile. Error bars 2 s.d.

As a result of oxidation, only a small amount of Cu was associated with the sulfide fraction in our study, which is consistent with the findings of Bea et al. (2010). This implies that most of the primary chalcopyrite and chalcocite was oxidized and hence reformed subsequently as secondary minerals. Furthermore, only a small amount of exchangeable bound or adsorbed Cu, and oxalate-extractable Cu was found at site Ch1 in the first 60 cm of the profile (with the exception of the fraction at 56 cm depth, Figure II.7 A).

At the other site, Ch12, the exchangeable fraction contained only minor amounts of Cu apart from the top sample (at 10 cm with 31 % exchangeable Cu). In contrast to Ch1, the bulk Cu content at site Ch12 reflects a more proportional mixture of all mineral fractions.

The difference of the bulk Cu contents between two sites may be explained by enhanced near-surface Cu removal at site Ch12 compare to site Ch1. This conclusion is supported by the significantly lower Cu content of the water soluble fraction in near-surface samples of site Ch12.



### 4.2.2 Isotope composition

In profile Ch1, the Cu isotope composition of the bulk samples and water-soluble fraction define a trend from lower  $\delta^{65}\text{Cu}$  at the top (bulk: -0.36 ‰; water-soluble: -0.53 ‰) towards higher  $\delta^{65}\text{Cu}$  values with depth (bulk: +0.66 ‰; water-soluble: +0.48 ‰; Figure II.7 B). The sulfide fraction (residual) for this side exhibits a trend from higher  $\delta^{65}\text{Cu}$  values at the top (+0.9 ‰) towards lower  $\delta^{65}\text{Cu}$  values (0.33 ‰ and 0.42 ‰) at depth. Although, the different separated Cu fractions of Ch12 (Figure II.7 D) display a significant Cu isotope fractionation. However, the bulk samples as well as most of the fractions show no systematic trend with depth at this site. An exception, in contrast to Ch1, are the residual and the sulfide fractions, which display an opposite trend than that observed for site Ch1. At the top of the profile these fractions have  $\delta^{65}\text{Cu}$  values around 0 ‰, but at depth significantly higher values of up to +3.1 ‰ were observed. The more negative  $\delta^{65}\text{Cu}$  values combined with the lower Cu contents, observed for the on shore site Ch12 compare to site Ch1 site, indicate preferential removal of the heavier Cu isotopes into the near ocean. This implication is in accord with the heavy  $\delta^{65}\text{Cu}$  compositions observed for seawater (Vance et al., 2008).

Copper sulfides can be oxidatively leached by either abiotic or biotic processes, i.e. mediated by microbial activity (Asael (2006), Mathur et al. (2005), Mathur and Fantle (2015), Mathur et al. (2012)) resulting in distinct directions of Cu isotope fractionation. Abiotic leaching of porphyry copper sample material under acidic conditions (pH 2.3) results in the enrichment of  $^{65}\text{Cu}$  in the dissolved Cu pool relative to the initial starting material (Mathur et al. (2005) with  $\text{Cu}_{\text{aq}}$  from chalcocite and chalcopyrite:  $\delta^{65}\text{Cu} = 5.34$  ‰ and  $\delta^{65}\text{Cu} = 1.90$  ‰, initial starting material:  $\delta^{65}\text{Cu} = 2.60$  ‰ and  $\delta^{65}\text{Cu} = 0.58$  ‰). Presumably, the fractionation is attributed to precipitation or adsorption of the light Cu isotope onto the dissolving mineral surface (formation of an oxidized layer), consequently enriching a solution in  $^{65}\text{Cu}$  (Kimball et al., 2009; Mathur et al., 2005). In contrast, microbial activity (leaching of chalcopyrite at pH 2.0) triggered a smaller fractionation in the opposite direction, resulting in an isotopically lighter solution and a heavier residual material ( $\Delta_{\text{aq-min}}^{\circ} = -0.57$  ‰, where  $\text{min}^{\circ}$  refers to the starting mineral) (Kimball et al., 2009).

The above mentioned results could be used to explain the rather high  $\delta^{65}\text{Cu}$  values and low Cu concentrations in the sulfide and residual fraction from site Ch1 in Chañaral. Dissolution of Cu sulfides is suggested due to acidic leaching and potentially biotic leaching by microorganisms. A similar observation with residual sulfides being enriched in heavy Cu isotopes was made by Pérez Rodríguez et al. (2013). Korehi et al. (2013) concluded that at least pyrite (and probably

also other sulfides) were oxidized biotically at site Ch1, because the horizons with the highest pyrite oxidation rate exhibited also the highest cell concentration. Moreover, the highest pyrite oxidation rate is at approximately 36 cm (Korehi et al., 2013) and at this depth a step in the Cu isotope composition of the sulfide fraction can be observed from 0.11 ‰ at 36 cm to 0.54 ‰ at 34 cm. This change of signature was also found for Fe at the same depth. Moreover, the sulfide fraction from this study exhibits an increase in the  $\delta^{65}\text{Cu}$  values from depth to surface, indicating that the sulfides are even more weathered and leached at the surface compared to the depth.

Finally, the dissolution of the Cu sulfides resulted in a solution enriched in light Cu isotopes. Due to evaporation the light solution from the depth migrated towards the surface where subsequently, in a second process, new isotopically light secondary Cu minerals formed (Figure II.7 B). Additionally, the high abundance of  $\text{Cl}^-$  and acidic conditions could result in the formation of relatively weak Cu-Cl bondings and as a result, the transport of Cu in Cu-Cl bondings prefers  $^{63}\text{Cu}$  (Fulton et al., 2000; Moynier et al., 2017) also promoting isotopically light secondary Cu minerals.

An additional process, generating a light isotope composition of the water-soluble fraction may be preferential adsorption of the heavier Cu isotope to the Fe (hydro)oxides. The adsorption of Cu on Fe(III)-oxides and hydroxides is demonstrated by Dold (2006, 2003) who applied a seven-step sequential extraction to samples from the Chañaral bay. In the first meter of borehole Ch1, they found that 36 % of the total Cu content was in the exchangeable and in the Fe(III) oxides and hydroxides fraction.

The adsorption of Cu on Fe oxy(hydr)oxides is strongly pH-dependent. According to Balistrieri et al. (2008), Cu does not adsorb at  $\text{pH} < 4.5$ . Furthermore, Pokrovsky et al. (2008) observed that Cu isotopes only fractionate during the adsorption on Fe and Al oxy(hydr)oxides at a pH between 4.2 and 6.1 with an enrichment of the heavy isotope  $^{65}\text{Cu}$  on the surface of the minerals ( $\Delta^{65/63}\text{Cu}_{\text{solid/solution}}$  of 0.6 – 1.3 ‰). This adsorption can result in depth-dependent  $\delta^{65}\text{Cu}$  values in soil profiles as shown e.g. by Bigalke et al. (2010). The authors suggest an equilibrium reaction between the dissolved and the adsorbed Cu species during the transport with the surfaces adsorbing preferentially the heavy isotope  $^{65}\text{Cu}$ , consequently leading to a soil solution with a lighter Cu isotope signature. In the Chilean mine tailings, during the capillary ascent of water with its load of dissolved elements, the  $^{65}\text{Cu}$  is adsorbed on mineral surfaces. This consequently resulted in a continuously evolution of  $\delta^{65}\text{Cu}$  solution towards lighter values. At

the top of the tailings, efflorescent salts are found, which most likely precipitated from such upwards-migrating isotopically light (with respect of Cu) solutions.

In our field study, we observed a stronger Cu isotope fractionation for site Ch1 in contrast to nearly no Cu isotope fractionation in the water-soluble fraction for site Ch12. This may be explained by the almost neutral pH at ~60 cm at site Ch1 (see Figure II.8), which is favorable for the adsorption of Cu at depth on Fe oxy(hydr)oxides, while at site Ch12 pH conditions were acidic. As a consequence, no distinct Cu isotope fractionation for the Fe hydroxide/oxide and the water-soluble fraction with depth has evolved. Figure II.8 shows how the pH developed with depth and that the Cu isotope composition of the water-soluble fraction correlates with pH, i.e. at higher pH the water-soluble fraction displays heavier Cu isotope compositions.

As an explanation for the Cu isotope fractionation during adsorption, Balistrieri et al. (2008) suggest equilibrium isotope fractionation between an aqueous solution and an adsorbed ion. Copper isotope fractionation during the adsorption is probably attributed to a change in the coordination number and shorter bond lengths: The coordination number for  $\text{Cu}^{2+}_{\text{aq}}$  is 6 and decreases to 4 during Cu(II) adsorption onto various Fe oxides. Moreover, the aqueous  $\text{Cu}^{2+}$  (hexa-aqua  $\text{Cu}^{2+}$  species) has four shorter Cu–O bonds (1.97 Å) and two longer axial bonds (2.38 Å) (Fulton et al., 2000). Adsorption of Cu(II) on Fe oxides results in contrast to the aqueous  $\text{Cu}^{2+}$  species in shorter Cu–O bond distances of ~1.85 to 2.05 Å (Balistrieri et al., 2008; Peacock and Sherman, 2004).

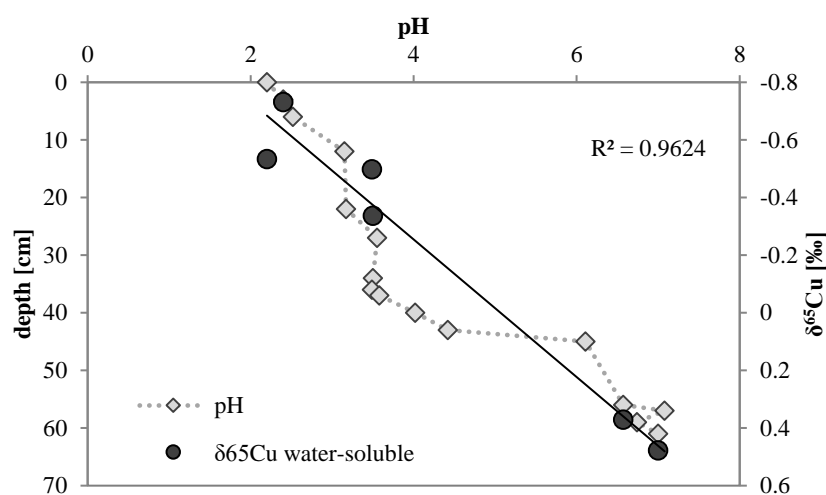


**Figure II.8.** Site Ch1. Correlation of the Cu isotope composition of the water-soluble fraction vs pH (circles) overlain to the pH relationship with depth (diamonds) from Fig. 1.

Mostly likely, the isotope signature of the water-soluble fraction is the result of several processes, (i) isotope fractionation during the dissolution of the sulfides, (ii) transport in Cu-Cl bondings, (iii) adsorption on Fe oxy(hydr)oxides and (iv) precipitation of secondary minerals from an isotopically light solution.

#### 4.2.3 Mass balance calculations

Finally, a mass balance calculation was carried out similar as for Fe (see above). For site Ch1 a similar mass loss as for Fe was determined (see Table II.5). The median between the measured and the calculated Cu concentration is -12 %. Similarly to Fe, this offset has little effect on the isotopic mass balance, in order to recalculate bulk  $\delta^{65}\text{Cu}$  values for site Ch1 from the individual extracts. An average deviation of 0.09 ‰ was determined (Table II.6) which is of little significance when compared to the isotopic differences observed between the single fractions.

**Table II.5.** Comparison of the measured bulk Cu concentration (in mg/kg) of core Ch1 before the sequential extraction and the concentration of each fraction after the procedure and the calculated bulk Cu content with the deviation between the measured and calculated bulk Cu content.

depth [cm]	bulk (measured)	water-soluble fraction	exchangeable fraction	oxalate fraction	residual/sulfide fraction	total (calculated)	deviation from bulk	in %
0	2114	2035	29	67	53	2184	70	3.3
3	2029	1674	34	122	62	1892	-137	-6.8
34	724	182	62	316	88	646	-77	-10.7
36	385	129	56	-	115	301	-84	-21.9
56	3920	19	2296	151	137	2603	-1317	-33.6
61	405	11	33	51	252	347	-58	-14.3

**Table II.6:** Isotopic mass balance for Cu isotope composition of core Ch1, the proportion and Cu isotope composition of each fraction and the calculated bulk  $\delta^{65}\text{Cu}$  and comparison with the bulk results without sequential extraction.

	depth [cm]	0	3	34	36	56	61
<b>Proportion of the fraction</b>	<b>Cu-water-soluble</b>	0.932	0.885	0.281	0.429	0.007	0.032
	<b>Cu-exchangeable</b>	0.013	0.018	0.095	0.187	0.882	0.095
	<b>Cu-oxalate</b>	0.031	0.065	0.488	0.000	0.058	0.148
	<b>Cu-residual/sulfides</b>	0.024	0.033	0.135	0.384	0.053	0.725
<b>Cu isotope composition [in ‰]</b>	<b><math>\delta^{65}\text{Cu}</math> water-soluble</b>	-0.533 $\pm 0.03$	-0.731 $\pm 0.02$	-0.337 $\pm 0.04$	-0.498 $\pm 0.04$	0.371 $\pm 0.02$	0.478 $\pm 0.05$
	<b><math>\delta^{65}\text{Cu}</math> exchangeable</b>	-0.800 $\pm 0.03$	-0.936 $\pm 0.03$	-0.491 $\pm 0.02$	-0.584 $\pm 0.01$	0.119 $\pm 0.01$	1.740 $\pm 0.02$
	<b><math>\delta^{65}\text{Cu}</math> oxalate</b>	-1.405 $\pm 0.03$	-0.685 $\pm 0.01$	-1.038 $\pm 0.01$	-	0.322 $\pm 0.01$	1.162 $\pm 0.02$
	<b><math>\delta^{65}\text{Cu}</math> residual/sulfides</b>	0.915 $\pm 0.01$	0.855 $\pm 0.01$	0.535 $\pm 0.01$	0.106 $\pm 0.05$	0.334 $\pm 0.02$	0.415 $\pm 0.02$
	<b>bulk <math>\delta^{65}\text{Cu}</math> calc. [‰]</b>	-0.529	-0.680	-0.576	-0.282	0.144	0.653
	<b>bulk <math>\delta^{65}\text{Cu}</math> meas. [‰]</b>	-0.356 $\pm 0.02$	-0.527 $\pm 0.03$	-0.46 $\pm 0.01$	-0.277 $\pm 0.01$	0.232 $\pm 0.03$	0.659 $\pm 0.03$
	<b>deviation</b>	-0.17	-0.15	-0.12	-0.01	-0.09	-0.01

## 5 Conclusions

Sequential extractions of Fe and Cu bearing primary and secondary minerals, in combination with metal isotope measurements, are a potential tool for understanding metal mobilization processes in mine tailings. As demonstrated in a case study from the Chañaral bay mine tailings in Chile, these tools may e.g. be used to unravel sulfide oxidation processes. Isotopic mass balance calculations demonstrate and support the applicability of the presented extraction scheme for mine tailings. Regarding the accuracy of the method, a small loss of Fe or Cu does not result in significant isotopic offsets of the isotopic mass balance. Therefore the presented extraction scheme may be applied to gain information about the distribution of Fe and Cu between different mineral phases and hence improve the understanding of metal migration in mine tailings.

With regard to Fe in the mine tailings in Chañaral (site Ch1), the Fe(hydr)oxide fraction exhibits positive  $\delta^{56}\text{Fe}$  values, presumably due to oxidative sulfide weathering and subsequent (re-)precipitation of Fe. As a result, the remaining sulfide fraction is enriched in light Fe isotopes. The Fe silicate fraction shows even more  $^{56}\text{Fe}$ -enriched values, because of preferential leaching of the light Fe isotopes resulting in a decrease from the bottom to the surface due to a longer weathering time of the deeper and earlier deposited tailings materials.

Regarding Cu, site Ch1 features a concentration increase in the water-soluble fraction from bottom to top with a simultaneous decrease in the  $\delta^{65}\text{Cu}$  values. This may be explained by the following scenario: 1) preferential oxidative and microbial dissolution of the light Cu isotopes during sulfide weathering, and 2) preferential adsorption of heavy Cu isotopes to the surface of Fe(hydr)oxide at depth, resulting in increasingly isotopically light Cu solution, which is migrating towards the surface to precipitate secondary Cu minerals.

## **6 Acknowledgments**

This work was funded by the State of Lower Saxony (Germany) as part of the Graduate School GeoFluxes. We thank R. Mathur and an anonymous reviewer for helpful comments and suggestions, and K. Johannesson for editorial handling.

**Chapter III:**

**Uranium isotope fractionation during anoxic mobilization  
of non-crystalline U(IV) by ligand complexation**

Accepted for publication in Environmental Science and Technology  
<https://doi.org/10.1021/acs.est.0c08623>

Y. Roebbert<sup>1</sup>; C. Rosendahl<sup>1</sup>; A. Brown<sup>2</sup>, A. Schippers<sup>3</sup>; R. Bernier-Latmani<sup>2</sup>; S. Weyer<sup>1</sup>

<sup>1</sup> Leibniz Universität Hannover, Institut für Mineralogie, Hannover, Germany

<sup>2</sup> École polytechnique fédérale de Lausanne, Lausanne, Switzerland

<sup>3</sup> Federal Institute for Geosciences and Natural Resources, Hannover, Germany

Ashley Brown conducted the U(IV)/U(VI) separation. All other laboratory work was conducted by Yvonne Röbbert. All data processing, interpretation and writing of the manuscript was done by Yvonne Röbbert, but all co-authors contributed with comments.

## Abstract

Uranium (U) isotopes are suggested as a tool to trace U reduction. However, non-crystalline U(IV), formed predominantly in near-surface environments, may be complexed and remobilized by ligands under anoxic conditions. This may cause additional U isotope fractionation and alter the signatures generated by U reduction. Here, we investigate the efficacy of non-crystalline U(IV) mobilization by ligand complexation and the associated U isotope fractionation. Non-crystalline U(IV) was produced via the reduction of U(VI) (400  $\mu\text{M}$ ) by *Shewanella oneidensis* MR-1 and was subsequently mobilized with EDTA (1 mM), citrate (1 mM), or bicarbonate (500 mM) in batch experiments. Complexation with all investigated ligands resulted in significant mobilisation of U(IV) and led to an enrichment of  $^{238}\text{U}$  in the mobilized fraction ( $\delta^{238}\text{U} = 0.4\text{-}0.7\text{ ‰}$  for EDTA;  $0.3\text{ ‰}$  for citrate;  $0.2\text{-}0.3\text{ ‰}$  for bicarbonate). For mobilization with bicarbonate, a Rayleigh approach was the most suitable isotope fractionation model, yielding a fractionation factor  $\alpha$  of 1.00026-1.00036. Mobilization with EDTA could be modelled with equilibrium isotope fractionation ( $\alpha$ : 1.00039-1.00049). The results show that U isotope fractionation associated with U(IV) mobilization under anoxic conditions is significant and needs to be considered when applying U isotopes in remediation monitoring or as a paleo-redox proxy.

Keywords:

Uranium

Fractionation

Laboratory batch experiments

Complexation

Ligands



## 1 Introduction

The industrial demand for uranium (U), because of its applications in nuclear energy and nuclear weapons production, resulted in widespread U mining and ore processing and left a legacy of U contamination of aqueous systems, soils and sediments all over the world (National Research Council, 2000; Riley and Zachara, 1992). Accordingly, environmental concerns and risks of the toxic element caused by anthropogenic spread are of public interest and methods are required to remediate contaminated sites.

In near-surface environments, U usually occurs as the uranyl ion ( $\text{UO}_2^{2+}$ ) which is soluble and mobile under oxic conditions in the presence of common ligands (e.g., carbonate). Reduction by microorganisms or redox-active minerals promotes transformation of U(VI) to U(IV) species such as uraninite ( $\text{UO}_2(\text{s})$ ) or non-crystalline U(IV) (Bernier-Latmani et al., 2010; Wang et al., 2013) and significantly decreases U mobility (Boyanov et al., 2011; Langmuir, 1978; Stylo et al., 2015b; Wall and Krumholz, 2006). This reduction process is often employed in bioremediation approaches in which biologically-mediated U reduction is stimulated in order to immobilize U in aquifers (Anderson et al., 2003; Bargar et al., 2013; Newsome et al., 2014; Williams et al., 2013). Several approaches were developed to monitor the remediation of U contaminated sites and U mines, including the application of U isotope signatures, as health concerns are considerable downstream of those sites (Abdelouas, 2006; Andersen et al., 2017; Basu et al., 2015; Bopp et al., 2010).

The largest U isotope variations in nature occur between oxidized and reduced reservoirs suggesting that U redox transformations control U isotope fractionation (Andersen et al., 2017; Weyer et al., 2008). Microbial U(VI) reduction results in the preferential removal of the heavier U isotope from the aqueous phase, due to a mass-independent isotopic fractionation attributed to the nuclear field shift (NFS) effect (Abe et al., 2008; Bigeleisen, 1996). Because of the significant U isotope fractionation, U isotope signatures were widely applied as an indicator of U reduction in nature, e.g., to monitor the success of remediation at *in situ* U mining site or to fingerprint U bioreduction (Basu et al., 2015; Bhattacharyya et al., 2017; Bopp et al., 2010; Dang et al., 2016; Stirling et al., 2015; Stylo et al., 2015a, 2015b). As U reduction results in the enrichment of heavy U isotopes in the solid phase, light U isotope signatures in groundwater may indicate U reduction. Isotope tools complement methods based on concentration measurements. The latter have limitations because common transport processes such as dilution or sorption could change the U concentration in the groundwater significantly without any long-term immobilization (Bopp et al., 2010).

Additionally, at remediation sites, it is not only important to monitor the extent of the reduction, but also the long-term stability of the immobilized U(IV). Similarly to reduction, U remobilization is difficult to trace using increasing U concentrations alone, as they may be affected by numerous processes in the groundwater (e.g., desorption). Thus, U isotopes are also suggested to trace reoxidation and mobilization of U(IV) after bioremediation (Jemison et al., 2018). A study consisted of oxidation experiments at a formerly bioremediated site and reported the accumulation of  $^{238}\text{U}$  in the groundwater upon oxidation.

In addition to the question of the reliability of U isotopes as a tool to monitor U reduction and thus, remediation, the question of the long-term stability of reduced U is also salient. It has been demonstrated that, in near-surface, organic-rich environments, the major product of U bioreduction is a non-crystalline U(IV) species associated with the organic matter (Bernier-Latmani et al., 2010). Recent investigations revealed that non-crystalline U may even be a major component in unmined U deposits (Bhattacharyya et al., 2017). Non-crystalline U(IV) is not well characterized and is proposed to be a family of compounds rather than a single one and includes coordination to carboxylic, phosphate, or silicate moieties (Alessi et al., 2014; Dreissig et al., 2011; Wang et al., 2013). It is significantly more labile than uraninite (Cerrato et al., 2013; Stylo et al., 2013a). It is defined by the absence of the 3.85 Å U–U pair correlation characteristic of  $\text{UO}_{2(s)}$  (observed using extended X-ray absorption fine structure spectra) and the absence of a crystalline lattice (Bernier-Latmani et al., 2010; Boyanov et al., 2011; Schofield et al., 2008). In biological systems, there is evidence that U(IV) is bound to phosphate groups (Alessi et al., 2014; Boyanov et al., 2011). Non-crystalline U(IV) was detected after U(VI) reduction by bacteria, by biogenic Fe(II)-bearing minerals or in reduced sediments (Alessi et al., 2014; Bargar et al., 2013; Bernier-Latmani et al., 2010; Boyanov et al., 2011; Campbell et al., 2011; Fletcher et al., 2010; Latta et al., 2014, 2012a; Sharp et al., 2011; Tsarev et al., 2016; Veeramani et al., 2011). In this study, non-crystalline U(IV) refers specifically to the U(IV) product generated through the biological reduction of U(VI) by the bacterium *Shewanella oneidensis* MR-1.

The biological production of uraninite vs. non-crystalline U(IV) appears to be correlated with the chemical speciation of the medium in which the reduction takes place (Bernier-Latmani et al., 2010; Boyanov et al., 2011). *Shewanella oneidensis* MR-1, forms a mixture of non-crystalline U(IV) and nano $\text{UO}_2$ , with more of the former under conditions in which extracellular polymeric substances (EPS) can form (Stylo et al., 2013a), and more of the latter in conditions in which EPS do not form.

Non-crystalline U(IV) is sensitive to reoxidation and thus more labile than crystalline UO<sub>2</sub> (Alessi et al., 2014, 2013, 2012; Cerrato et al., 2013). Uranium (IV) can be remobilized by oxidants such as dissolved oxygen, Fe(III) and nitrate or through complexation by ligands such as bicarbonate, siderophores, citrate and humic substances (Alessi et al., 2012; Finneran et al., 2002; Frazier et al., 2005; Ginder-Vogel et al., 2010, 2006; Gu et al., 2005; Loreggian et al., 2020; Luo and Gu, 2011, 2009; Sani et al., 2005; Wan et al., 2005). Ligands (e.g., citrate, EDTA) are used for example in the processing of radioactive waste because of their strong complexing capabilities (Hummel et al., 2005; Riley and Zachara, 1992; Suzuki et al., 2010). They are, therefore, present at some subsurface contamination sites and are capable of complexing U(IV) and U(VI), leading to increased U solubility and mobility (AbdEl-Sabour, 2007; Duquène et al., 2008; Huang et al., 1998; Luo and Gu, 2011; Riley and Zachara, 1992). Isotope fractionation associated with mobilization of metals by ligands has already been studied. For example, copper isotope fractionation occurs between free Cu(II) and Cu complexed with organic ligands, resulting in an enrichment of the heavy isotope (<sup>65</sup>Cu) in the complexed form (Ryan et al., 2014). Redox-independent dissolution of chromium with ligands causes variations in the  $\delta^{53}\text{Cr}$  from -0.27 to 1.23 ‰ (Saad et al., 2017).

The objective of this study is to investigate U isotope fractionation during the anoxic mobilization of non-crystalline U(IV) with organic ligands and bicarbonate. As the subsurface stability of U may be affected by a variety of complexation reactions (Boyanov et al., 2011), potential isotope effects must be considered for the correct interpretation of subsurface U isotope signatures. Here, we test whether U isotope fractionation may be an appropriate tool to unravel the mechanism of U mobilization. The results of these investigations, performed under controlled laboratory conditions, may lead to a better understanding of processes affecting the long-term stability of U(IV) at remediated sites.

## **2 Materials and methods**

### **2.1 Preparation of non-crystalline U(IV)**

For all experiments, the U isotope standards IRMM-184 or CRM-112A were used (Brennecka et al., 2011b; Noordmann et al., 2015; Weyer et al., 2008). The stock solution of U(VI) was prepared by evaporation and replacement of the nitric acid with hydrochloric acid. In an initial step, the standard was heated in 6 M HCl, evaporated and finally diluted with suprapure hydrochloric acid (0.1 M).

Non-crystalline U(IV) was produced as previously described in Stylo et al. (2013a). Everything used for the experiments was sterilized before use. *Shewanella oneidensis* MR-1 cultures were grown in sterile Luria–Bertani broth (LB medium) until cell growth reached the beginning of the exponential phase (optical density  $OD_{600}=2.0$ ). Cells were harvested by centrifugation at 8,000 rpm for 10 min and washed in simple buffered medium (referred to as BP medium), composed of 30 mM  $\text{NaHCO}_3$  and 20 mM 1,4-piperazinediethane sulfonic acid (PIPES buffer) adjusted to pH 6.8, giving a final pH of 7.3. The washed cells were suspended in a phosphate-containing medium (Widdel Low Phosphate, WLP) to a final optical density  $OD_{600}$  of 1.0.

U(VI) reduction was performed in 30 ml bottles inside a MBraun Labmaster Pro SP anoxic chamber with  $\text{N}_2$  atmosphere. Sterile centrifuge tubes (50 ml) and anoxic solutions were used. Either IRMM-184 or CRM-112A was used and the appropriate initial  $^{238}\text{U}/^{235}\text{U}$  value was carried into calculations. The U standard (approximately 400  $\mu\text{M}$ ) was reduced enzymatically by *Shewanella oneidensis* MR-1 in pH-buffered WLP medium (containing 20 mM PIPES, pH 6.8, final experimental pH 7.3). The full medium constituents can be found in the SI (Table S III.1). Speciation modelling using MINEQL+ (version 5.0, 2015, with updated equilibrium constants and reactions included in the latest critically revised thermodynamic databases) (Grenthe et al., 2004; Guillaumont et al., 2003; Schecher and McAvoy, 2007) revealed that in WLP, U(VI) was predominantly present as the soluble  $\text{CaUO}_2(\text{CO}_3)_3^{2-}$  and  $\text{Ca}_2\text{UO}_2(\text{CO}_3)_3$  species. Lactic acid (final concentration 20 mM) was added as an electron donor. After complete reduction (as indicated by removal of U from solution), the solid phase was separated by centrifugation for 30 min at 8,000 rpm and washed for several hours with 50 mM  $\text{NaHCO}_3$  to desorb any potentially remaining U(VI). Sodium bicarbonate powder and MQ water were autoclaved separately in gas-tight bottles, flushed with  $\text{N}_2$  for an hour and mixed inside an anaerobic box shortly before the washing step. After washing, the suspension was centrifuged again and the supernatant discarded. These washing steps also ensured that the initial medium (including the electron donor) was completely removed. The non-crystalline U(IV) product was associated with cell biomass, which is retained with the solid product. However, it was shown that the viability of *S. oneidensis* cells decreases rapidly after 48 hours in this medium. Thus, we expect that little to no active biomass will be present, especially given the removal of the electron donor (Molinas et al., 2021). After washing, the non-crystalline U(IV) product was resuspended in NaCl and MOPS. Previous work has shown that this product is stable in a simple buffered medium (e.g., PIPES-bicarbonate (Alessi et al., 2012)), indicating that these washing steps do not alter the U(IV) speciation.

## 2.2 Ligand mobilization experiment

Non-crystalline U(IV) (initial U(IV) concentration ~400  $\mu\text{M}$ ) was incubated with one of three ligands: EDTA (1 mM), citrate (1 mM), or bicarbonate (500 mM). For bicarbonate, a higher ligand concentration was necessary, as a concentration of 30-50 mM does not complex significant amounts of U (Alessi et al., 2012). For each ligand, two separate experimental runs (referred to as 1 or 2) were conducted, each with freshly prepared solutions and bacterial cultures. Furthermore, each experiment was conducted in duplicate (referred to as a or b) in which the same solutions and bacterial cultures were used to produce non-crystalline U(IV) in separate bottles. In other words, (a) and (b) include separate mixtures of the same stock solutions and bacterial cultures. In addition, a control experiment was conducted to probe whether U was mobilized over time in the absence of ligands.

In each reaction bottle, the following ingredients were added to a final volume of 30 ml: deionized water (18.2 M $\Omega$ .cm), MOPS pH buffer (5 mM; pH 7), NaCl (10 mM), ligand, and non-crystalline U(IV). The ingredients were continuously mixed at 130 rpm using a magnetic stirrer. Samples (0.5 ml) were collected at distinct time intervals and filtered through 0.22  $\mu\text{m}$  nylon membranes.

## 2.3 Anion exchange resin separation of U(IV) and U(VI)

To determine whether both the starting solid phase and the mobilized fractions were entirely reduced, an anion exchange resin separation of U(IV) and U(VI) was performed on selected samples (Molinas et al., 2021). Briefly, polypropylene columns were slurry-packed with 2.5 ml Dowex 1x8 (100-200 mesh) anionic chloride form resin which was pre-washed three times with 0.1 N HCl. The resin was subsequently cleaned with 10 bed volumes of 0.1 N HCl and 10 bed volumes of 4.5 N HCl. The packed columns were equilibrated with the glovebox atmosphere for several days.

A small volume (0.5 ml) of acidified sample (>4 N HCl) containing around 10  $\mu\text{M}$  U was loaded onto the columns. Uranium (IV) was collected with 10 bed volumes of 4.5 N HCl. Then, U(VI) was eluted with 10 bed volumes of 0.1 N HCl. All steps were performed inside an anoxic chamber ( $\text{O}_2 < 0.1$  ppm) and all solutions were flushed with nitrogen for more than 2 hours before usage. Ultrapure reagents were used at every step.

## 2.4 Uranium concentration and isotope analyses

For U concentration measurements, a Thermo-Scientific Element-XR inductively coupled plasma source mass spectrometer (ICP-MS) at Leibniz Universität Hannover (Germany) was employed. For the calibration of the instrument and the external standardization of the

concentration measurements, multi-element standard solutions were prepared gravimetrically. Internal standardization was performed with an iridium solution (Alfa-Aesar, Germany) which was added to all samples and standards, to achieve a final concentration of 5 ng/g Ir. The precision of the ElementXR analyses was typically below 5% (2 s.d.). Because of difficulties during the concentration measurements of the EDTA experiment (1a/b) (signal instabilities indicating that the complete amount of uranium was not available for analysis), the samples in the second experiment were treated with aqua regia and H<sub>2</sub>O<sub>2</sub>/HNO<sub>3</sub> prior to the concentration measurement (instead of after the measurement) in order to destroy any complexes that may have formed with EDTA.

For MC-ICP-MS analysis, the samples were weighted and evaporated to dryness. To destroy the ligand complexes, aqua regia (3 ml 11 M HCl and 1 ml 14 M HNO<sub>3</sub>) was added, boiled at 130°C for 48 h and subsequently evaporated. The samples were then treated with a mixture of 200 µl 14 M HNO<sub>3</sub> and 200 µl H<sub>2</sub>O<sub>2</sub> (30 %). For mass balance calculation, samples were filtered, as described, in order to separate the non-crystalline U(IV) (filter residue) from the mobilized U in solution. Uranium was dissolved from the filters with 90°C 11 M HCl and treated like all samples with aqua regia and H<sub>2</sub>O<sub>2</sub> + HNO<sub>3</sub>.

Uranium was purified by ion-exchange chromatography according to a method described in Weyer et al. (2008). The samples were dissolved in 1 mL 3 M HNO<sub>3</sub> and U was purified on Eichrom UTEVA resin. Prior to the chemical separation, a weighed aliquot of the <sup>236</sup>U/<sup>233</sup>U double spike solution (IRMM 3636-A, <sup>236</sup>U/<sup>233</sup>U = 0.98130) was added to the samples in order to correct for isotope fractionation during U purification and instrumental mass discrimination during MC-ICP-MS analysis. Spike/sample mixtures for all samples and standards were adjusted to similar ratios (<sup>236</sup>U/<sup>235</sup>U ≈ 3 ± 10%) to minimize peak tailing effects (from the ion beams of <sup>238</sup>U on <sup>236</sup>U and of <sup>236</sup>U on <sup>235</sup>U).

U isotope measurements were performed at Leibniz Universität Hannover with a Thermo-Finnigan Neptune multi-collector ICP-MS (MC-ICP-MS), similar to the protocol published by Noordmann et al. (2015). For sample introduction, a desolvation unit of a Cetac Aridus-II in combination with a perfluoroalkoxy alkane (PFA) nebulizer with a sampling rate of 100 µl/min (Elemental Scientific) was used to enhance sensitivity and to reduce solvent-based interferences such as oxides and hydrides. Furthermore, a standard Ni sampler cone and a Ni X skimmer cone were used in combination with a 0.8 mm copper ring (spacer). With this setup, a 70 ng/g solution achieved a ~80 V signal on <sup>238</sup>U in low mass resolution.

The abundance sensitivity was determined before each analysis term and typically  $\leq 0.1$  ppm of the  $^{238}\text{U}$  signal at mass 236 (determined on a spike-free solution), resulting in negligible tail correction.

All samples and standards were measured with  $\sim 4$  min total integration time and mass bias correction was performed with the IRMM 3636-A double spike (Richter et al., 2010) and the exponential law (Russell et al., 1978). During analyses a standard sample bracketing method was applied, i.e. two sample measurements were bracketed by two standard measurements. The results for all sample analyses are presented in the delta notation relative to the U standard that was used for the respective experiment (i.e. either IRMM-184 or CRM-112A):

$$\delta^{238}\text{U} = \left[ \frac{(^{238}\text{U}/^{235}\text{U})_{\text{sample}}}{(^{238}\text{U}/^{235}\text{U})_{\text{standard}}} - 1 \right] * 1000 \quad [\text{‰}] \quad (1)$$

Each sample was analyzed three times and the precision is given as two standard deviations (2 S.D.) of the replicate analysis for each sample (typically  $\leq 0.1\text{‰}$ ).

Additionally, reproducibility and accuracy was determined by replicate analyses of the U-standards IRMM-184 and REIMEP 18-A relative to CRM-112A during each analysis session and the results agreed with those previously reported in the literature (Brennecka et al., 2011b; Noordmann et al., 2015; Richter et al., 2010; Weyer et al., 2008), within uncertainties.

### 3 Results and discussion

The batch experiments data indicate that a significant amount of non-crystalline U(IV) was mobilized by the ligands, in agreement with previous findings (AbdEl-Sabour, 2007; Duquène et al., 2008; Huang et al., 1998; Lozano et al., 2011; Luo and Gu, 2011; Shahandeh and Hossner, 2002). All ligands are found at U contamination sites or in natural environments.

Control experiments (without ligand amendment) did not exhibit significant U mobilization over time ( $< 0.4 \mu\text{M}$  U, Table S III.5). The initial  $\delta^{238}\text{U}$  value of the non-crystalline U(IV) for all experiments was approximately 0 ‰. This result indicates that U was reduced quantitatively prior to the experiment as incomplete reduction would result in an isotopically heavy U solid phase (Dang et al., 2016; Stirling et al., 2015; Stylo et al., 2015b, 2015a).

Experimental data for U mobilization with 1 mM EDTA (pH 6.9-7.1) show an increase of the U concentration in the solution over time (Figure III.1 A) and the mobilization of approx. 45-70 % of the solid phase U after two days. Differences in the concentrations of mobilized U observed between the two EDTA experiments (1 and 2) may be partially due to difficulties during the measurement of the U concentration for EDTA-containing solutions for experiment

1, as discussed in the methods section. For the experiment with bicarbonate, a higher ligand concentration of 500 mM was required to mobilize U (at pH 8.4-8.5) and about 52-70 % U was mobilized after two days, with more rapid initial mobilization in experiment 1 than 2 (Figure III.1 C). U mobilization with 1 mM citrate (pH 7-7.2) resulted in increasing U concentration with time and different proportions of total U mobilization, 38-40 % for experiment 1 and 13-15 % for experiment 2 (Figure III.1 E).

**Table III.1.** Overview of the non-crystalline U(IV) batches produced and whether their speciation was determined.

<b>Experiment (1)</b>		<b>Experiment (2)</b>	
Individual non-crystalline U(IV) batches	Speciation of NCU(IV) determined?	Individual non-crystalline U(IV) batches	Speciation of NCU(IV) determined?
(1a)-EDTA*	-	(2a) EDTA	yes
(1b)-EDTA*	-	(2b) EDTA	-
(1a)-bicarbonate	-	(2a) bicarbonate	yes
(1b)-bicarbonate	-	(2b) bicarbonate	-
(1a)-citrate	yes	(2a) citrate	yes
(1b)-citrate	-	(2b) citrate	-

\* some minor issues occurred during concentration measurement of EDTA (1a/b) as explained in the method chapter, mostly at time 2h, 3.25h and 4.5h



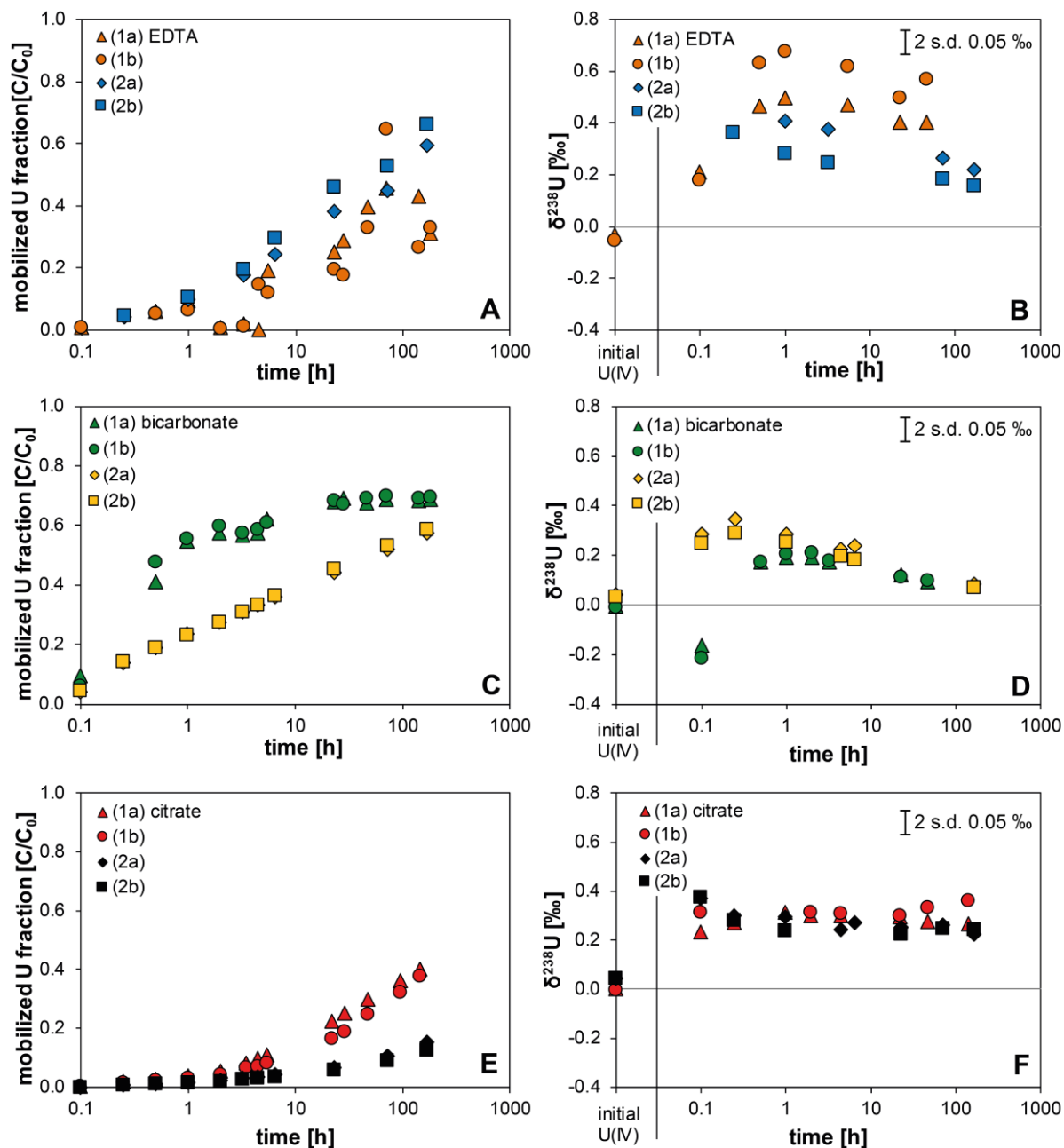


**Figure III.1.** The left-hand figures show the mobilized U concentration  $[C/C_0]$  over time [in h]. On the right-hand side, the measured  $\delta^{238}\text{U}$  values [in ‰] are plotted versus time [in h]; initial U(IV) indicates the U isotope composition of the unfiltered starting material. 1a, 1b, 2a, 2b, represent four replicate non-crystalline U(IV) materials for each condition (see Table III.1 for further detail).

Comparing all ligands, more U was mobilized by EDTA than by citrate (up to 70 % and 41 %, respectively) for the same amount of ligand. At significantly higher ligand to U ratio, bicarbonate mobilized about 70 % of the initial U, similar to EDTA. It is also noticeable that, for bicarbonate and citrate, experiments (1a/b) exhibited a greater fraction of U in solution and a more rapid rate of mobilization as compared to experiments (2a/b).

To determine whether these differences in mobilization rates and extents between batches arose from incomplete reduction of U(VI) in the starting material, anion exchange resin separation of U(IV) and U(VI) was performed on selected samples (Table III.1). This technique allows the separation and quantification of the two oxidation states of U. Thus, it was possible to probe for possible persistence by U(VI) in the starting material and, separately, for the mobilization of U(IV) after reaction with each ligand. Table S III.2 indicates that for experiment (1a)-citrate, the starting material contained approximately 16 % U(VI), suggesting that the biological reduction of U for batch experiments (1a) and (1b) was potentially incomplete for all ligands, and that some U(VI) remained associated with the solid phase, despite washing the product with 50 mM bicarbonate.

To determine whether the remaining U(VI) was preferentially extracted by citrate, selected samples of mobilized U (0.22  $\mu\text{m}$  filtered) from the same batch of non-crystalline U(IV) (i.e., (1a)-citrate) were also subjected to ion exchange chromatography (Table S III.2). After 1 h, 43 % of the mobilized U was U(VI) (22  $\mu\text{M}$  U;  $\sim$ 35 % of the initial U(VI) content), followed by 47 % U(VI) (16  $\mu\text{M}$ ;  $\sim$ 26% of the initial U(VI) content) after 5.5 h. Then, after 22 h, 35 % was U(VI) (28  $\mu\text{M}$ ;  $\sim$ 45 % of the initial U(VI) content). In summary, *ca* half of the initial U(VI) associated with the solid was mobilized within the first 22 h.

To determine whether the mobilization of U(VI) had a significant impact on the observed isotope signatures of the mobilized U, all experiments were repeated with fresh solid phase U (experiments (2a) and (2b)), for which we avoided the potential oxidation of non-crystalline U(IV) by performing the reduction, the complexation, and the oxidation state analyses within the same anoxic chamber. Once harvested, three of the six solid phases ((2a) and (2b) destined for complexation by each ligand (i.e., replicate (2a) for each ligand) were tested for their starting composition before addition of the ligand (Table III.1). The mean U(IV) content was found to be 97 % ( $\pm$  2 %) (Table S III.3). Each of the conditions was sampled again 6.5 hours after addition of the appropriate ligand to probe the composition of the mobilized U (0.22  $\mu\text{m}$  filtered). Here, the mean U(IV) content was 96% ( $\pm$  3 %), indicating that U(IV) was mobilized in the same proportions as that of the starting solid phase, with no preferential mobilization of U(VI) (Table S III.3).

It is likely that these differences in the contribution of U(VI) to the solid between batches 1 and 2 explain the observed variability in rate and extent of mobilization.

The main focus of this study was the isotope fractionation during mobilization and our results show that this is relatively independent from the total amount of mobilized U(IV) and from the

ratio of mobilized U(IV) to U(VI). Likewise, the fractionation behavior is also quite similar regardless of the presence of U(VI) in the starting material, except for one time point for the bicarbonate case.

The  $^{238}\text{U}/^{235}\text{U}$  ratios presented in this study clearly demonstrate that all ligands generated U isotope fractionation, with variable enrichment of  $^{238}\text{U}$  in the mobilized fraction of U. Mobilization with EDTA displayed initially high  $\delta^{238}\text{U}$  values (0.4-0.7 ‰) that decreased with proceeding U mobilization to values of  $\sim 0.2$  to  $0.3$  ‰ (Figure III.1 B). Uranium mobilization with 1 mM citrate resulted in  $\delta^{238}\text{U}$  values between  $\sim 0.2$  and  $0.4$  ‰ and did not change significantly during the course of the experiment (Figure III.1 F). Mobilization with bicarbonate also resulted in a positive  $\delta^{238}\text{U}$ , decreasing from initial values of  $+0.3$  ‰ to  $\sim +0.1$  ‰ during ongoing U mobilization for experiments (2a/b). For experiments (1a/b), light U isotopes were initially mobilized ( $\delta^{238}\text{U} \sim -0.2$  ‰). However, the direction of isotope fractionation changed, just a few minutes after the experiment started, towards heavy U isotope compositions, decreasing from  $\delta^{238}\text{U}$  of  $\sim +0.2$  ‰ to  $\sim +0.1$  ‰ during the course of the experiment (Figure III.1 D). Several mechanisms may explain the observation of initially light  $\delta^{238}\text{U}$ , although it is unclear which of these explains the data: (1) The preferential dissolution of light isotopes in the solution at the start of the experiment might be caused initially by kinetic isotope fractionation, which changes to equilibrium isotope fractionation during the course of the experiment. A similar effect was previously observed for Fe isotope fractionation during ligand-controlled dissolution of goethite (Wiederhold et al., 2006). (2) An alternative and more parsimonious explanation might be that the remaining unreduced U(VI) may have a light isotopic signature, because during bacterial U reduction the remaining U(VI) becomes depleted in  $^{238}\text{U}$  (Stirling et al., 2015; Stylo et al., 2015b). As it is expected that U(VI) is more readily complexed than U(IV), this would result in transient negative  $\delta^{238}\text{U}$  values at the beginning of the experiments. Mass balance calculations of experiments (1a) were used to validate the isotope results. The measured  $\delta^{238}\text{U}$  values for solution and corresponding non-crystalline U(IV) were multiplied by their fraction in the bulk sample and summed according to Equation (2) where  $X_j$  represents the mole fractions and  $\delta_j$  the isotope composition of solution or non-crystalline U(IV).

$$\delta^{238}\text{U}_{bulk} = \sum_{j=1}^n X_j \delta_j \quad (2)$$

The mobilized U fraction exhibits mostly high  $\delta^{238}\text{U}$  whereas the residues, the remaining non-crystalline U(IV) fractions, were depleted in  $^{238}\text{U}$  (Table S III.4 and Figure S III.2 in SI). Mass

balance fits well and was identical to that of the starting material in most cases within analytical uncertainties (2s.d.  $\leq 0.1\%$ ).

In order to further characterize the mechanism of U isotope fractionation, we attempted to fit the isotopic signatures of the mobilized U fraction with either an equilibrium fractionation model (assuming that the mobilized U and the remaining solid U remain in isotopic equilibrium throughout the experiment), or a Rayleigh Distillation model. A Rayleigh model implies the assumption of no back-reaction between the mobilized U and solid U. In this case, the variation of  $\delta^{238}\text{U}_{\text{mobilized}}$ , as a function of the fraction of remaining solid phase U(IV), can be described by the following equation:

$$\delta^{238}\text{U}_{\text{mobilized}} = (\delta^{238}\text{U}_{\text{mobilized}_t0} + 1000)F_{\text{remaining}}^{(\alpha-1)} - 1000 \quad (3)$$

$\delta^{238}\text{U}_{\text{mobilized}}$  represents the U isotopic ratio of the mobilized U fraction and  $\delta^{238}\text{U}_{\text{mobilized}_t0}$ , the initial U isotope composition of the mobilized fraction. The fraction of remaining solid phase U(IV) is given by  $F = C/C_0$ , where  $C$  represents mobilized U, and  $C_0$  the initial U concentrations (as non-crystalline U(IV));  $\alpha$  is defined as

$$\alpha = \frac{R_{\text{mobilized}}}{R_{\text{non-crystalline U(IV)}}} \quad (4)$$

$R_{\text{mobilized}}$  and  $R_{\text{non-crystalline U(IV)}}$  are the U isotopic ratios ( $^{238}\text{U}/^{235}\text{U}$ ) of the mobilized fraction and the non-crystalline U(IV).

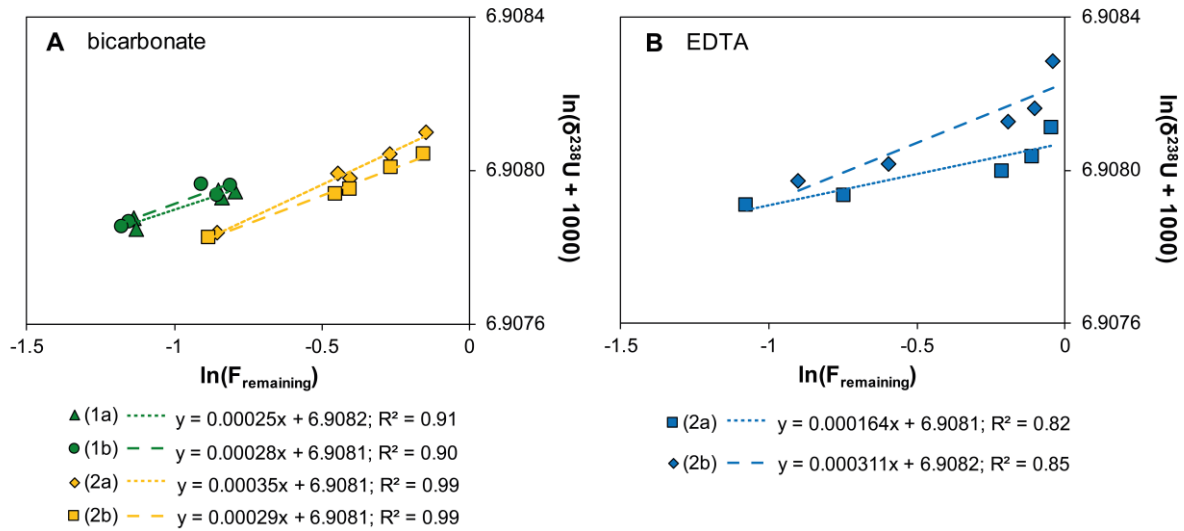


**Figure III.2.** Rayleigh fitting  $\ln F$  versus  $\ln(\delta^{238}\text{U} + 1000)$  for **A:** 500 mM bicarbonate mobilization, **B:** 1 mM EDTA mobilization (experiment (2a/b) only). For bicarbonate, the initial lighter U isotope values were excluded from the calculation (as they indicate a very different initial mobilization mechanism than for all other experiments, see Figure III.1).

A Rayleigh behavior during U mobilization is indicated by a straight line in a plot of  $\ln F$  vs.  $\ln(\delta^{238}\text{U} + 1000)$ , where the slope is equal to  $(\alpha-1)$ , permitting the calculation of an isotope fractionation factor (Figure III.2). Such a linear relationship was observed for most of the

experiments (Figure III.2). The modeled Rayleigh behavior of U during the mobilization with ligands is furthermore indicated in Figure III.3 A&B which shows the relationship of  $\delta^{238}\text{U}$  and  $C/C_0$ . For comparison, modeled equilibrium isotope fractionation, which corresponds to a linear relationship of  $\delta^{238}\text{U}$  and  $C/C_0$ , is indicated in Figure III.3 C&D.

For bicarbonate, a Rayleigh model implies  $\alpha$  values ranging from 1.000256 to 1.000359 with (theoretical) initial  $\delta^{238}\text{U}$  values for the mobilized fraction of 0.33 to 0.44 ‰ with  $R^2$  of 0.90 to 0.99 (Figure III.2 A and Table III.2). For EDTA, the correlation of the second experiment with a Rayleigh model is slightly worse than that observed for the bicarbonate experiments, indicating  $\alpha = 1.000164$  ( $R^2=0.85$ ) for experiment (2a) and  $\alpha = 1.000311$  ( $R^2=0.82$ ) for experiment (2b) (Figure III.2 B and Table III.2). The first EDTA experiment does not match a Rayleigh fit very well (Figure S III.3 and Figure S III.4). The misfit could arise from difficulties during the U concentration measurement of EDTA-containing solutions for batch experiment 1, as discussed in the methods section. By excluding one data point (outlier at 20% U mobilization in (1b), indicated as (1b\*) in Fig S3) from the calculations, the  $R^2$  values of a Rayleigh fit are 0.67 for (1a) and 0.75 for (1b\*).

A Rayleigh fractionation model does not fit results from the mobilization experiments with citrate, as the  $\delta^{238}\text{U}$  values remain essentially constant during U mobilization (Figures S III.5 and S III.6). The reason for this observation is unclear, however, it is possibly the result of a mixture of distinct mechanisms of U isotope fractionation during U mobilization (e.g., kinetic and equilibrium isotope fractionation). Moreover, less U was mobilized with citrate (for experiments (2a) and (2b) only ~16 % of the initial U(IV), as compared to ~70 % for bicarbonate or ~66 % EDTA), making any fit of the observed  $\delta^{238}\text{U}$  values during progressive U mobilization challenging.

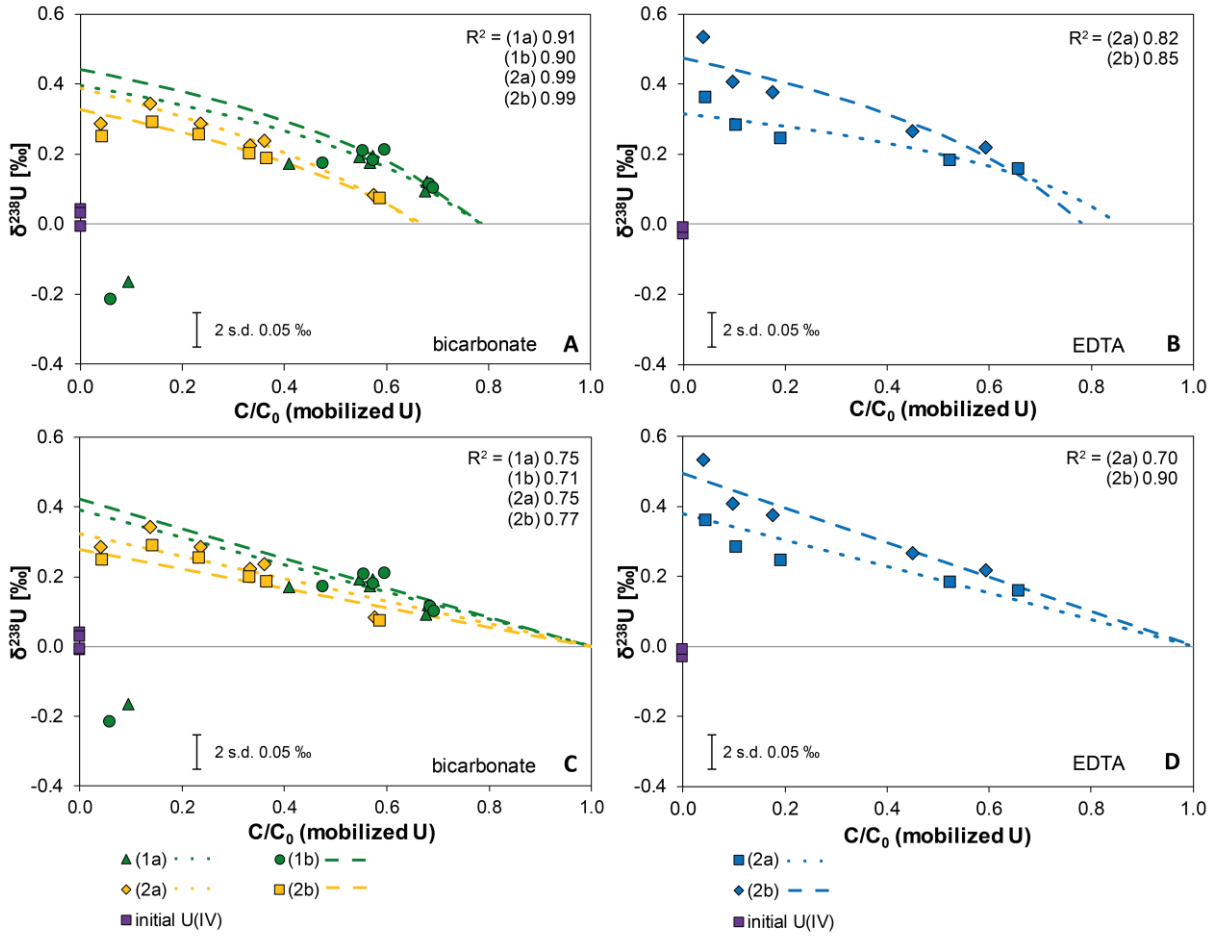


**Figure III.3.** Measured experimental  $\delta^{238}\text{U}$  values [in ‰] for the mobilized U versus the fraction of mobilized U ( $C/C_0$ ). **A:** Rayleigh model for 500 mM bicarbonate ((1a/b) and (2a/2b) performed simultaneously). **B:** Rayleigh model for 1 mM EDTA, experiments (2a/b). **C:** Equilibrium model for 500 mM bicarbonate. **D:** Equilibrium model for 1 mM EDTA, experiments (2a/b).

Equilibrium isotope fractionation, assuming reversible isotope exchange between solid and mobilized U(IV), was also modeled for bicarbonate and EDTA. An isotope fractionation factor  $\alpha$  was calculated using the approximation:  $\delta_A - \delta_B \approx 1000 \ln \alpha_{A-B}$ . For the calculation, the first isotopically light  $\delta^{238}\text{U}$  values of bicarbonate experiment (1a/b) were excluded (similarly to the Rayleigh modelling). In this case,  $\alpha$  for all four bicarbonate experiments range from 1.000277 to 1.000422, with  $\delta^{238}\text{U}_{t0}$  of 0.28 to 0.42 and  $R^2$  of 0.71 to 0.77 (Table III.2). For EDTA,  $\alpha$  ranges from 1.000380 to 1.000494, with initial  $\delta^{238}\text{U}_{t0}$  of 0.38 to 0.49 ‰ and  $R^2$  of 0.7 and 0.9 for experiments (2a/b). Accordingly, the equilibrium model also fits the observed U isotope fractionation, although for experiments with bicarbonate, this model exhibits slightly lower correlation coefficient ( $R^2$ ) than the Rayleigh model. For mobilization with EDTA, both models fit the data with a similar correlation coefficient. Potentially, the mechanism of U mobilization, may include partial re-equilibration of some of the remaining solid with the mobilized U(IV),

resulting in a U isotope fractionation behavior that cannot be precisely described by either of the above modeled processes.

**Table III.2.** Fractionation factor ( $\alpha$ ),  $\delta^{238}\text{U}_{\text{t0}}$  and  $R^2$  for modelled Rayleigh fractionation and equilibrium isotope fractionation for bicarbonate and EDTA experiments.

		Rayleigh			Equilibrium		
		$\alpha$	$\delta^{238}\text{U}_{\text{t0}}$	$R^2$	$\alpha$	$\delta^{238}\text{U}_{\text{t0}}$	$R^2$
bicarbonate	1a	1.000256	0.40	0.91	1.000390	0.39	0.74
	1b	1.000284	0.44	0.90	1.000422	0.42	0.71
	2a	1.000359	0.39	0.99	1.000324	0.32	0.75
	2b	1.000294	0.33	0.99	1.000277	0.28	0.77
EDTA	2a	1.000164	0.32	0.82	1.000380	0.38	0.70
	2b	1.000311	0.47	0.85	1.000494	0.49	0.90

Although several mechanisms of U isotope fractionation may be involved in generating the observed isotope fractionation, all of the investigated ligands generated a heavy isotope signature for the mobilized and complexed U. For instance, a change in the coordination of U during the mobilization and complexation may play an important role, resulting in a change in the bond lengths and bonding strength. For U redox reactions, the direction of U isotope fractionation (in isotopic equilibrium) is dominantly generated by the NFS effect which is opposite in direction to that expected from mass-dependent equilibrium isotope fractionation (MDF) (Bigeleisen, 1996). As a result, the lighter U isotope,  $^{235}\text{U}$  is preferentially enriched in the stronger bonding environment, i.e., U(VI) in redox reactions (Bigeleisen, 1996; Moynier et al., 2013; Schauble, 2006). Assuming that in non-redox reactions NFS similarly dominates isotope fractionation, rather than MDF, this would suggest that the mobilized U(IV) components in our experiments exhibit weaker bonding than that of the non-crystalline U(IV). However, the effect and portion of NFS on U isotope fractionation during non-redox reactions is yet poorly constrained.

#### 4 Implications for the use of the U isotope proxy

The suitability of U isotopes as a monitoring tool for remediation processes is still under evaluation. Initial promising results showed that  $^{238}\text{U}/^{235}\text{U}$  may be used as an indicator for U reduction (Basu et al., 2015; Bopp et al., 2010). Variability in the observed U isotope signatures of natural systems may result from additional U isotope fractionation during U sorption (Brennecka et al., 2011b; Jemison et al., 2016a) or during U remobilization, under oxic (Jemison et al., 2018) or anoxic conditions (this study).

The findings of this study may be particularly important for the interpretation of groundwater U isotope signatures. In a recent study by Jemison et al. (2018), the U isotope composition of groundwater was suggested as an indicator for oxic remobilization of U in remediated U deposits. This suggestion was based on the observation that the  $\delta^{238}\text{U}$  of groundwater displayed a negative correlation with  $1/\text{U}$  (i.e., a positive correlation with U concentration) in the groundwater. This was interpreted to be the result of oxic remobilization of U with a heavy  $\delta^{238}\text{U}$  signature. Our study indicates that, increased  $\delta^{238}\text{U}$  values and concentrations in natural or engineered environments may also be explained by anoxic mobilization of non-crystalline U with ligands. Thus, a correlation of  $\delta^{238}\text{U}$  and  $1/\text{U}$  does not necessarily indicate oxic U mobilization, rather, U mobilization may also occur under anoxic conditions and may generate heavy  $\delta^{238}\text{U}$ .

Several studies observed a large range of U isotope compositions for sedimentary U deposits, which formed as a result of U reduction, also including very low  $\delta^{238}\text{U}$  values (from -0.16 ‰ to -1.33 ‰, average of -0.31 ‰ (Basu et al., 2015); -0.30 ‰ to 1.52 ‰ (Uvarova et al., 2014); -1.30 ‰ to 0.55 ‰ with one sample as low as -4.13 ‰ (Murphy et al., 2014)). This heterogeneity may be explained by reservoir effects during progressive U reduction (resulting in a low  $\delta^{238}\text{U}$  in the remaining reservoir) or by different mechanisms of U reduction (Bhattacharyya et al., 2017). Alternatively, the low  $\delta^{238}\text{U}$  values may also indicate U remobilization by ligands. Similar to U(IV) residues in the filters that remained after mobilization in our experiments (Table S III.4), ligand-driven partial U remobilization may result in low  $\delta^{238}\text{U}$  values in the remaining U(IV) and may explain the variations observed, e.g., by Basu et al. (2015).

Beyond the effect on U isotope signatures of U deposits, anthropogenic U contamination, or remediated sites, the findings of this study may also challenge previous interpretation of the U isotope signatures of modern and ancient sediments. Most studies assume redox reactions as the dominant driver for U isotope fractionation as they are known to induce the largest isotope fractionation. In particular, the U isotopic range observed for shales is assumed to be essentially the product of U isotope fractionation during U reduction from a variably fractionated water column (Andersen et al., 2018; Brüske et al., 2020b; Bura-Nakić et al., 2018). Partial remobilization of U by ligands, however, may additionally fractionate sedimentary U isotopes and thus, enhance the range of observed U isotope signatures in black shales.

Understanding of sedimentary U isotope signatures is particularly important, as they are frequently used to reconstruct the redox evolution of Earth's oceans and atmosphere (Asael et



al., 2013; Kendall et al., 2013; Lau et al., 2016; Montoya-Pino et al., 2010; Satkoski et al., 2015). However, ligands likely existed in the environment since the mid-Archean (e.g., by the degradation of organic material and metabolites by microorganisms) (Boenigk et al., 2015; Dalai et al., 2016) and may have mobilized small amounts of U, imposing the associated U isotope fractionation. In particular, in the Archean, the findings of our study may challenge the interpretation of variable  $\delta^{238}\text{U}$  which are commonly interpreted as the onset of oxidative geochemical U cycling (Brüske et al., 2020a; Kendall et al., 2013; Wang et al., 2018). Heavy isotope signatures in Archean or early Proterozoic shales may be interpreted to be the product of partial U reduction during deposition of the sediments. In such a model, it is assumed that U was mobilized during U weathering with little isotope effects and that the heavy shale signature, thus, indirectly indicates the onset of oxic weathering with quantitative U mobilization. The findings of this study, however, imply that heavy U isotope signatures in Archean sediments may also be the result of partial ligand-driven anoxic U mobilization during weathering (assuming ligands available in the Archean generated similar isotope effects) and thus, may potentially predate the first rise of oxygen. However, it should be noted that only mobilization of non-crystalline U(IV) was investigated in this study and it is unclear which U phases predominated in the Archean continental crust and whether U mobilization from minerals, such as e.g., uraninite would show similar isotopic effects during weathering.

The present study has important implications for environmental studies on the mobility of U in (remediated) aquifer and, in particular, for the application of U isotopes as a monitoring tool for remediation. Ligand-driven mobilization of U and thus, transport and bioavailability, have to be considered when examining the long-term feasibility of remediation. Furthermore, this study shows that anoxic U mobilization with ligands isotopically fractionates U, towards high  $\delta^{238}\text{U}$ . These increased  $\delta^{238}\text{U}$  values in the aqueous phase may affect the interpretation of natural data in several ways: (a) they may overprint the isotopic effect of U reduction and thus challenge interpretation of the remediation success; (b) they may be used as an indicator for U (re-) mobilization processes with ligands; or (c) they may enhance the heavy aqueous U isotopic signature observed for oxidation processes. Hence, the results of this study may complicate the interpretation of natural and anthropogenic U isotope signatures but also offer new explanations, e.g., for the interpretation of Archean sediment data which may be difficult to explain by redox reactions alone.

## **Acknowledgements**

We thank Walter Schenkeveld, Stephan Krämer, Luca Loreggian, Zezhen Pan, Stephan Schuth, Maria Kirchenbaur, Ingo Horn, Minoru Abe, Sabrina Hedrich and Isabell Kruckemeyer for their support during generation and discussion of the data. Associate Editor Daniel Giammar, Xiangli Wang and two anonymous reviewers are thanked for their helpful comments. Funding for this work was provided by DFG/SNSF grants (WE 2850-16/1 and 200021E-164209: Fate of tetravalent uranium under reducing conditions) and an ERC consolidator grant of R. Bernier-Latmani (725675: UNEARTH: “Uranium isotope fractionation: a novel biosignature to identify microbial metabolism on early Earth”).

## **Chapter IV:**

# **Abiotic and biotic U oxidation processes and associated U isotope fractionation**

Y. Roebbert<sup>1</sup>; C. Rosendahl<sup>1</sup>, A. Schippers<sup>2</sup>; S. Weyer<sup>1</sup>

<sup>1</sup> Leibniz Universität Hannover, Institut für Mineralogie, Hannover, Germany

<sup>2</sup> Federal Institute for Geosciences and Natural Resources, Hannover, Germany

The pre-experiments were performed by Yvonne Röbbert. Oxidation with bacteria was part of the master thesis written by Chris Rosendahl under supervision of Yvonne Röbbert. All data processing, interpretation and writing of the manuscript was done by Yvonne Röbbert, but all co-authors contributed with comments.

## Abstract

Subsurface uranium (U) isotope signatures at remediation sites, in acid mine drainage and in bioleaching environments are influenced by various environmental factors which are not yet fully understood in detail. Uranium isotopes are suggested as a tool to monitor remediation success based on the assumption that isotopic signatures are essentially shaped during U reduction of the mobile U(VI) to more immobile U(IV), e.g. by stimulated microbial reduction. However, the subsurface stability of U(IV), typically present as non-crystalline U, may be affected by reactions with oxidants or bacteria. These processes may result in U mobilization associated with additional and variable isotope fractionation, which are important to be understood in order to correctly interpret U isotope signatures. Apart from remediation, mining causes acid mine drainage with mobilized U and methods of U mining like *in situ* leaching also result in a change of the oxidation state and may fractionate U isotopes. These processes may be mirrored in the U isotope signatures of ground water; however, interpretation of such signatures remains challenging as potential U isotope fractionation during oxidative U mobilizations is yet poorly understood.

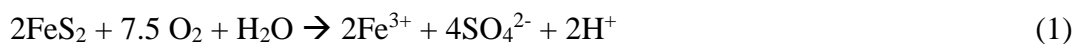
Here, we investigated pathways of oxidative uranium mobilization and the associated U isotope fractionation in laboratory batch experiments. First, an U(VI) isotope standard was reduced by *Shewanella oneidensis* MR-1 in a phosphate-containing medium (WLP) under anoxic conditions to produce non-crystalline U(IV), the dominant product of U remediation. This non-crystalline U was used as the starting material for all experiments. Subsequently, U(IV) was mobilized (1) by oxidation with Fe(III), and with molecular oxygen at low pH in presence of the bacterium *Acidithiobacillus ferrooxidans* (either grown on (2) elemental sulfur or (3) tetrathionate). Aliquots collected at various intervals were analyzed for their U concentration and  $^{238}\text{U}/^{235}\text{U}$  isotope ratios.

The reaction with Fe(III) caused oxidative U mobilization, but no U isotope fractionation was observed. For oxidation with biomass of *At. ferrooxidans*, also no significant U isotope fractionation was observed. Either, isotope fractionation of all relevant (i.e. slow) processes was very small or different isotope effects in opposite direction eliminated each other. The latter may be indicated by the observation of high aqueous  $\delta^{238}\text{U}$  values ( $\sim 0.8$  ‰) in corresponding abiotic experiments, which may be the result of adsorption processes after oxidative U mobilization. Assays with living and with dead cells (inhibited with 0.5 mM formate) show the same mobilization and isotope fractionation behavior. Accordingly, U oxidation is not related

to an electron transfer across the cell membrane, but rather may be generated by a ligand-related effect driven by proteins or cell wall structures of the biomass.

## 1 Introduction

In recent years, the demand for uranium increased and the study of microbial oxidation is of particular interest because it can be used to develop new bioleaching methods, it occurs in combination with environmental harmful acid mine drainage, and it also influences the long-term success of remediation strategies based on reductive immobilization. Many U ores have been mined and the deposits are becoming increasingly depleted. In addition, awareness of the environmental problems with traditional mining methods has grown. This has led to research into efficient, simple and less environmentally harmful methods in U mining which are also applicable for low grade ores (Johnson, 2014; Zammit et al., 2014). Recently, U is mostly mined with *in situ* leaching: U is extracted through wells via oxidative dissolution (Borch et al., 2012; Campbell et al., 2015; International Atomic Energy Agency and Agency, 2014; Zammit et al., 2014). Bioleaching is an alternative extraction method, a process in which bacteria or products of the bacterial metabolism are used for the oxidation and thus mobilization of metals. The crushed and agglomerated ore is placed in heaps where it is sprinkled with sulfuric acid and aerated to initiate the microbial oxidation of iron and sulfur compounds (Abhilash et al., 2011; Abhilash and Pandey, 2013; Brierley, 2008; Choi et al., 2005; Johnson, 2014; Kalinowski et al., 2004; Muñoz et al., 1995; Pal et al., 2010; Roberto, 2017; Yan et al., 2017; Zammit et al., 2014). Uranium ores are often accompanied with metal sulfides like pyrite, so that pyrite oxidation leads to a simultaneous release of uranium (Schippers et al., 1995). Therefore, iron-oxidizing acidophilic bacteria and archaea could be used in bioleaching processes for the recovery of base metals and uranium from mine waste and tailings (DiSpirito and Tuovinen, 1981; Schippers et al., 2014). Uranium is indirectly (chemically) leached oxidatively by bacteria: microorganisms metabolize reduced iron and/or sulfur compounds in the ore, producing Fe(III) and sulfuric acid (Zammit et al., 2014). Fe(III) oxidizes U abiotically ( $\text{UO}_2(\text{s}) + 2\text{Fe}^{3+} \rightarrow \text{UO}_2^{2+} + 2\text{Fe}^{2+}$ ) and subsequently the product Fe(II) is bacterially reoxidized to Fe(III) again via the following reactions (Hamidian et al., 2009; Tuovinen and Bhatti, 1999; Zammit et al., 2014):



For the bioleaching process, *Acidithiobacillus ferrooxidans* is one of the most widely employed microorganisms (Choi et al., 2005). It lives in extremely acidic conditions (with an optimal pH of 2.0) by fixing CO<sub>2</sub> and nitrogen and tolerates metal ions up to a certain level which helps to survive in extreme areas like metal mines (Zhang et al., 2018). It is a Gram-negative, chemoautotrophic, acidophilic aerobe microorganism (Yan et al., 2010). It obtains energy by oxidizing Fe<sup>2+</sup>, S<sup>0</sup> or reduced sulfur compounds and uses O<sub>2</sub> or Fe<sup>3+</sup> as electron acceptor (Kelly and Wood, 2000; Osorio et al., 2013; Temple and Colmer, 1951; Valdés et al., 2008; Zhang et al., 2018). Previous investigations on the oxidation of U directly with *At. ferrooxidans* (Alan A. DiSpirito and Tuovinen, 1982a, 1982b; DiSpirito and Tuovinen, 1981) showed that the oxidation rate depends on the cell concentration, the previous growth history of the organisms, the amounts of U(IV) and of inhibitors, pH and the presence of iron sulfates. DiSpirito and Tuovinen (1981) also tested autoclaved cells, cells grown on glucose or bacteria inhibited by pentachlorophenol and observed minor to no oxygen uptake in the presence of uranous sulfate and therefore concluded that the activity of the bacteria is essential for U oxidation. It was also shown that the oxidation was coupled to CO<sub>2</sub> fixation as well as O<sub>2</sub> consumption and the reduction of cytochrome and rusticyanin (a protein which is part of an electron transfer chain for Fe(II) oxidation) (Alan A. DiSpirito and Tuovinen, 1982a, 1982b; DiSpirito and Tuovinen, 1981; Tuovinen and Bhatti, 1999).

However, the same mechanism that is used to profitably mine uranium also causes increased acid rock drainage (ARD) or acid mine drainage (AMD) released in natural and anthropogenic environments. Because sulfide minerals react with oxygen and water during mining, this triggers an increase of acidity which may be further accelerated by microorganisms. AMD causes environmental damage and releases toxic elements associated with sulfide minerals (e.g., Akcil and Koldas, 2006; Simate and Ndlovu, 2014). This has already been studied extensively, however, previous investigations did not focus on U mobilization (Balci et al., 2012) and potentially associated U isotope fractionation, which may be used as a tool to understand the mechanism of U mobilization.

Apart from sites where uranium oxidation associated with bioleaching or AMD occurs, U isotopes are one possible approach to monitor the success of remediation efforts. Understanding

processes of U(IV) oxidation is important because of the enhanced mobility of oxidized U(VI) which results in increasing environmental damage. Uranium isotopes may help to trace these processes. The largest U isotope variations in nature occur between oxidized and reduced reservoirs suggesting that U redox transformations control U isotope fractionation (Andersen et al., 2017; Weyer et al., 2008).

At remediation sites, U reduction results in the enrichment of heavy U isotopes in the solid phase, light U isotope signatures in groundwater may indicate U reduction (Basu et al., 2015; Bhattacharyya et al., 2017; Bopp et al., 2010; Dang et al., 2016; Stirling et al., 2015; Stylo et al., 2015a, 2015b). However, in order to fully utilize these isotope signatures as indicator for U reduction, all other processes that may affect the  $\delta^{238}\text{U}$  values must be investigated. Tracing of U remobilization by increasing U concentration alone is challenging, because the U concentration may be affected by numerous processes in the groundwater (e.g., desorption). For this purpose, for example, the influence of organic ligands and the associated mobilization was investigated in the previous chapter of this thesis. Field experiments studying U isotope fractionation during reoxidation were performed at a formerly bioremediated site and an enrichment of the heavy  $^{238}\text{U}$  in the groundwater upon oxidation was observed (Jemison et al., 2018).

Uranium isotope fractionation during oxidation by abiotic oxidants was already shown in previous studies. Uranium oxidation with dissolved oxygen results in initial mobilization of U(VI) which is depleted in  $^{238}\text{U}$ . However, as the reaction continues,  $\delta^{238}\text{U}$  increase towards values of  $\sim 0\text{‰}$  (Wang et al., 2015a). Equilibrium isotope fractionation occurs between dissolved U(IV) and U(VI) with U(IV) enriched in  $^{238}\text{U}$  ( $1.64 \pm 0.16\text{‰}$ , Wang et al., 2015b). The U isotope fractionation associated with biotic U oxidation was not yet investigated. However, investigations on other isotope systems indicate that biotic oxidation may result in isotope fractionation of metals. For example, biological Fe oxidation has been shown to result in isotopically heavier  $\delta^{56}\text{Fe}$  (Balci et al., 2006a; Croal et al., 2004; Kappler et al., 2010) and for Cu, bacteria seem to preferentially oxidize light Cu isotopes or no isotope fractionation was observed as the bacteria are apparently a sink for heavy Cu isotopes (heavy copper present in the bacteria cells with  $\delta^{65}\text{Cu} = 5.59 \pm 0.16\text{‰}$ ) (Kimball et al., 2009; Mathur et al., 2005).

As starting material for the experiments, non-crystalline U(IV) was used for the oxidation experiments (described in detail in the previous chapter) which is sensitive to reoxidation and thus more labile compared to crystalline  $\text{UO}_2$  (Alessi et al., 2014, 2013, 2012; Cerrato et al., 2013). Recent investigations revealed that non-crystalline U is not only the dominant U species

generated during remediation of U mining sites, but may also be a major component in unmined U deposits (Bhattacharyya et al., 2017). Non-crystalline U(IV) was produced by reduction of the U isotope standard IRMM-184 with *Shewanella oneidensis* MR-1 in a phosphate-containing medium (Bernier-Latmani et al., 2010; Stylo et al., 2013b). Oxidation was performed either abiotically with (1) Fe(III) or biotically with *Acidithiobacillus ferrooxidans* (grown on (2) elemental sulfur or (3) tetrathionate).

The U(IV) oxidation with Fe(III) (1) was previously shown (Sani et al., 2005) but no U isotope data have been conducted so far. *At. ferrooxidans* (experiment (2/3)) and other acidophiles can be found in low-pH natural environments, e.g. hydrothermal sites, acid sulfate soils and acidic fens, naturally exposed ore deposits (gossans) as well as in man-made acidic environments such as mine sites including mine waste dumps and tailings, acid mine drainage and biomining operations (Hedrich and Schippers, 2020; Zhang et al., 2018).

The objective of this chapter is to experimentally investigate U isotope fractionation during abiotic and biotic U oxidation of non-crystalline U(IV) with Fe(III) and *At. ferrooxidans* under controlled laboratory conditions which should help to improve the interpretation of subsurface U isotope signatures at remediation sites, in acid mine drainage and in bioleaching environments.

## 2 Methods

As starting material for all experiments, non-crystalline U(IV) was produced as described in chapter 3 of this thesis according to Bernier-Latmani (2010) and Stylo et al. (2013). U(VI) of the U isotope standard IRMM-184 was reduced by *Shewanella oneidensis* MR-1 in a phosphate-containing growth medium (WLP medium). The experiments were performed at least in duplicates. Aliquots (0.5 ml) were withdrawn at distinct time intervals and filtered through 0.22 µm nylon membranes for collecting the oxidized and dissolved U(VI) fraction (solid U(IV) remained in the filter).



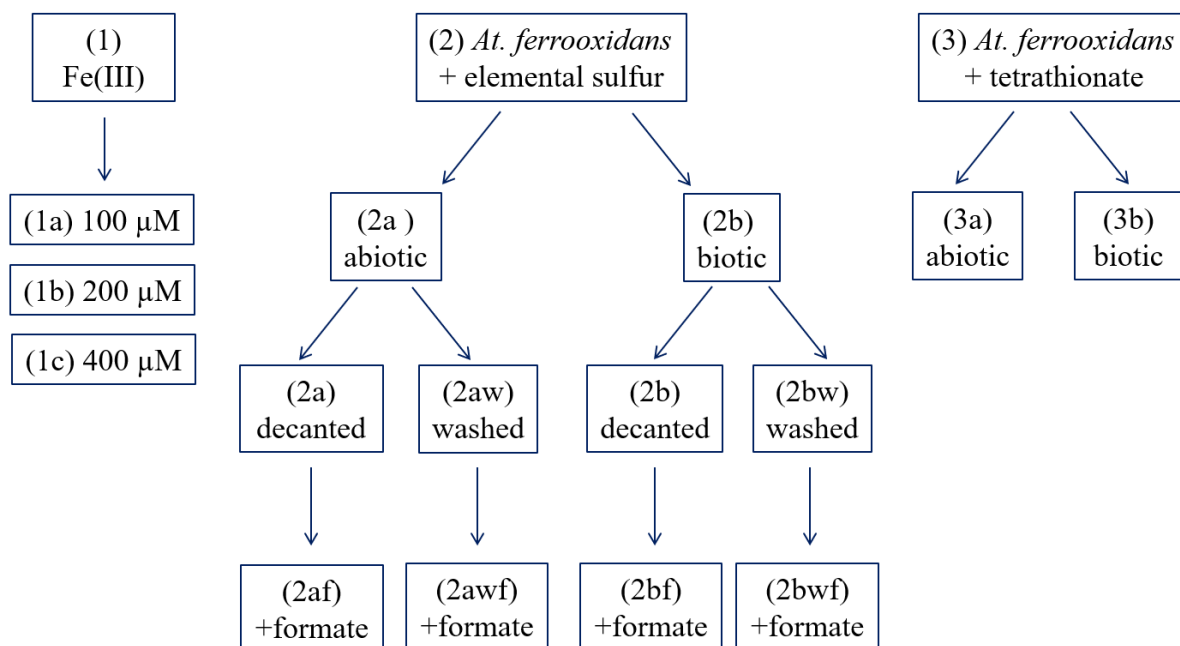


**Figure IV.1.** Overview of the experiments. (1) U(IV) oxidation with Fe(III), (2) with *At. ferrooxidans* grown on elemental sulfur, (3) *At. ferrooxidans* grown on tetrathionate. a = abiotic experiments, b = biotic experiments. w = non-crystalline U(IV) was not only decanted but also washed with 50 mM bicarbonate. f = addition of formate to the basalt salt medium (see Table S IV.1 in SI for further details).

## 2.1 Experiment (1) – Fe(III)

Uranium oxidation with Fe(III) was performed in an anaerobic chamber to exclude U oxidation by molecular oxygen, the suspension of non-crystalline U(IV) and reduction medium was centrifuged 20 min at 8000 rpm and subsequently washed in 50 mM bicarbonate solution to desorb any remaining U(VI) from the non-crystalline U(IV) and associated organic matter. For the experiments, the non-crystalline U(IV) was resuspended in anoxic basalt salt medium (Wakeman et al., 2008) with pH 2.0 to a final concentration of 200 μM U and Fe(III) concentration of 100/200/400 μM. All experiments were performed in duplicates (Figure IV.1, Table S IV.1). The basal salts medium contained (mg/L): Na<sub>2</sub>SO<sub>4</sub>·10H<sub>2</sub>O (150), (NH<sub>4</sub>)<sub>2</sub>SO<sub>4</sub> (450), KCl (50), MgSO<sub>4</sub>·7H<sub>2</sub>O (500), KH<sub>2</sub>PO<sub>4</sub> (50) and Ca(NO<sub>3</sub>)<sub>2</sub>·4H<sub>2</sub>O (14).

## 2.2 Experiment (2) – Sulfur & *At. ferrooxidans*

For the U oxidation, *Acidithiobacillus ferrooxidans* (type strain ATCC 23270, DSM 14882) was grown in 50 ml basalt salt medium (Wakeman et al., 2008). Additionally, 10 μl of a 10 mM FeSO<sub>4</sub> solution and 1 ml trace elements were added. The trace elements solution contained (g/L): ZnSO<sub>4</sub>·7H<sub>2</sub>O (10), CuSO<sub>4</sub>·5H<sub>2</sub>O (1.0), MnSO<sub>4</sub>·4H<sub>2</sub>O (1.0), CoSO<sub>4</sub>·7H<sub>2</sub>O (1.0), Cr<sub>2</sub>(SO<sub>4</sub>)<sub>3</sub>·15H<sub>2</sub>O (0.5), H<sub>3</sub>BO<sub>3</sub> (0.6), Na<sub>2</sub>MoO<sub>4</sub>·2H<sub>2</sub>O (0.5), NiSO<sub>4</sub>·6H<sub>2</sub>O (1.0), Na<sub>2</sub>SeO<sub>4</sub>·10H<sub>2</sub>O (1.0), Na<sub>2</sub>WO<sub>4</sub>·2H<sub>2</sub>O (0.1) and NaVO<sub>3</sub> (0.1). The medium was adjusted to pH 2.5 with sulfuric acid and sterilized by autoclavation for 15 min at 121°C. As growth substrate

0.05% elemental sulfur (0.025 g in 50 ml) was used. 100 ml culture flasks with 50 ml medium were incubated with 1 ml (2 %) microbial culture for 5 days at 30 °C on a shaker with 120 rpm, resulting in a slight turbidity.  $10^6$  to  $10^7$  cells per ml were counted after 5 days with a thoma cell counting chamber under a phase contrast microscope. After 5 days of growth, the bacteria were transferred into an anaerobic chamber ( $N_2$  atmosphere). Non-crystalline U(IV) was prepared in advance as described above. The U suspension was centrifuged 25 min at 8000 rpm in anaerobic tubes. For the first experiments, the WLP medium (used for U reduction) was decanted (experiments (2b), b = biotic, Figure IV.1, Table S IV.1). For some of the later experiments (2bw, w = washed with sodium bicarbonate), the non-crystalline U(IV) was washed with 50 mM bicarbonate: The non-crystalline U(IV) suspension was centrifuged, washed with 50 mM bicarbonate followed with two subsequent MQ wash steps. The bicarbonate solution was used to desorb any remaining U(VI) from the non-crystalline U(IV) and associated organic matter. To initiate U oxidation, the solid non-crystalline U(IV) phase was resuspended with 3-4 ml basalt salt medium (containing the grown *At. ferrooxidans*) of one culture flask and added to the culture flask with a final concentration of approx. 240  $\mu$ M U.

To further test if the cell metabolism plays a role for U oxidation and isotope fractionation, the experiments were performed with cells treated with 0.5 mM formate to inhibit bacteria (Ballerstedt et al., 2017; Zhang et al., 2020): after 5 days of growth, formate was added to the culture flasks with *At. ferrooxidans* before addition of non-crystalline U(IV) (2bf und 2bwf, f = formate, Figure IV.1, Table S IV.1). Flasks with and without formate treatment were analyzed by cell counting via microscopy and a thoma cell counting chamber and compared to ensure that the formate treatment inhibited the bacteria successfully. All experiments had an initial U concentration of approx. 200  $\mu$ M.

It was furthermore tested if abiotic U oxidation occurred with molecular oxygen at low pH conditions: the experimental setup was identical but without bacteria (2a, a = abiotic): the non-crystalline U(IV) suspension was only centrifuged and the supernatant was discarded, (2af) contained additionally formate. For (2aw) the non-crystalline U(IV) was washed with bicarbonate, and (2awf) contained formate (Figure IV.1, Table S IV.1).

### **2.3 Experiment (3) – Tetrathionate & *At. ferrooxidans***

*At. ferrooxidans* was grown as described for experiment (2) in a basalt salt medium but instead of elemental sulfur, tetrathionate with a final concentration of 16.7 mM was used as growth substrate (sterilized by filtration through 0.22  $\mu$ m nylon filter) For the microbial oxidation of tetrathionate, a pH of 2.5 was adjusted and *At. ferrooxidans* was grown with 16.7 mM

tetrathionate (Eccleston and Kelly, 1978). The U suspension was centrifuged 25 min at 8000 rpm and the supernatant was discarded. To initiate U oxidation, the solid non-crystalline U(IV) phase was resuspended with basalt salt medium (containing the grown *At. ferrooxidans* as in experiment 2) to the culture flask with a final concentration of approx. 240  $\mu\text{M}$  U (experiment 3b). It was furthermore tested if abiotic U oxidation occurred with molecular oxygen at low pH conditions; the experimental setup was identical but without bacteria (3a). As no stable culture of *At. ferrooxidans* on tetrathionate could be maintained, no experiments with formate were conducted.

### 2.3.1 High-performance liquid chromatography

With an additional control experiments, a chemical reduction of U(VI) by K-tetrathionate under aerobic conditions was excluded. For this, 25 ml basalt salt medium (pH 2.5) with a U(VI) concentration of 200  $\mu\text{M}$  was prepared in duplicates similar to the biotic experiments. Experiments were performed with either 10 mM, 5 mM or 1 mM K-tetrathionate and aliquots were taken in a time series. Aliquots were buffered 1:4 with a 0.1 M phosphate buffer (pH 7.0) and frozen to stop the reaction (Schippers, 1998; Schippers et al., 1996). High-performance liquid chromatography (HPLC) analysis was performed after Steudel et al. (1987). Reduction of U(VI) would result in degradation of K-tetrathionate would.

### 2.4 Concentration and isotope measurements

A detailed description of the measurement protocol (concentration and isotope fractionation) is given in chapter 3 of this thesis.

Briefly, for concentration measurements a Thermo-Scientific Element-XR inductively coupled plasma source mass spectrometer (ICP-MS, ElementXR) at Leibniz Universität Hannover (Germany) was employed. The precision of the analyses was typically below 5% (2 s.d.).

For U isotope analysis, the samples were weighted and evaporated to dryness. To destroy any organic compounds, aqua regia (3 ml 11 M HCl and 1 ml 14 M HNO<sub>3</sub>) was added, boiled at 130°C for 48 h and subsequently evaporated. The samples were then treated with a mixture of 200  $\mu\text{l}$  14 M HNO<sub>3</sub> and 200  $\mu\text{l}$  H<sub>2</sub>O<sub>2</sub> (30 %). Uranium was purified by ion-exchange chromatography according to a method described by Weyer et al. (2008). U isotope measurements were performed at Leibniz Universität Hannover with a Thermo-Finnigan Neptune multi-collector ICP-MS (MC-ICP-MS), similar to the protocol published by Noordmann et al. (2015).

### 3 Results and discussion

#### 3.1 Experiment (1) – Fe(III)

The abiotic batch experiments with Fe(III) resulted in rapid oxidation of non-crystalline U(IV). Within the first 15 minutes, 23 to 34% U(IV) were oxidized and mobilized (Figure IV.2). After 48 h 200  $\mu\text{M}$  Fe(III) mobilized ~80 %, 400  $\mu\text{M}$  Fe(III) ~50 % and 100  $\mu\text{M}$  Fe(III) 30% or 57 % U(IV), respectively. Experiment (1a)-2 100  $\mu\text{M}$  slightly differs from all other experiments, apparently U mobilization is faster with 57 % U mobilized after 2 hours.

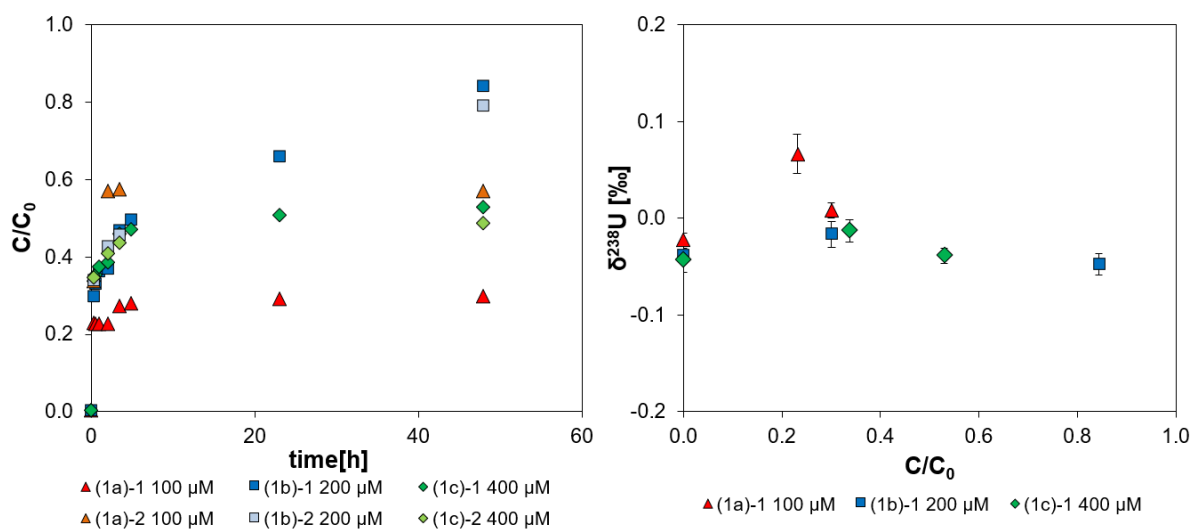


**Figure IV.2.** Left: Oxidized U fraction ( $C/C_0$ ) vs. time [h] after oxidation with 100  $\mu\text{M}$ , 200  $\mu\text{M}$  and 400  $\mu\text{M}$  Fe(III). Right:  $\delta^{238}\text{U}$  [‰] of U in solution (separated from solid U(IV) by filtration) vs. the oxidized fraction of uranium.

Oxidation with Fe(III) was shown in previous studies (e.g. Sani et al., 2005), but this work showed that the oxidation with Fe(III) is not causing any significant isotope fractionation bigger than the analytical error (2s.d.  $\leq \pm 0.05$  ‰), all values are between -0.05 ‰ and 0.07 ‰. It seems that two processes mobilized U, a first very fast mechanism within the first minutes, and afterwards a second one, by which the mobilization was slower and tended to stagnate almost at some point. However, both mechanisms did not fractionate U isotopes significantly. Likely, a layer effect played a role: i.e. each layer must be completely oxidized before the next layer can be oxidized, which was similarly observed by Wang et al. (2015a) during U(IV) oxidation with oxygen.

#### 3.2 Experiment (2) – Sulfur & *At. ferrooxidans*

Experiments with *At. ferrooxidans* grown on Fe(II) as substrate were excluded, since the product of the biological Fe(II) oxidation Fe(III) would rapidly chemically oxidize U(IV) as shown in chapter 3.1. Therefore, U oxidation with *At. ferrooxidans* which was grown on elemental sulfur was tested. For the first experiments, the WLP solution (used for U reduction)

was decanted and then all other components were added (Figure IV.1, Figure IV.3 A & B, 2b, b = biotic). In the later experiments, the solids were rinsed first with 50 mM bicarbonate and then with MQ to desorb any remaining U(VI) (Figure IV.1, Figure IV.3 C & D, 2bw, w = non-crystalline U(IV) was washed prior to U oxidation with sodium bicarbonate). The cells of *At. ferrooxidans* grown on elemental sulfur oxidized U(IV) almost quantitatively (~90 %) within one week. Notably, the final U(VI) concentration in solution was similar for the untreated (2b, Figure IV.3 A) and the bicarbonate washed experiments (2bw, Figure IV.3 D), however, at the beginning the concentration rose slower in the untreated experiments (2b, 29-57 % in the first 3 hours) and faster in the bicarbonate washed samples (2bw, 67-77 % after 3 hours). For the untreated experiments (2b, Figure IV.3 B), preferential oxidation of  $^{235}\text{U}$  (-0.4 to -0.2 ‰) was initially observed, however, in the course of the experiments  $\delta^{238}\text{U}$  values rose quickly with time and settled down around the initial value of non-crystalline U(IV) or slightly above at about 35 % mobilization. In case of the bicarbonate-washed experiments (2bw), no significant initial mobilization of light U isotopes was observed and the  $\delta^{238}\text{U}$  values varied slightly around 0 ‰. However, it is striking that all four biotic experiments with bicarbonate wash (2bw) showed a similar very small pattern. The initial values were on average 0.04 ‰, the  $\delta^{238}\text{U}$  of the first mobilized U had a value of -0.06 ‰ and then increased to values of 0.09 ‰. The errors were 0.02-0.06 ‰ in each case. So, it is not clearly quantifiable, but a slight trend, as seen in more pronounced form in the biotic experiments without bicarbonate wash (2b), might be suspected.

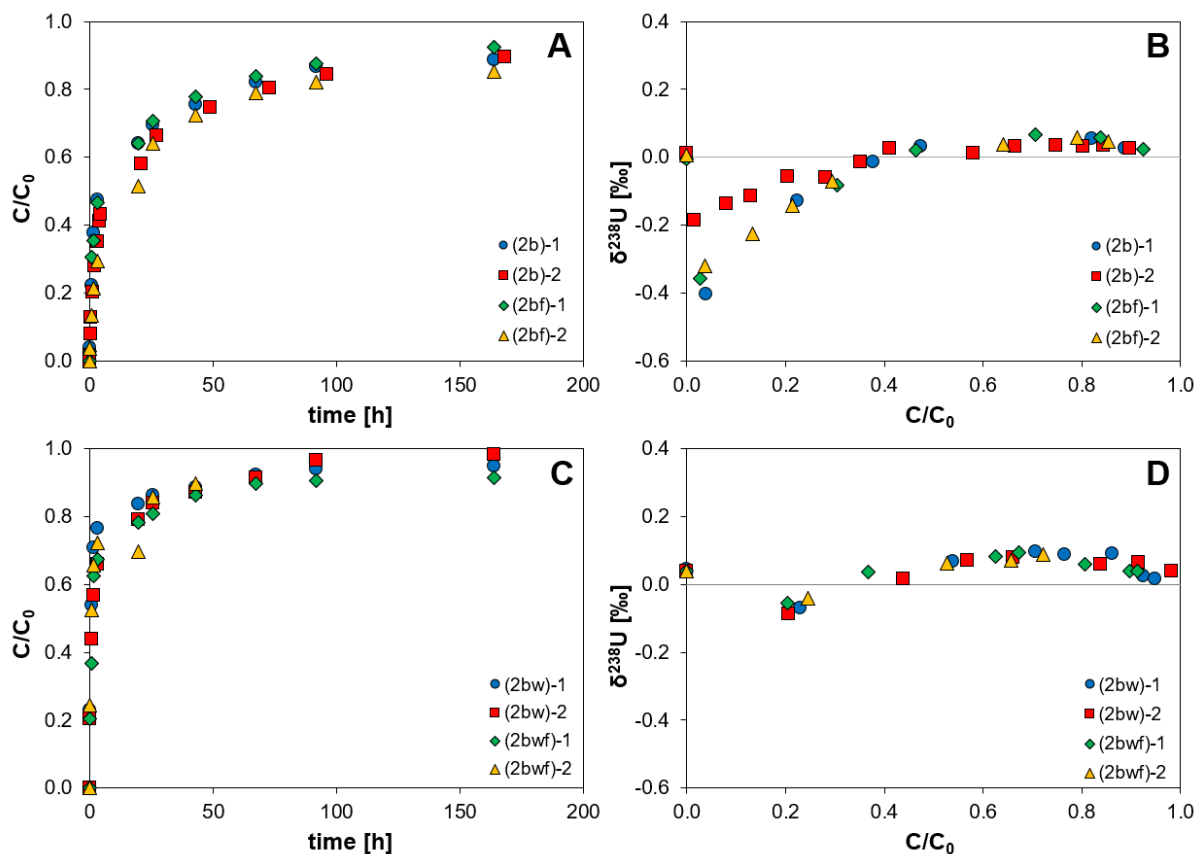


**Figure IV.3.** Biotic U oxidation (bacteria grown on elemental sulfur), on the left-hand side the oxidized U fraction ( $C/C_0$ ) vs. time [h] is plotted, ( $C/C_0$ ) vs.  $\delta^{238}\text{U}$  [‰] of U(VI) can be seen on the right-hand side. Figures A and B show the results with decanted growth medium (2b), U(IV) from Figures C and D was washed prior to the experimental start with bicarbonate and MQ (2bw). (2b/2bw) = biotic experiments with live cells. (2bf/2bwf) show the results for the cells killed with formate.

Treatment with 0.5 mM formate killed the bacteria. Interestingly, no significant differences in the mobilization or in the isotope behavior were observed between experiments conducted with living and dead cells (Figure IV.3). It seems that U(IV) oxidation is independent of a microbial metabolism and not related to an electron transfer across the cell membrane. Rather, it seems to be rather a ligand-related effect driven by proteins or cell wall structures of the cells related to U biosorption.

#### Fitting of initial U isotope fractionation

The light isotope values in the untreated experiments probably arose from U(VI) that was still present in the non-crystalline U(IV) as the only difference in the experiments is the washing with bicarbonate to desorb residual U(VI). Any remaining unreduced U(VI), adsorbed to non-crystalline U(IV), may had a light isotopic signature, because during bacterial U reduction the remaining U(VI) becomes depleted in  $^{238}\text{U}$  (Stirling et al., 2015; Stylo et al., 2015b).

In order to further characterize the initial mechanism of U isotope fractionation in the experiments without any bicarbonate washing before the start of the experiment, the U(VI)

isotopic signatures were modeled with both an equilibrium isotope fractionation-, and a Rayleigh Distillation model. For the Rayleigh model a closed system with no back-reaction of the oxidized U(VI) and solid U(IV) is assumed. In this case, the variation of  $\delta^{238}\text{U}_{\text{U(VI)}}$  as function of the fraction of remaining U(IV) can be described by the following equation:

$$\delta^{238}\text{U}_{\text{U(VI)}} = (\delta^{238}\text{U}_{\text{U(VI),t0}} + 1000)F_{\text{U(IV)}}^{(\alpha-1)} - 1000 \quad (4)$$

$\delta^{238}\text{U}_{\text{U(VI)}}$  represents the U isotopic ratio of the oxidized U fraction and  $\delta^{238}\text{U}_{\text{U(VI),t0}}$  the initial U isotope composition of the oxidized fraction. The fraction of remaining U(IV) is given by  $F = C/C_0$ , where C and  $C_0$  represent the oxidized U and initial U concentrations (as non-crystalline U(IV)) respectively,  $\alpha$  is defined as

$$\alpha = \frac{R_{\text{oxidized}}}{R_{\text{non-crystalline U(IV)}}} \quad (5)$$

$R_{\text{oxidized}}$  and  $R_{\text{non-crystalline U(IV)}}$  are the U isotopic ratios ( $^{238}\text{U}/^{235}\text{U}$ ) of the oxidized fraction and the non-crystalline U(IV).

A Rayleigh model results in a linear relationship between  $\ln F$  and  $\ln(\delta^{238}\text{U} + 1000)$ , with a slope  $\alpha-1$  (Figure IV.4 A&B). Such a relationship was observed for U oxidation with a correlation coefficient of 0.91-0.99 and  $\alpha$  of 0.9992-0.09996, respectively (Table IV.1).

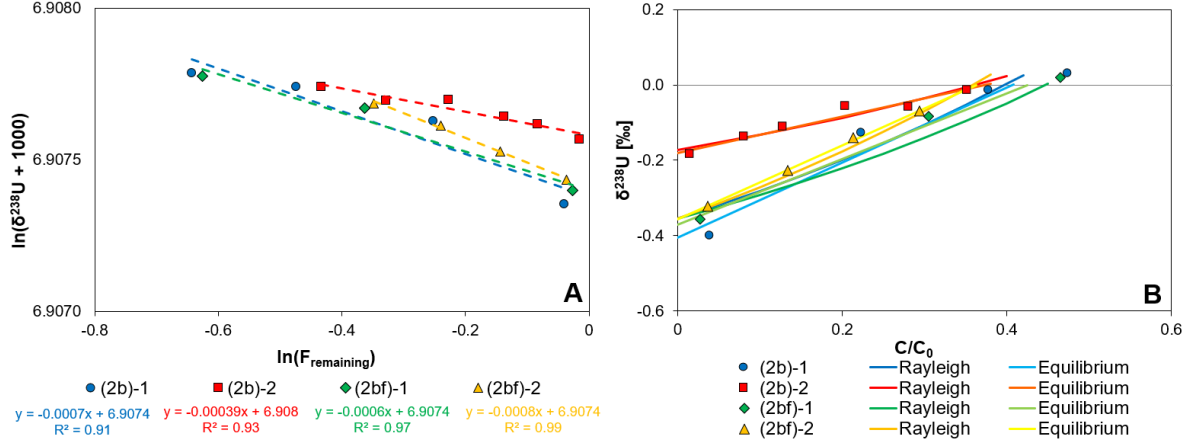


**Figure IV.4.** Left side: Rayleigh fitting  $\ln F$  versus  $\ln(\delta^{238}\text{U} + 1000)$  for initial values until mobilized fractions reach a steady state at  $\sim 0$  ‰. Right side: Measured experimental  $\delta^{238}\text{U}$  values [in ‰] for the mobilized U versus the fraction of mobilized U ( $C/C_0$ ) and modeled Rayleigh and Equilibrium isotope fractionation (b = biotic, f = formate).

**Table IV.1.** Fractionation factor ( $\alpha$ ),  $\delta^{238}\text{U}_{\text{t0}}$  and  $R^2$  for modelled Rayleigh fractionation and equilibrium isotope fractionation for the biotic (2b) oxidation experiments without bicarbonate wash (f = formate).

	Rayleigh			Equilibrium		
	$\alpha$	$\delta^{238}\text{U}_{\text{t0}}$	$R^2$	$\alpha$	$\delta^{238}\text{U}_{\text{t0}}$	$R^2$
(2b)-1	0.9993	-0.36	0.91	0.99959	-0.41	0.95
(2b)-2	0.9996	-0.17	0.93	0.99982	-0.18	0.95
(2bf)-1	0.9994	-0.36	0.97	0.99963	-0.37	0.99
(2bf)-2	0.9992	-0.36	0.99	0.99964	-0.36	0.99

Equilibrium isotope fractionation, assuming reversible isotope exchange between solid and oxidized U(VI), results in a linear relationship between  $\delta^{238}\text{U}_{\text{U(VI)}}$  and  $C/C_0$  (Figure IV.4 B). Such a relationship with a  $R^2$  value of 0.95-0.99 was observed for the first 35-40% of U mobilization (considered here as initial mobilization) and resulted in an isotope fractionation factor  $\alpha$ , using the approximation  $\delta_A - \delta_B \approx 1000 \ln \alpha_{A-B}$ , of 0.99959-0.99982. Thus, for the limited portion of initial U mobilization, both models fit similarly well the observed isotope fractionation behavior for the same area (Figure IV.4) with minimal better correlation coefficients for equilibrium isotope fractionation.

### 3.3 Experiment (3) – Tetrathionate & *At. ferrooxidans*

Experiments with *At. ferrooxidans* grown tetrathionate were also tested as further sulfur substrate (besides elemental sulfur) ((3a), Figure IV.5,  $10^6$  to  $10^7$  cells per ml). Non-crystalline U(IV) was added to the bacterial medium inside the glove box and then the experiments were run and sampled under normal atmospheric conditions. It was furthermore tested if abiotic U oxidation occurred with molecular oxygen at low pH conditions (3a). The abiotic experiments exhibited a minor increase in the oxidized fraction at the beginning (~10 %) but with ongoing experiment duration the U concentration in solution decreased. Biotic oxidation by *At. ferrooxidans* resulted in enhanced initial U mobilization (41 % after 0.5 h) and approx. half the U amount was oxidized after 3 hours (47 %) of the experiment. However, with time, the U concentration in solution decreased and stagnated at values of ~25% oxidized U. The U isotope signature in the abiotic experiment changed at the beginning of the experiment to values of -0.15 ‰ and then increased after one day to 0.51 ‰ and 0.98 ‰ after four days. Oxidation



with *At. ferrooxidans* resulted in initial  $\delta^{238}\text{U}$  values of 0.14 ‰ (within the first hours) and subsequently an increase to stagnate values of  $\sim 0.55$  ‰ was observed.

In order to address the decreasing U concentration in both, biotic and abiotic experiments with time, i.e. the potential role of a chemical reduction of U(VI) by tetrathionate, HPLC (high-performance liquid chromatography) measurements have been conducted. No decrease of the K-tetrathionate concentration was observed indicating that the observed decrease in the U concentration in the previous experiments was not caused by an interaction of U(VI) with K-tetrathionate. Another possibility may be reduction of previously mobilized U(VI) through the *Shewanella oneidensis* cells, which were still associated with the non-crystalline U(IV), or adsorption of U(VI) onto the biomass. However, despite promising first results, no stable culture of *At. ferrooxidans* on tetrathionate could be maintained, so that the further discussion mainly relates to the experiments with *At. ferrooxidans* grown on elemental sulfur.

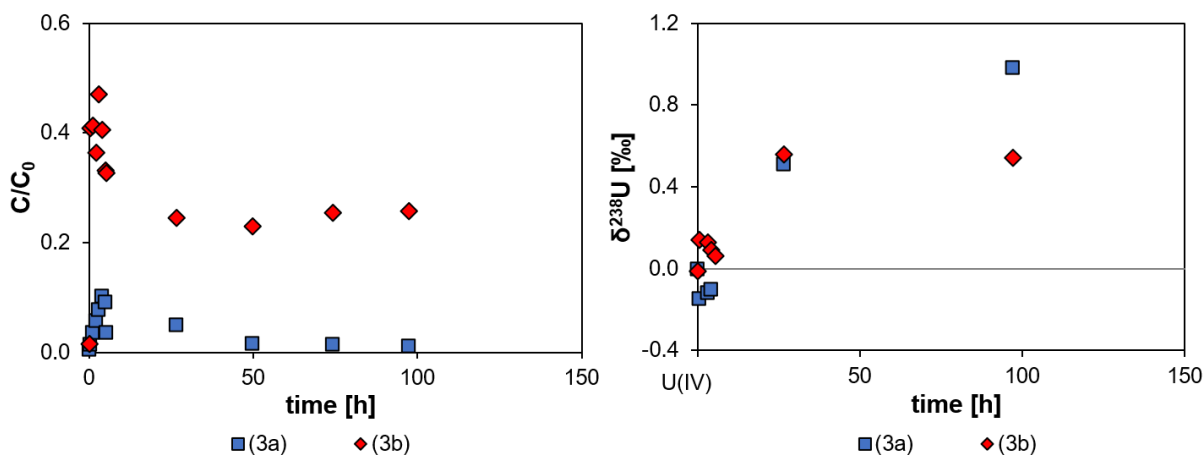


**Figure IV.5.** Oxidation with *At. ferrooxidans* grown on tetrathionate (3b) and concurrent abiotic oxidation experiment with molecular oxygen (3a), oxidized U fraction ( $C/C_0$ ) vs. time [h] on the left-hand side, time vs.  $\delta^{238}\text{U}$  [‰] of U(VI) on the right-hand side.

Comparable biotic experiments were performed with copper by Kimball et al. (2009) and Mathur et al. (2005). The Cu minerals chalcocite and chalcopyrite were inoculated with *Acidithiobacillus ferrooxidans*, but no significant Cu isotope fractionation was directly observed in solution (Mathur et al., 2005). Kimball et al. (2009) performed biotic Cu leaching experiments to further interpret stream water samples affected by acid mine drainage. Their experimental set up was similar to Mathur et al. (2005), but they used a 200 times higher inoculum, additionally the mineral enargite and tested live and heat-killed bacteria. Experiments with *At. ferrooxidans* resulted in lighter leached Cu ( $\Delta_{\text{aq-min}} = -0.57$  ‰) for chalcopyrite, significant less compared to the former experiments, and with no difference between autoclaved and not autoclaved cells. For enargite no significant Cu isotope

fractionation was observed ( $\Delta_{\text{aq-min}^{\circ}} = 0.03 \text{ ‰}$  for nonautoclaved cells, 0.26 ‰ for autoclaved cells).

To explain the absence of isotope fractionation in the leach fluid, Mathur et al. (2005) analyzed the bacteria pellet and detected isotopically heavy Cu associated with the bacteria cells and surrounding precipitates ( $\delta^{65}\text{Cu} = 5.59 \pm 0.16\text{‰}$ ). Mathur et al. (2005) and Kimball et al. (2009) observed (similar to the U oxidation in this study) no isotopic fractionation or light isotopes are preferentially oxidized because the heavy Cu is accumulated in/at the bacteria. They assumed that cellular uptake or adsorption caused the heavy Cu isotopes associated with the bacteria and proved that further with TEM images and EDS spectra and a mass balance calculation, in which the isotopic composition of the residual mineral, the Cu in the aqueous leach fluid and in the bacteria pellet was considered. Acidophilic microorganisms such as *At. ferrooxidans* have developed resistance mechanisms to the extreme conditions of their environment and, among other abilities, are able to live with high concentrations of metals (Dopson et al., 2003; Kimball et al., 2009; Valls and De Lorenzo, 2002). The passive uptake to the surface of microbial cells (live and dead) is caused by the electronegative charge of Gram-positive and Gram-negative bacterial cell envelopes (biosorption). Ligands in the cell wall (e.g., carboxyl, amine, hydroxyl, phosphate and sulfhydryl groups) are able to chemically sorb and bind metals (Lloyd and Macaskie, 2000; Newsome et al., 2014). Experiments investigating the cellular uptake of uranium showed that the uptake increased with higher U concentrations and is further influenced by pH (DiSpirito et al., 1983). Uranium was mainly found in association with the cell wall and membrane and only minor quantities were found in the cytoplasmic, lipopolysaccharide and periplasmic space material. Dead cells (poisoned with potassium cyanide) had 8 to 11 times more uranium in the cytoplasm than living cells. Experiments at different pH values exhibited that above pH 2 the U uptake decreased about 50 % in comparison to pH 1.0 and 1.5. Hence, it might be possible that in our experiments the bacterial biomass adsorbed some uranium (biosorption) rather than taking it up into the cells (bioaccumulation) as described for the Cu experiments by Kimball et al. (2009) and Mathur et al. (2005). Uranium biosorption to *At. ferrooxidans* cells was proofed by Merroun and Selenska-Pobell (2001). The initially dissolved U was isotopically slightly lighter than the starting material (although still identical within uncertainties) for the bicarbonate washed experiments (2bw, Figure IV.3 D), or isotopically lighter in the untreated experiments (2b, Figure IV.3 B), indicating that either  $^{235}\text{U}$  is preferentially oxidized or  $^{238}\text{U}$  is adsorbed by the cells. After mobilization of 35-40% the isotopic signatures become positive. However, this interpretation is contradicted by the fact

that at the end of the experiments almost all uranium was in solution, i.e., only a little amount could be precipitated or adsorbed. Moreover, it was not observed that dead cells (inhibited with formate) adsorbed more U than living cells, as no difference in the aqueous U concentration was observed.

The hypothesis that isotope fractionation occurs during bacterial U oxidation could be supported with a closer look at microbial Fe isotope fractionation. During abiotic and biotic oxidation of iron, significant Fe isotope fractionation was observed (Balci et al., 2006a; Bullen et al., 2001; Croal et al., 2004; Johnson et al., 2004a; Kappler et al., 2010). Iron behaves chemically oppositely to U; the reduced Fe is in solution and the oxidized form precipitates at circumneutral pH. Oxidation of Fe(II)<sub>aq</sub> by anaerobic, photoautotrophic bacteria lead to precipitation of Fe(III) that was ~1.5‰ heavier than the initial iron. To investigate Fe isotope fractionation during microbially stimulated Fe oxidation, laboratory experiments were conducted with *At. ferrooxidans* at low pH (<3) from Balci et al. (2006) and the coexisting phases Fe(II)<sub>aq</sub>, Fe(III)<sub>aq</sub> and precipitated Fe(III)<sub>ppt</sub> were analyzed as well as abiotic control experiments. Fe(II) oxidizes to different Fe(III)<sub>aq</sub> complexes (depending on ligand concentration and pH) which are then almost immediately precipitated (Jambor, 2003). Aqueous Fe(II) exhibits lower  $\delta^{56}\text{Fe}$  values compared to the coexisting Fe(III)<sub>aq</sub> and Fe(III)<sub>ppt</sub> phases. The isotopic effect during precipitation was further studied and the main Fe isotope fractionation occurred rather during the oxidation step than during the precipitation. Aqueous Fe(III) has  $\delta^{56}\text{Fe}$  values similar to or greater than the values for Fe(III)<sub>ppt</sub> with a decrease correlated to an increasing precipitation rate and decreasing grain size. The authors conclude that the behavior in their experiments is mainly controlled by non-biological equilibrium and kinetic factors. However, it is assumed that the precipitation of Fe(III) oxides, and thus unidirectional kinetic fractionation, causes mainly the observed Fe isotope signatures (Johnson, 2020; Staubwasser et al., 2007). Consequently, with regard to Fe and Cu, it could therefore be assumed that biotic isotope fractionation could be possibly occur with uranium, but might be not detected at first sight by measurements of the solution. However, since small amounts of oxygen were also in the system, further reactions may have occurred. For this reason, additional abiotic experiments were carried out in order to understand the entire system.

### Abiotic isotope fractionation

For abiotic control experiments the same medium was used but was not inoculated with *At. ferrooxidans*. In all abiotic controls, an initial U concentration increase followed by a decrease was observed (Figure IV.6 A&C). All controls not pre-treated with bicarbonate (2a, Figure IV.6 A) showed only minor U mobilization within the first hours (~8 %) whereas the experiments washed with bicarbonate prior to U oxidation (2aw, Figure IV.6 C) exhibited U mobilization of up to ~34-51 % after 3 hours. Subsequently, the U fraction in solution decreased in all cases. The control experiments with formate reacted similar to those without formate, indicating that formate had no impact on the U speciation. The isotope values for the abiotic experiments exhibited an increase of  $\delta^{238}\text{U}$  to values of 0.71 – 0.88 ‰ without bicarbonate wash followed by a small decrease to  $\delta^{238}\text{U} = 0.55 – 0.72$  ‰ (experiments 2a, Figure IV.6 B), and 0.85 ‰ with the wash or 0.61 ‰ followed by a decrease to 0.43 ‰ (2aw, Figure IV.6 D). Only one abiotic control (2a-1) exhibited an initial decrease of the  $\delta^{238}\text{U}$  value (-0.24 ‰) followed by higher values.

Particularly noticeable is the large initial abiotic oxidation of non-crystalline U(IV) that was washed with bicarbonate prior to experiment start (~ 50 % mobilization after 3 hours), compared to those experiments without bicarbonate wash (< 10 % mobilization). This difference can also be noticed quite easily in the biotic experiments (Figure IV.3), where the concentration rose to 29-57 % in the first three hours in the untreated experiments (2a) and to 67-77 % in the bicarbonate washed samples (2aw). Presumably, the abiotic mobilization also played a small part there and causes the differences. Therefore, the bicarbonate pretreatment may likely be one dominant cause for abiotic U mobilization (apart from oxidation with molecular oxygen) and needs to be further considered.

With higher bicarbonate concentration (and also higher temperatures) the dissolution of  $\text{UO}_{2(s)}$  increases under oxidizing conditions (de Pablo et al., 1997). Moreover, experiments show that the dissolution rate of  $\text{UO}_{2(s)}$  increases with decreasing pH between pH 3 and 6.5 and increases with higher oxygen concentration (Ginder-Vogel and Fendorf, 2007; Torrero et al., 1997). Torrero et al. (1997) also analyzed the solid phase with XPS and found an oxidized surface layer that, especially at low pH, contained a high proportion of U(VI).

Regarding the experiments in this study, the first abiotic experiments exhibited a pH of 3.35-3.73, while all later experiments (with bicarbonate wash) had a lower pH (pH 2.60-2.72) (see table S IV. 2 and S IV.3 in SI). All biotic experiments had also a lower pH (pH 1.92-2.51), consequently, it is possible that some mobilization in the biotic experiments is additionally

caused by abiotic processes. For our experiments we can assume the following explanation: 1) Either residues of bicarbonate were still present in the oxidation solution, 2) bicarbonate has reacted during the U(VI) desorption step directly with the non-crystalline U(IV) or 3) a partially oxidized surface layer may have formed when reacting with the low pH medium of the bacteria and dissolved the uranium. The low pH value is probably the most likely cause, as it correlated closely with the measured concentration values. The overserved U isotope fractionation can be used to understand the subsequent decrease of the U concentration in the solution.

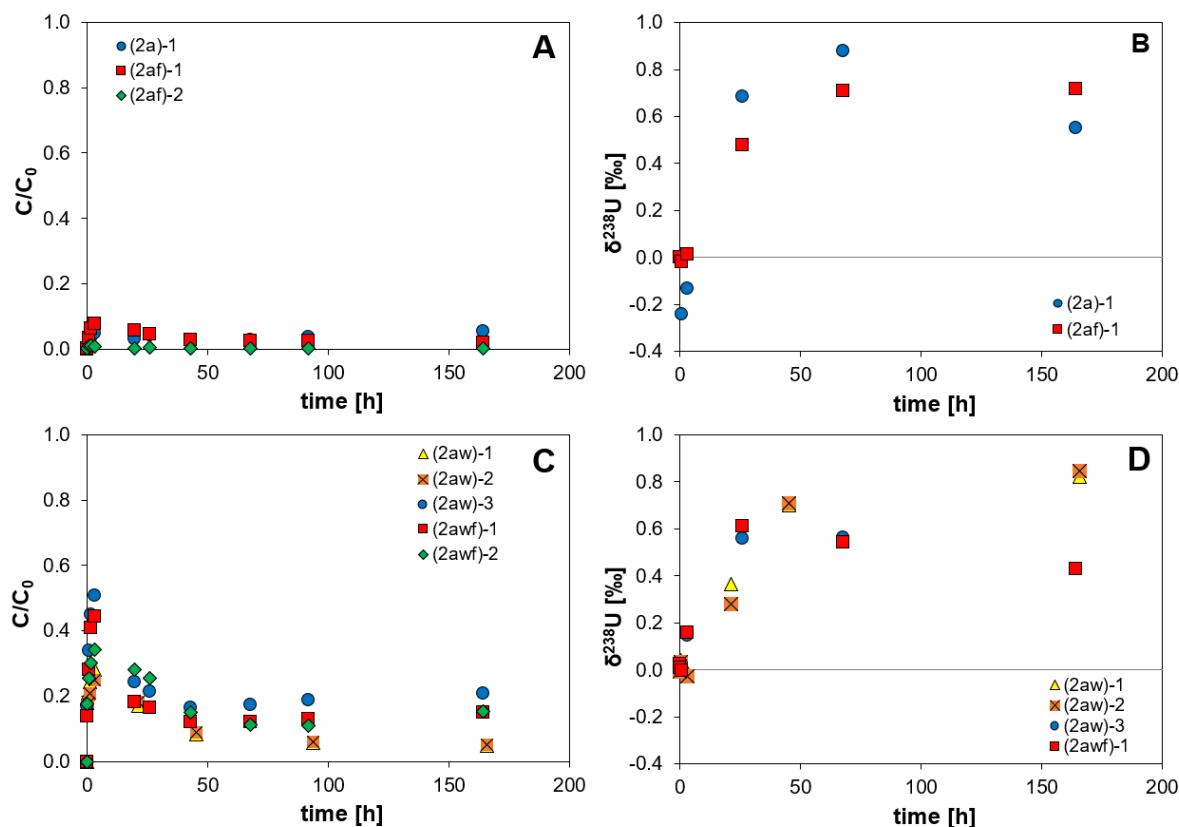


**Figure IV.6.** U concentration ( $C/C_0$ ) vs. time [h] for abiotic control experiments (A/B: decanted growth medium (2a); C/D: bicarbonate-washed (2aw), f = addition of formate). Corresponding  $\delta^{238}\text{U}$  values for those experiments vs. time [h].

Wang et al. (2015a) performed abiotic U oxidation experiments in order to characterize the associated U isotope fractionation. In acidic media, light U isotopes preferentially were oxidized from dissolved U(IV), U(VI) being approx.  $1.1 \pm 0.2$  ‰ lighter than the remaining U(IV). Oxidation of solid U(IV) at a higher pH (9.4) resulted in minor U isotope fractionation in the opposite direction with  $\delta^{238}\text{U}$  values of  $\sim 0.1$  to  $0.3$  ‰ for U(VI). The authors explain this by a layer effect: each layer must be completely oxidized before the next layer can be oxidized and the minor isotope effects may only arise from adsorption effects. Interestingly, these authors observed (in a more frequently sampled experiment) negative initial isotope signatures as in our experiment for the U(VI) during oxidation from solid U(IV). The first sample exhibits

a  $\delta^{238}\text{U}$  value of -0.13 ‰ followed by an immediate increase to more positive values (+0.34 ‰) and a further decrease during the course of the experiment in the direction of the starting material with almost quantitative oxidation (94 %) at the end of the experiment. In our study, minor oxidative U mobilization was caused indirectly by a bit of molecular oxygen and it resulted in sometimes initial low values (-0.24 ‰) and later higher  $\delta^{238}\text{U}$  values (~0.7 ‰). We only mobilized U partly in our experiments (a maximum of ~20 % in solution is reached at the experimental end), therefore we may not observe the decrease as in the study of Wang et al. (2015a).

The initial U(VI) isotope fractionation, being slightly lighter, may probably be due to an initial kinetic isotope fractionation which is then quickly overlaid by isotope fractionation generated in the opposite direction by a different mechanism. Furthermore, Wang et al. (2015a) speculate that the experiment duration was too short and thus there was not enough time for equilibration between U(IV) and U(VI), so no equilibrium isotope fractionation may be observed like, for example, during reductive dissolution of Fe(III), where more pronounced isotope effects are generated (~3 ‰) (Crosby et al., 2007, 2005; Wu et al., 2009). The later isotope fractionation resulting in an enrichment of  $^{238}\text{U}$  in solution in Wang et al. (2015a) is explained by minor adsorption effects as also seen by Brennecka et al. (2011) and Jemison et al. (2016). These effects can explain exactly the results of our abiotic experiments. Brennecka et al. (2011) observes a preferential adsorption of light  $^{235}\text{U}$  on synthetic K-birnessite, the adsorbed U is ~0.2 ‰ lighter. In the experiments, the U remaining in the solution is heavier and reaches values of up to 0.3 ‰. Jemison et al. (2016) performed further adsorption experiments onto common aquifer minerals and observed an average fractionation of -0.15 ‰. Most experiments were conducted at pH 8 and with addition of bicarbonate to produce uranyl carbonate complexes, but one experiment was performed without bicarbonate addition and behaved similarly to our experiments, indicating that the results are also comparable to the experiments in our study. In the adsorption experiments performed by Jemison et al. (2016), the solution becomes significantly heavier with time, reaching even values of 0.41 ‰ in some cases. In our study, we see a slight mobilization despite the absence of bacterial biomass, but after a short time the concentration in the solution decreases again and simultaneously the isotope fractionation becomes larger. Hence, it is likely that the observed abiotic U isotope fractionation results from adsorption of light U. However, it should be noted that the isotope values in this study are even higher than those observed by Brennecka et al. (2011) and Jemison et al. (2016). It would be necessary that the adsorbed U is not in equilibrium with the U remaining in the solution and

some kind of Rayleigh process would happen, adsorbing most of the uranium. Also in the experiments with *At. ferrooxidans* grown on tetrathionate (experiment 3a, Figure IV.5) the U isotope fractionation is very similar to the abiotic controls. In the corresponding abiotic experiment, about 10% U was mobilized. That the concentration decreases, presumably due to subsequent adsorption on the non-crystalline U(IV) (which is also associated with cell biomass of *S. oneidensis* from U reduction, which is retained with the non-crystalline U(IV)), can also be seen and probably causes the observed U isotope fractionation in the abiotic and biotic experiment with tetrathionate.

If the isotope values of the abiotic mobilization are plotted against  $C/C_0$  and the corresponding tables are consulted (Table S IV.4 in SI, see also Figure IV.6), it can be seen that two different processes seem to take place in the abiotic experiments. In a first step, the U concentration in the solution increases, but no isotope fractionation is observed. From the point of maximum concentration in solution, a second process seems to start, the U concentration decreases again, and the decreasing U concentration correlates with increasing  $\delta^{238}\text{U}$  value. This correlation can be directly seen, when plotting  $C/C_0$  vs.  $\delta^{238}\text{U}$  and excluding the first samples (Figure IV.7).

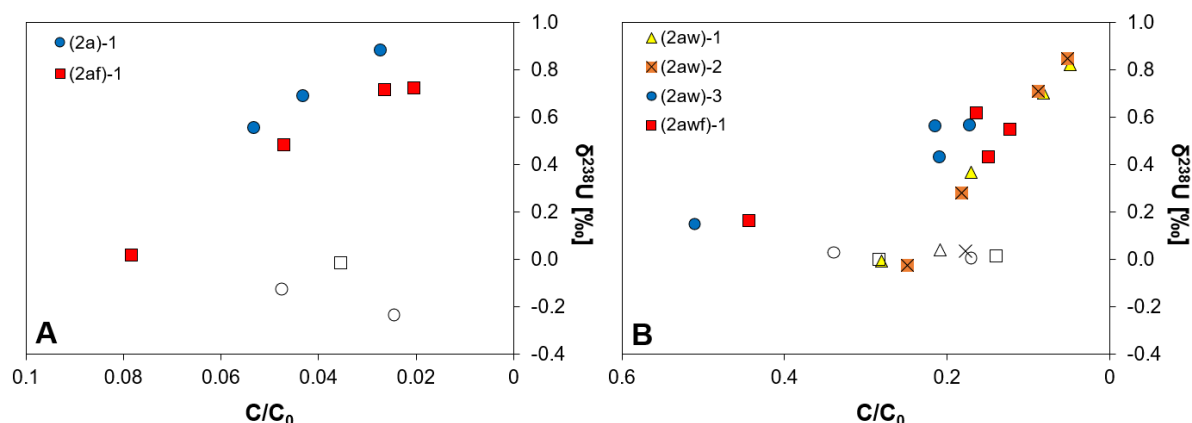


**Figure IV.7.** U fraction in solution ( $C/C_0$ ) vs.  $\delta^{238}\text{U}$  values for all abiotic experiments (A: decanted growth medium (2a), B: bicarbonate washed non-crystalline U(IV) (2aw, f = formate). Symbols without color display the first mobilization mechanisms resulting in increasing U concentration in solution, filled symbols show the samples with decreasing U concentration and corresponding increasing  $\delta^{238}\text{U}$  values, most likely due to adsorption.

Similar to the fitting of the initial U mobilization in the biotic experiments, Rayleigh and equilibrium isotope fractionation was modeled for this second mechanism (Figure IV.8 and Table IV.2). However, it must be said that the calculations neglect the fact that further U oxidation might occur in parallel with adsorption. The experiments without bicarbonate wash ((2a), as already presented in Figure IV.6) show a distinctly lower U concentration in solution and  $\alpha$  is 1.01207/1.01192 with  $R^2$  of 0.999/0.98 for a Rayleigh fractionation behavior vs. 1.00122/1.00180 with  $R^2$  of 0.999/0.95 for equilibrium. The bicarbonate washed samples show

two different behaviors (2aw-1 and 2aw-2) behave similar with less U in solution and higher  $\delta^{238}\text{U}$  values: Rayleigh fitting has a correlation coefficient of 0.996-0.999 and equilibrium isotope fractionation of 0.999. (2aw-3 and 2awf-1) have a higher U concentration and lower  $\delta^{238}\text{U}$  values and  $R^2$  values of 0.84-0.91 for Rayleigh and 0.83-0.92 for equilibrium. The calculation for all abiotic oxidation experiments show that it is not clearly distinguishable between both fractionation mechanisms, but the high correlation coefficients confirm the strong correlation between the decreasing U concentration and increasing  $\delta^{238}\text{U}$  values, further supporting the hypothesis that U is probably adsorbed.

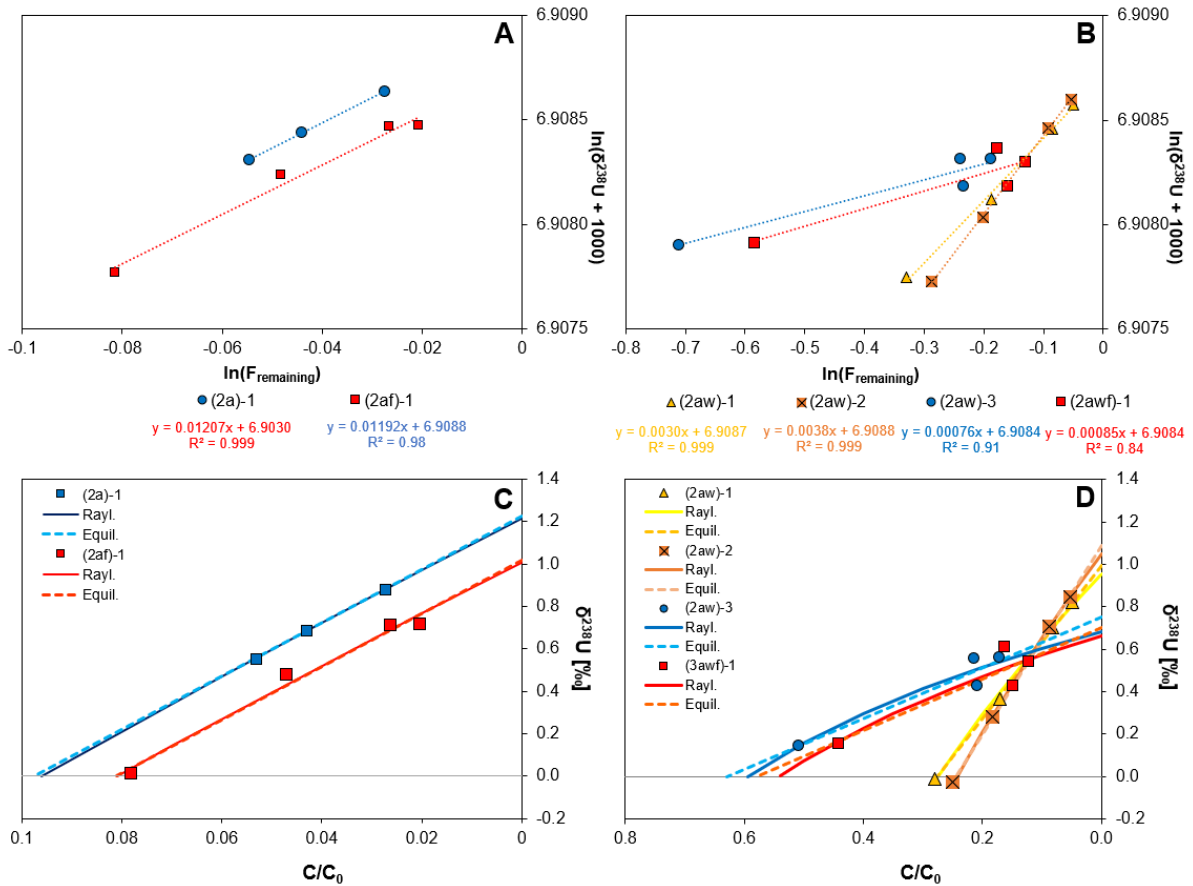


**Figure IV.8.** Rayleigh fitting  $\ln F$  versus  $\ln(\delta^{238}\text{U} + 1000)$  for second mobilization mechanism (A: deacanted growth medium (2a), B: bicarbonate-washed (2aw)). C + D: Measured experimental  $\delta^{238}\text{U}$  values [in ‰] for the mobilized U versus the fraction of mobilized U ( $C/C_0$ ) and modeled Rayleigh and Equilibrium isotope fractionation (a = abiotic, w = non-crystalline U(IV) washed with bicarbonate, f = addition of formate).



**Table IV.2.** Fractionation factor ( $\alpha$ ),  $\delta^{238}\text{U}_{10}$  and  $R^2$  for modelled Rayleigh fractionation and equilibrium isotope fractionation for the second abiotic mechanisms.

	Rayleigh			Equilibrium		
	$\alpha$	$\delta^{238}\text{U}_{10}$	$R^2$	$\alpha$	$\delta^{238}\text{U}_{10}$	$R^2$
(2a)-1	1.01207	1.22	0.999	1.00122	1.22	0.999
(2af)-1	1.01192	1.01	0.98	1.00180	1.02	0.95
(2aw)-1	1.00298	0.96	0.996	1.00099	0.99	0.999
(2aw)-2	1.00377	1.05	0.999	1.00109	1.09	0.999
(2aw)-3	1.00076	0.68	0.91	1.0007503	0.75	0.92
(2awf)-1	1.00085	0.66	0.84	1.00703	0.70	0.83

Another process that produces heavy U isotope signatures is anoxic mobilization of U(IV) (chapter 3 of this thesis), but this can be ruled out here because the delta values only increase as the U concentration in solution decreases. Uranium reduction (e.g., by remaining *S. oneidensis* cells) can also be excluded as an explanation for the concentration decrease as microorganisms preferentially reduce  $^{238}\text{U}$ , resulting in an isotopically lighter solution.

During abiotic Cu sulfides oxidation by Mathur et al. (2005) (corresponding to the previously mentioned biotic experiments), the heavy Cu isotope was preferentially mobilized to aqueous copper (from  $\delta^{65}\text{Cu} = 2.60$  to  $\delta^{65}\text{Cu} = 5.34\text{‰}$  and from  $\delta^{65}\text{Cu} = 0.58$  to  $\delta^{65}\text{Cu} = 1.90\text{‰}$  [ $\pm 0.16$  at  $2\sigma$ ]). Kimball et al. (2009) observed similarly in the abiotic cases, that the leachates are isotopically heavier ( $\Delta_{\text{aq-min}} = \delta^{65}\text{Cu}_{\text{aq}} - \delta^{65}\text{Cu}_{\text{min}}$  for chalcopyrite: 1.37 ‰ and enargite 0.98‰,  $\pm 0.14\text{‰}$ ). The authors assume that in case of the abiotic experiments, an oxidized layer at the surface of an isotopically homogeneous mineral is formed and that partial oxidation leads to isotopically heavy  $\text{Cu}^{2+}$  which is preferentially leached in the solution compared to  $\text{Cu}^+$ . Hence, in the experiments of Kimball et al. (2009) and Mathur et al. (2005), heavy isotope enrichment is seen in the oxidized phase in the abiotic experiments just as in the U oxidation studied here.

In order to understand the entire system of U oxidation by *At. ferrooxidans*, we now combine the results of the biotic and abiotic experiments. There are several explanations for the lack of isotopic fractionation during biotic U oxidation. The simplest explanation may be that no isotope fractionation occurs during oxidation by biomass of *At. ferrooxidans*. However, it is

also possible that two different processes are taking place that are fractionating the isotopes in different directions, superimposing each other. Abiotic oxidation experiments by Wang et al. (2015a) showed that U(IV) dissolved with oxygen at acidic pH leads to isotopically lighter U(VI). Moreover, Wang et al. (2015b) suggests that equilibrium between the oxidized and mobilized U(VI) and the non-crystalline U(IV) may at least partially occur: equilibrium isotopic fractionation between dissolved U(IV) and dissolved U(VI) under anoxic conditions at low pH (0.2) results in a  $\delta^{238}\text{U}$  value  $1.64 \pm 0.16$  ‰, with U(IV) being enriched in  $^{238}\text{U}$  relative to U(VI). However, the isotopic equilibrium was reached after 19 days, but already after 0.7 days a  $\delta^{238}\text{U}$  value of -0.18 ‰ for U(VI) was measured. If we now assume for our experiments that the U(VI) has only experienced the process of oxidation and/or equilibrium exchange, we can speculate that we would obtain light isotopic values. However, our abiotic experiments indicate another process that fractionates U isotopes in the opposite direction. From the above conclusions, we assume that even small amounts of adsorbed U cause the solution to become heavier. Combining both processes may crudely result in the elimination of both isotope effects, i.e. a potential light signature from oxidation and heavy signatures of U(VI) remaining in solution after preferential adsorption of  $^{235}\text{U}$  onto the cells. In the case of iron, one can see that microbial oxidation leads to isotopic fractionation, which might not be measured directly in the case of uranium and, to some extent, copper. However, in the case of Fe, the observed isotope fractionation seem to be mainly caused in combination with precipitation (Johnson, 2020). This could support the hypothesis that biotic isotopic fractionation also occurs in the case of uranium, but is eliminated by the opposing values of abiotic fractionation. Another explanation could be that layer effects results in measurable U isotope fractionation as observed by Wang et al. (2015a): each layer must be completely oxidized before the next layer can be oxidized and the minor isotope effects may only arise from adsorption effects. Or some kind of kinetic effects during the dissolution step may fractionate the U isotopes in the opposite direction that adsorption does.

#### Environmental implications

In nature, many different processes overlap and it is complicated to reveal distinct biogeochemical processes related to U isotope fractionation. The suitability of U isotopes as a monitoring tool for remediation processes is still in development. In addition to U reduction with its distinct isotopic signature, other processes need to be studied in detail in order to understand the overall U isotopic cycle. Jemison et al. (2018) have conducted field experiments by re-oxidizing previously biologically reduced uranium in groundwater environments through

nitrate injections. As a result of the preceding reduction, initial U isotope fractionation towards heavy  $\delta^{238}\text{U}$  was observed. If such initial precipitates are re-mobilized, the passing groundwater will also become isotopically heavier. In addition, the previous chapter of this thesis has shown that organic ligands also lead to mobilization of non-crystalline U(IV), enriching the heavy U isotopes in solution. Thus, this study shows that U isotope fractionation results from U reduction and from mobilization with ligands rather than from microbial oxidation.

However, the acidic conditions of these experiments are far from natural conditions in the groundwater and only directly applicable for acid mine drainage and also bioleaching sites. There, it seems that bacteria, especially *At. ferrooxidans*, do not produce a distinct U isotope signatures which could be used as an indicator for underlying processes, but the abiotic control experiments indicate that U isotope fractionation could occur through oxidative mobilization by molecular oxygen, at higher carbonate concentrations (at a higher pH), and through possible subsequent adsorption. Further studies with a variety of microorganisms could strengthen the results.

To sum up, U(IV) oxidation with Fe(III) apparently does not result in U isotope fractionation. Abiotic experiments conducted in this study exhibit an increased  $\delta^{238}\text{U}$  value in the solution which was probably generated by adsorption processes after minor U oxidation. Oxidation with *At. ferrooxidans* does not appear to result in detectable U isotope fractionation which could be due to either the lack of a process that fractionates the isotopes or the presence of two processes that superimpose each other. The implication is that the isotopic signatures found in nature are more likely to be due to other processes such as reduction, abiotic oxidation, or mobilization with ligands.

## Conclusions and Perspectives

The analysis of isotope ratios of redox-sensitive elements provides the possibility to elucidate and trace numerous redox reactions and associated changes in elemental mobility and solubility. This thesis revealed that a sequential extraction, in combination with Fe and Cu isotopic measurements, can trace diverse mobilization and secondary enrichment processes in mine tailings. Consequently, mine tailings can be more specifically observed and remediated to avoid further environmental pollution, but also prospection-worthy mineralization can be detected easily. In future, this newly developed method can be applied to numerous depth profiles and/or mine tailings to discover and use processes like secondary elemental enrichment also on a larger scale profitably.

Moreover, U *in-situ* leaching areas and (bio)remediation sites often produce large amounts of non-crystalline U(IV), which is known for its low long-term stability. Mobilized U can be transported from the mining area and may contaminate e.g., drinking water. Methods that are solely based on concentration measurements, are severely limited because common transport processes such as dilution or adsorption could change the U concentration in the groundwater significantly, thus biasing the results. Therefore, U isotope fractionation is (1) a powerful tool, as it is proved by this thesis, to distinguish between U reduction, U complexation or (a)biotic U oxidation, and it (2) helps to further characterize and enhance remediation efforts. Future work can apply the performed methods (U complexation and U oxidation) to even more complex samples in column experiments or to natural samples, by applying the knowledge on individual isotope signatures of this study.

## Supporting Information

### Supporting Information for Chapter II

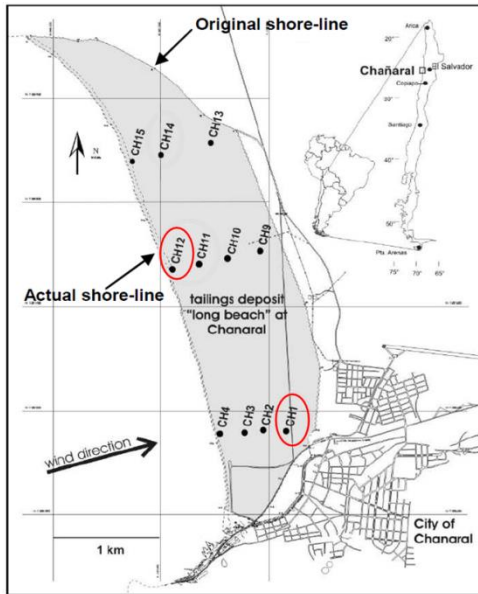


**Figure S II.1.** Sample area in the Chañaral bay (modified after Dold, 2007).

**Table S II.1.** Steps for Cu, Fe and Zn separation modified after Borrok et al. (2007).

Step	Acid	Amount [ml]
wash resin	7 M HCl	10
wash resin	MQ / 5 % HNO <sub>3</sub> / MQ	10+10+10
HCl conditioning	9 M HCl	12
load sample	9 M HCl	1
matrix wash	9 M HCl	1+3+3
Cu fraction	5 M HCl	1+2+5+5+5
Fe fraction	1 M HCl	1+1+5+5
Zn fraction	MQ	1+1+5+5

## Supporting Information for Chapter III

### Organic ligands

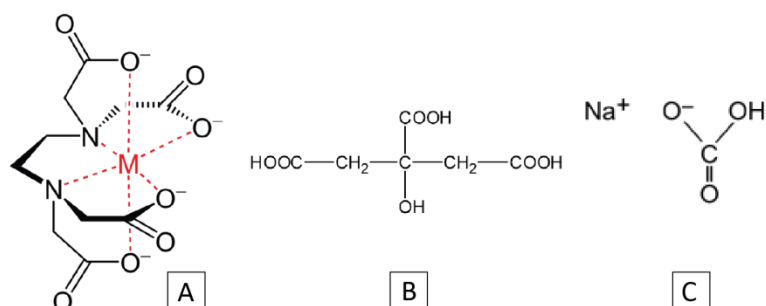


**Figure S III.1.** (A) Ethylenediaminetetraacetic acid (EDTA), (B) citric acid, (C), sodium bicarbonate (Gavrilescu et al., 2009; Jesús et al., 2011).

### Widdel Low Phosphate (WLP) medium

**Table S III.1.** Composition of WLP medium

Compound	Concentration (mM)
CaCl <sub>2</sub> · 2H <sub>2</sub> O	0.68
KCl	6.71
KH <sub>2</sub> PO <sub>4</sub>	0.22
MgCl <sub>2</sub> · 6H <sub>2</sub> O	2.46
NaCl	85.56
NH <sub>4</sub> Cl	4.67
NaHCO <sub>3</sub>	30
Pipes	20
pH	7.3

## Anion exchange resin separation of U(VI) and U(IV)

**Table S III.2.** Recovery of U after ion exchange separation of U(VI) from U(IV) for the citrate experiment ((1a)-citrate). U(IV)/U(VI) composition in the starting material (solid phase) and after 1, 5.5 and 22h (filtered mobilized fraction).

time [h]		[ $\mu$ M]	[%] of total collected	% U recovered post-separation <sup>2</sup>	$\delta^{238}\text{U}$ [‰]
start material	U(IV) solid	337.94	84.5		
	U(VI) solid	62.14	15.5		
	Sum U(IV) + U(VI) solid	400.08			
	total pre-separation <sup>1</sup>	353.99		113.02	0.00
1	U(IV) mobilized	28.92	56.6		
	U(VI) mobilized	22.21	43.4		
	Sum U(IV) + U(VI) solid	51.12			
	total pre-separation <sup>1</sup>	56.97		89.73	0.31
5.5	U(IV) mobilized	18.56	53.1		
	U(VI) mobilized	16.41	46.9		
	Sum U(IV) + U(VI) solid	34.97			
	total pre-separation <sup>1</sup>	37.32		93.72	0.30
22	U(IV) mobilized	52.17	64.9		
	U(VI) mobilized	28.16	35.1		
	Sum U(IV) + U(VI) solid	80.34			
	total pre-separation <sup>1</sup>	98.38		81.66	0.29

<sup>1</sup> one aliquot of the sample was analyzed for U concentration before anion exchange resin separation

<sup>2</sup> % U recovered post-separation % = (total U mobilized (or solid))/(100 x total U pre-separation), i.e., how much of the initially measured U concentration was recovered after the ion exchange separation

**Table S III.3.** Results for U(VI) and U(IV) separation of samples from experiments ((2a)-EDTA, (2a)-bicarbonate, and (2a)-citrate). The first table corresponds to the solid phase before addition of the ligand (after the bicarbonate wash step) and the second table to mobilized U, 6.5h after addition of the ligand (filtered).

<b>After bicarb wash, before addition of the ligand</b>		<b>[<math>\mu</math>M]</b>	<b>[%] of total U</b>	<b><math>\delta^{238}\text{U}</math> [‰]</b>	
NCU4 (for EDTA)	U(IV)	307.5	94.4	-0.03	<b>Starting material</b>  <b>mean U(IV)%</b> <b>s.d.</b> <hr style="width: 100%;"/> 96.7                  2.0
NCU4 (for EDTA)	U(VI)	18.4	5.6		
NCU4 (for citrate)	U(IV)	326.3	97.5	0.05	
NCU4 (for citrate)	U(VI)	8.5	2.5		
NCU4 (for bicarb)	U(IV)	248.2	98.2	0.04	
NCU4 (for bicarb)	U(VI)	4.5	1.8		
<b>t6.5h, 0.22<math>\mu</math>m filtered</b>		<b>[<math>\mu</math>M]</b>	<b>[%] of aqueous phase</b>	<b><math>\delta^{238}\text{U}</math> [‰]</b>	
EDTA + NCU4	U(IV)	61.3	99.2	0.33	<b>t6.5h</b>  <b>mean U(IV)%</b> <b>s.d.</b> <hr style="width: 100%;"/> 95.5                  3.3
EDTA + NCU4	U(VI)	0.5	0.8		
Citrate + NCU4	U(IV)	12.1	93.1	0.27	
Citrate + NCU4	U(VI)	0.9	6.9		
Bicarb + NCU4	U(IV)	90.5	94.2	0.24	
Bicarb + NCU4	U(VI)	5.6	5.8		



## Mass balance calculations

**Table S III.4.** Mass balance calculations for solution (mobilized U fraction) and the remaining, unreacted non-crystalline U(IV) (collected on the filter).

	solution			filter / non-crystalline U(IV)		mass balance
	Time [h]	$\delta^{238}\text{U}$	Fraction of initial U	$\delta^{238}\text{U}$	fraction	total
(1a) 1 mM EDTA	1	0.50 ‰	0.092	-0.07 ‰	0.908	-0.02 ‰
	23	0.40 ‰	0.251	-0.30 ‰	0.749	-0.13 ‰
(1a) 500 mM bicarbonate	1	0.19 ‰	0.547	-0.14 ‰	0.453	0.04 ‰
	23	0.12 ‰	0.680	-0.20 ‰	0.320	0.02 ‰
(1a) 1 mM citrate	0.5	0.05 ‰	0.060	0.05 ‰	0.940	0.05 ‰
	2	0.14 ‰	0.126	0.00 ‰	0.874	0.02 ‰
	71	0.29 ‰	0.432	-0.13 ‰	0.568	0.05 ‰

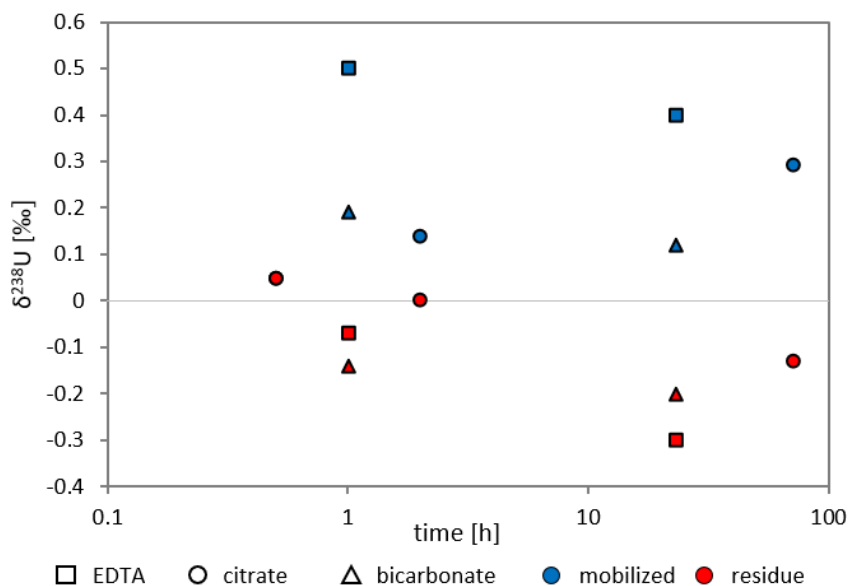


**Figure S III.2.**  $\delta^{238}\text{U}$  [‰] for solution/mobilized U fraction in blue, the filter residues in red, showing lighter  $\delta^{238}\text{U}$  values for residual U(IV) compared to the mobilized fraction (squares: EDTA, circles: citrate, triangle: bicarbonate).

## Rayleigh fractionation model

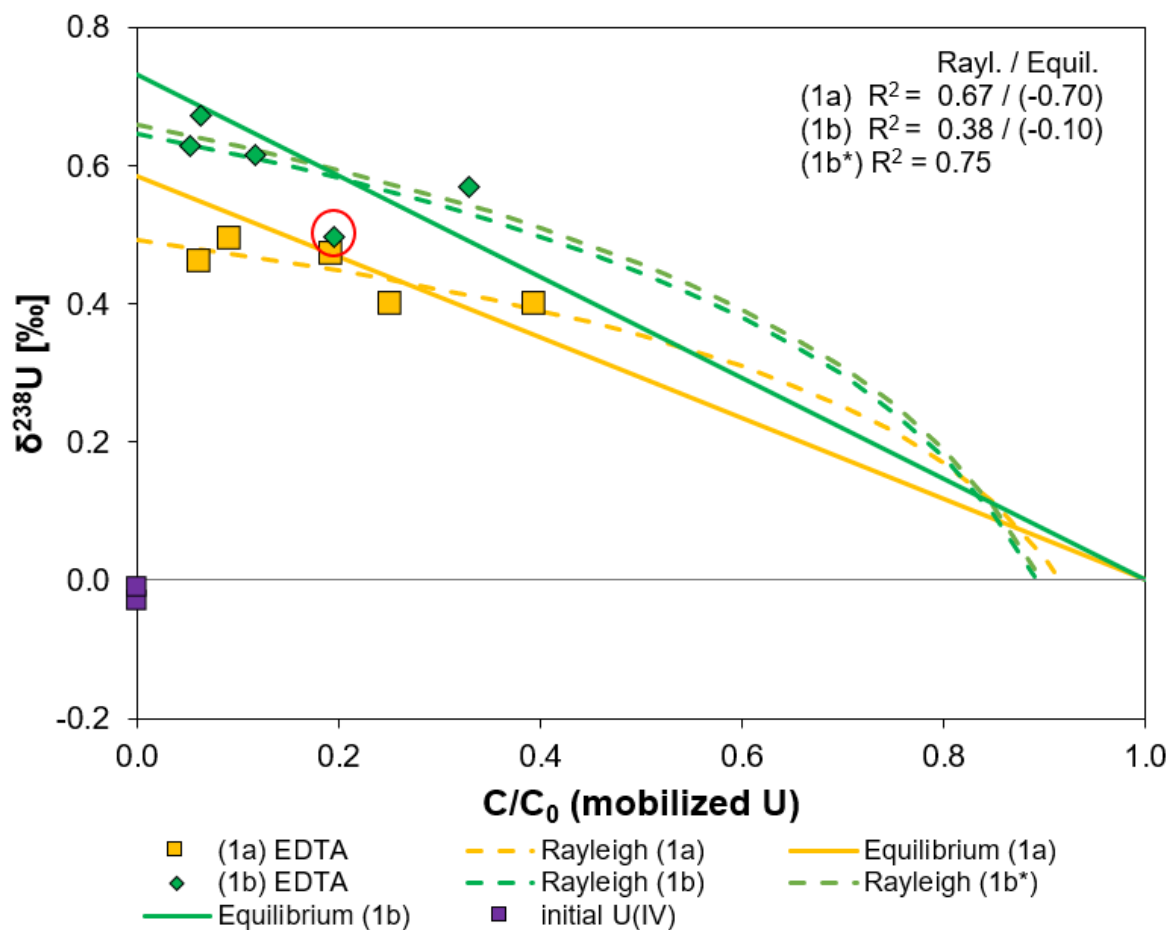


**Figure S III.3.** Rayleigh and equilibrium models for measured experimental  $\delta^{238}\text{U}$  values [in ‰] for the mobilized U versus the fraction of mobilized U ( $C/C_0$ ) for EDTA experiments (1a) and (1b). Due to its obvious deviation from the rest of the data point, the point at 20% mobilization ( $\delta^{238}\text{U} = 0.5$  ‰, marked with a red circle) was excluded in the calculation (1b\*). As a result, the  $R^2$  value improves from 0.38 to 0.75. The model for equilibrium isotope fractionation does not fit the data.

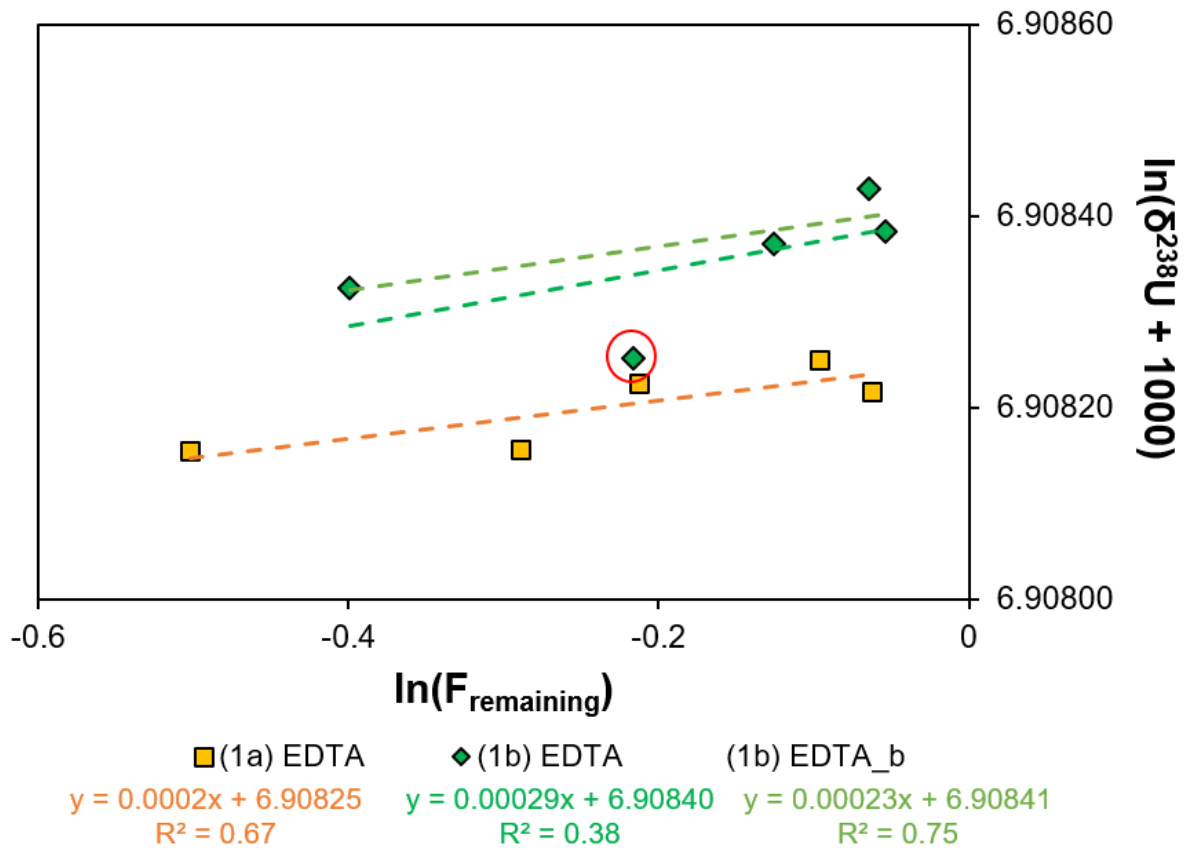


**Figure S III.4.** Rayleigh fitting  $\ln F$  versus  $\ln(\delta^{238}\text{U} + 1000)$  for experiment 1 with 1 mM EDTA. (1a) with a yellow fit line, (1b) with a dark green fit line. For (1b)-EDTA, the data point at 20% mobilization ( $\delta^{238}\text{U} = 0.5 \text{ ‰}$ , marked with a red circle) was excluded (light green fit line), resulting in an improved fit.

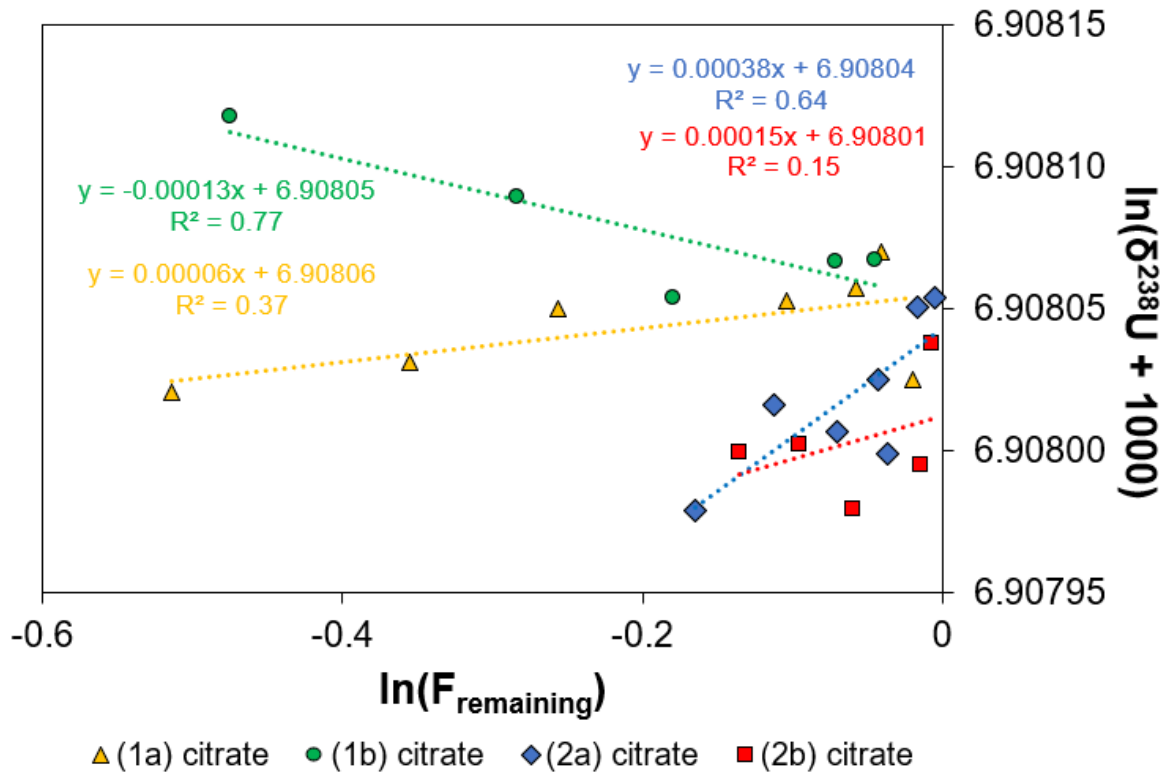


**Figure S III.5.** Measured experimental  $\delta^{238}\text{U}$  values [in ‰] for mobilized U versus the fraction of mobilized U ( $C/C_0$ ) for 1 mM citrate. No Rayleigh or equilibrium model could be fitted.

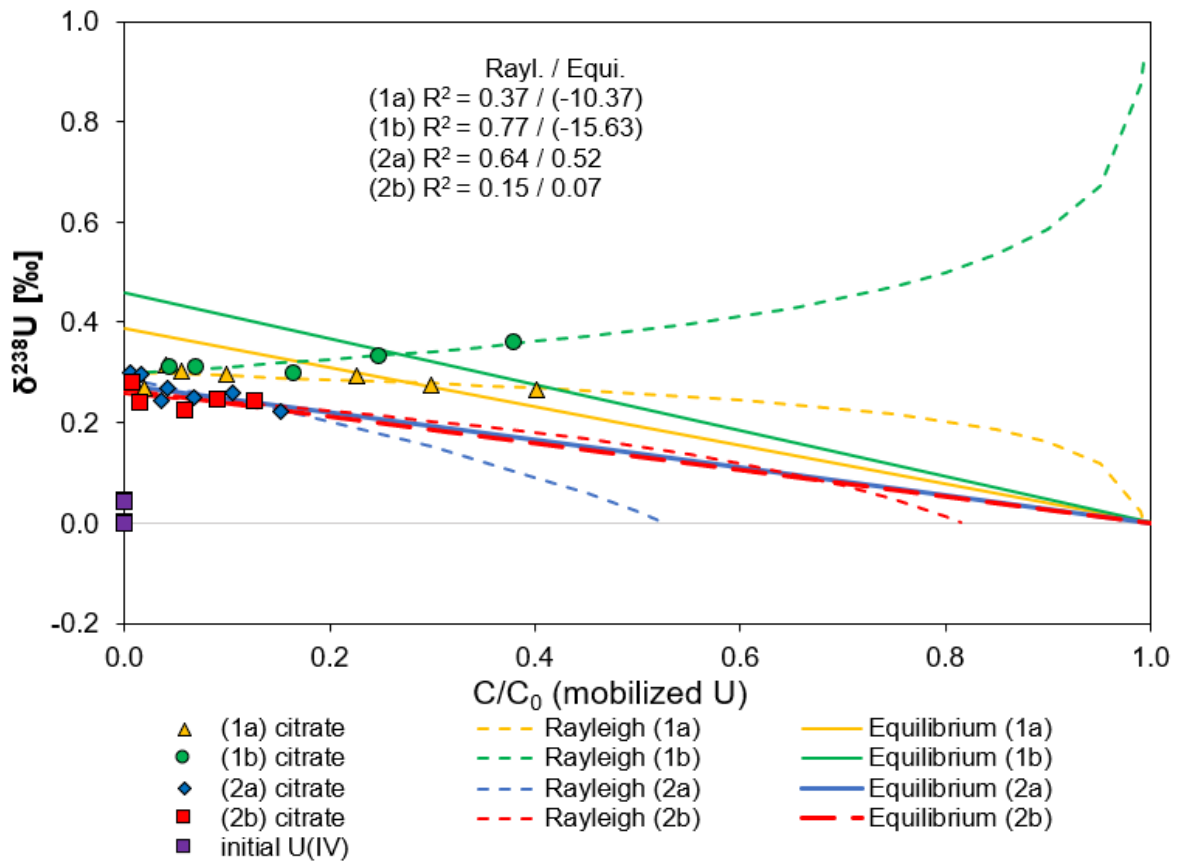


Figure S III.6. Rayleigh fitting  $\ln F$  versus  $\ln(\delta^{238}\text{U} + 1000)$  for experiment 1 and 2 with 1 mM citrate.

## Concentration and isotope data

### Control experiment

**Table S III.5.** Control experiment (initial U(IV) concentration ~400  $\mu\text{M}$ )

time [h]	mobilized U fraction [ $\mu\text{M}$ ]
0	0.41
1	0.42
2	0.37
5.5	0.39
23	0.32
29	0.39
48	0.41
144	0.41

### EDTA

**Table S III.6.** (1a) 1 mM EDTA

time [h]	$\mu\text{M}$	C/C <sub>0</sub>	$\delta^{238}\text{U}$ [‰]	2 s.d.
0	0.28			
0.1	3.28	0.007	0.21	0.06
0.5	29.85	0.060	0.46	0.06
1	45.34	0.092	0.50	0.05
2	3.15	0.006		
3.25	9.08	0.018		
4.5	1.03	0.002		
5.5	94.59	0.192	0.47	0.05
23	123.84	0.251	0.40	0.05
28	142.31	0.288		
47	194.84	0.395	0.40	0.01
71	224.45	0.455		
143	212.48	0.431		
181	153.28	0.311		
initial U(IV)	493.41		-0.03	0.05

**Table S III.7.** (1b) 1 mM EDTA

<b>time [h]</b>	<b><math>\mu\text{M}</math></b>	<b><math>C/C_0</math></b>	<b><math>\delta^{238}\text{U}</math> [‰]</b>	<b>2 s.d.</b>
0	0.35			
0.1	4.42	0.009	0.18	0.01
0.5	26.12	0.053	0.63	0.00
1	30.82	0.062	0.67	0.01
2	2.44	0.005		
3.25	4.98	0.010		
4.5	73.10	0.148		
5.5	58.49	0.118	0.62	0.03
23	96.55	0.195	0.50	0.06
28	87.00	0.176		
47	163.02	0.329	0.57	0.03
71	320.19	0.646		
143	131.61	0.266		
181	163.50	0.330		
initial U(IV)	495.46		-0.06	0.03

**Table S III.8.** (2a) 1 mM EDTA

<b>time [h]</b>	<b><math>\mu\text{M}</math></b>	<b><math>C/C_0</math></b>	<b><math>\delta^{238}\text{U}</math> [‰]</b>	<b>2 s.d.</b>
initial U(IV)	408		-0.03	0.04
0.25	16.6	0.04	0.53	0.04
1	39.7	0.10	0.41	0.01
3.25	72.2	0.18	0.38	0.08
6.5	98.8	0.24	0.33	0.05
23	155.6	0.38		
72	183.6	0.45	0.26	0.02
168	242.5	0.59	0.22	0.01

**Table S III.9.** (2b) 1 mM EDTA

<b>time [h]</b>	<b><math>\mu\text{M}</math></b>	<b><math>C/C_0</math></b>	<b><math>\delta^{238}\text{U}</math> [‰]</b>	<b>2 s.d.</b>
initial U(IV)	377		-0.01	0.03
0.25	17.5	0.05	0.36	0.07
1	39.5	0.10	0.28	0.02
3.25	72.7	0.19	0.24	0.05
6.5	110.8	0.29	0.24	0.03
23	173.4	0.46		
72	198.3	0.53	0.18	0.01
168	248.7	0.66	0.16	0.02

## Bicarbonate

Table S III.10. (1a) 500 mM bicarbonate

time [h]	$\mu\text{M}$	$\text{C}/\text{C}_0$	$\delta^{238}\text{U}$ [‰]	2 s.d.
0	0.29	0		
0.1	56.03	0.094	-0.16	0.01
0.5	243.47	0.409	0.17	0.02
1	325.35	0.547	0.19	0.03
2	340.50	0.573	0.19	0.02
3.25	337.18	0.567	0.17	0.01
4.5	341.79	0.575		
5.5	368.42	0.619		
23	404.27	0.680	0.12	0.03
28	411.93	0.693		
47	402.04	0.676	0.09	0.05
71	408.53	0.687		
143	405.38	0.682		
181	407.97	0.686		
initial U(IV)	594.72	0.000	-0.01	0.06

Table S III.11. (1b) 500 mM bicarbonate

time [h]	$\mu\text{M}$	$\text{C}/\text{C}_0$	$\delta^{238}\text{U}$ [‰]	2 s.d.
0	0.89	0.000		
0.1	34.69	0.060	-0.22	0.04
0.5	275.76	0.476	0.17	0.03
1	321.35	0.555	0.21	0.03
2	345.37	0.596	0.21	0.02
3.25	332.71	0.574	0.18	0.03
4.5	340.39	0.588		
5.5	353.82	0.611		
23	396.72	0.685	0.11	0.03
28	388.81	0.671		
47	401.21	0.693	0.10	0.04
71	403.94	0.697		
143	399.92	0.690		
181	402.69	0.695		
initial U(IV)	579.35	0.000	-0.01	0.01



**Table S III.12.** (2a) 500 mM bicarbonate

<b>time</b>	<b><math>\mu\text{M}</math></b>	<b><math>\text{C}/\text{C}_0</math></b>	<b><math>\delta^{238}\text{U}</math> [‰]</b>	<b>2s.d.</b>
initial U(IV)	378	0	0.04	0.05
0.1	15.2	0.04	0.29	0.03
0.25	51.7	0.14	0.34	0.01
0.5	71.8	0.19		
1	88.9	0.24	0.29	0.08
2	104.1	0.28		
3.25	117.0	0.31		
4.5	125.5	0.33	0.22	0.06
6.5	135.9	0.36	0.24	0.03
23	166.5	0.44		
72	196.1	0.52		
168	217.2	0.58	0.08	0.06

**Table S III.13.** (2b) 500 mM bicarbonate

<b>time</b>	<b><math>\mu\text{M}</math></b>	<b><math>\text{C}/\text{C}_0</math></b>	<b><math>\delta^{238}\text{U}</math> [‰]</b>	<b>2s.d.</b>
initial U(IV)	375	0.00	0.03	0.01
0.1	16.3	0.04	0.25	0.07
0.25	53.5	0.14	0.29	0.01
0.5	70.6	0.19		
1	87.5	0.23	0.25	0.07
2	102.6	0.27		
3.25	116.7	0.31		
4.5	125.0	0.33	0.20	0.03
6.5	137.3	0.37	0.18	0.01
23	169.9	0.45		
72	199.0	0.53		
168	220.6	0.59	0.07	0.06

## Citrate

**Table S III.14.** (1a) 1 mM citrate

<b>time [h]</b>	<b><math>\mu\text{M}</math> total</b>	<b><math>C/C_0</math></b>	<b><math>\delta^{238}\text{U}</math> [‰]</b>	<b>2s.d.</b>
0	0.0	0.000		
0.1	0.9	0.002	0.23	0.08
0.25	8.6	0.020	0.27	0.05
0.5	11.8	0.027		
1	17.5	0.040	0.31	0.01
2	24.6	0.056	0.30	0.07
3.5	36.2	0.082		
4.5	43.4	0.099	0.30	0.04
5.5	48.2	0.110		
22	99.0	0.226	0.29	0.04
29	110.5	0.252		
47	131.0	0.299	0.28	0.07
96	158.8	0.362		
144	176.2	0.402	0.27	0.06
initial U(IV)	438.5	0.000	0.00	0.03

**Table S III.15.** (1b) 1 mM citrate

<b>time [h]</b>	<b><math>\mu\text{M}</math> total</b>	<b><math>C/C_0</math></b>	<b><math>\delta^{238}\text{U}</math> [‰]</b>	<b>2s.d.</b>
0	0.0	0.000		
0.1	0.9	0.002	0.31	0.02
0.25	7.1	0.016		
0.5	10.2	0.022		
1	15.0	0.033		
2	20.2	0.044	0.31	0.04
3.5	30.2	0.066		
4.5	31.7	0.069	0.31	0.04
5.5	37.1	0.081		
22	75.3	0.164	0.30	0.02
29	86.5	0.189		
47	113.2	0.247	0.33	0.01
96	148.2	0.323		
144	173.4	0.378	0.36	0.05
initial U(IV)	458.5	0.000	0.00	0.04

**Table S III.16.** (2a) 1 mM citrate

<b>time</b>	<b><math>\mu\text{M}</math></b>	<b><math>\text{C}/\text{C}_0</math></b>	<b><math>\delta^{238}\text{U}</math> [‰]</b>	<b>2s.d.</b>
initial U(IV)	375	0	0.05	0.06
0.1	0.4	0.00	0.37	0.01
0.25	2.1	0.01	0.30	0.06
0.5	4.2	0.01		
1	6.1	0.02	0.30	0.03
2	9.0	0.02		
3.25	11.6	0.03		
4.5	13.5	0.04	0.24	0.03
6.5	15.7	0.04	0.27	0.07
23	25.4	0.07	0.25	0.02
72	39.7	0.11	0.26	0.05
168	56.9	0.15	0.22	0.02

**Table S III.17.** (2b) 1 mM citrate

<b>time</b>	<b><math>\mu\text{M}</math></b>	<b><math>\text{C}/\text{C}_0</math></b>	<b><math>\delta^{238}\text{U}</math> [‰]</b>	<b>2s.d.</b>
initial U(IV)	431	0	0.04	0.04
0.1	0.5	0.00	0.38	0.01
0.25	2.9	0.01	0.28	0.03
0.5	4.4	0.01		
1	6.2	0.01	0.24	0.03
2	8.9	0.02		
3.25	11.4	0.03		
4.5	13.1	0.03		
6.5	15.7	0.04		
23	25.1	0.06	0.22	0.01
72	39.2	0.09	0.25	0.02
168	54.7	0.13	0.24	0.02

## Supporting Information for Chapter IV

**Table S IV.1.** Overview over all performed experiments.

(1) Fe(III)		(2) <i>At. Ferrooxidans</i> grown on tetrathionate	(3) <i>At. Ferrooxidans</i> grown on elemental sulfur	
(1a)-1	100 µM Fe(III)	(2b) biotic	(3b)-1	biotic
(1a)-2	100 µM Fe(III)		(3b)-2	biotic
(1b)-1	200 µM Fe(III)	(2a) abiotic	(3bf)-1	biotic + formate
(1b)-2	200 µM Fe(III)		(3bf)-2	biotic + formate
(1c)-1	400 µM Fe(III)		(3bw)-1	biotic + bicarbonate wash
(1c)-2	400 µM Fe(III)		(3bw)-2	biotic + bicarbonate wash
			(3bwf)-1	biotic + bicarbonate wash + formate
			(3bwf)-2	biotic + bicarbonate wash + formate
			(3a)-1	abiotic
			(3af)-1	abiotic + formate
			(3af)-2	abiotic + formate
			(3aw)-1	abiotic + bicarbonate wash
			(3aw)-2	abiotic + bicarbonate wash
			(3aw)-3	abiotic + bicarbonate wash
			(3awf)-1	abiotic + bicarbonate wash + formate
			(3awf)-2	abiotic + bicarbonate wash + formate

**Table S IV.2.** pH values for abiotic experiment. The first experiments without bicarbonate wash show a higher pH than the other experiments.

experiment	pH	
	before start	after start
(3a)-1	2.52	3.35
(3af)-1	2.59	3.29
(3af)-2	2.48	3.73
(3aw)-1	-	2.72
(3aw)-2	-	2.72
(3aw)-3	2.45	2.60
(3awf)-1	2.55	2.66
(3awf)-2	2.58	2.61

**Table IV.3.** pH values for biotic experiment.

experiment	pH before start	pH after start
(3b)-1	1.96	2.08
(3b)-2	2.44	2.14
(3bf)-1	2.10	2.51
(3bf)-2	2.02	2.17
(3bw)-1	1.92	1.92
(3bw)-2	2.00	2.00
(3bwf)-1	1.97	1.97
(3bwf)-2	1.91	1.98

**Table IV.4.** Mobilized fraction ( $C/C_0$ ) and corresponding  $\delta^{238}\text{U}$  values (in ‰) for all abiotic experiments. Remarkable is that during the first concentration increase no U isotope fractionation is observed. When the U concentration decreases (after reaching a maximum), the  $\delta^{238}\text{U}$  values increase.

(3a)-1		(3af)-1		(3aw)-1		(3aw)-2		(3aw)-3		(3awf)-1	
$C/C_0$	$\delta^{238}\text{U}$ [‰]	$C/C_0$	$\delta^{238}\text{U}$ [‰]	$C/C_0$	$\delta^{238}\text{U}$ [‰]	$C/C_0$	$\delta^{238}\text{U}$ [‰]	$C/C_0$	$\delta^{238}\text{U}$ [‰]	$C/C_0$	$\delta^{238}\text{U}$ [‰]
0.00	0.00	0.00	0.00	0.00	0.02	0.00	-0.01	0.00	0.02	0.00	0.02
0.00	-	0.00	-	0.21	0.04	0.18	0.03	0.17	0.00	0.14	0.01
0.02	-0.24	0.04	-0.02	0.24	-	0.21	-	0.34	0.02	0.28	0.00
0.03	-	0.06	-	0.28	-0.01	0.25	-0.03	0.45	-	0.41	-
0.05	-0.13	0.08	0.01	0.17	0.36	0.18	0.28	0.51	0.15	0.44	0.16
0.03	-	0.06	-	0.08	0.70	0.09	0.71	0.24	-	0.18	-
0.04	0.69	0.05	0.48	0.05	0.82	0.05	0.85	0.21	0.56	0.16	0.61
0.02	-	0.03	-	-	-	0.17	-	0.17	-	0.12	-
0.03	0.88	0.03	0.71	-	-	0.17	0.56	0.17	0.56	0.12	0.54
0.04	-	0.03	-	-	-	0.19	-	0.19	-	0.13	-
0.05	0.55	0.02	0.72	-	-	0.21	0.43	0.21	0.43	0.15	0.43

## References

- AbdEl-Sabour, M.F., 2007. Remediation and bioremediation of uranium contaminated soils. *Electron. J. Environ. Agric. Food Chem.* 6, 2009–2023.
- Abdelouas, A., 2006. Uranium mill tailings: Geochemistry, mineralogy, and environmental impact. *Elements* 2, 335–341. <https://doi.org/10.2113/gselements.2.6.335>
- Abe, M., Suzuki, T., Fujii, Y., Hada, M., Hirao, K., 2008. An ab initio molecular orbital study of the nuclear volume effects in uranium isotope fractionations. *J. Chem. Phys.* 129. <https://doi.org/10.1063/1.2992616>
- Abhilash, Mehta, K.D., Kumar, V., Pandey, B.D., Tamrakar, P.K., 2011. Bioleaching - An alternate uranium ore processing technology for India. *Energy Procedia* 7, 158–162. <https://doi.org/10.1016/j.egypro.2011.06.021>
- Abhilash, Pandey, B.D., 2013. Microbially assisted leaching of uranium - A review. *Miner. Process. Extr. Metall. Rev.* 34, 81–113. <https://doi.org/10.1080/08827508.2011.635731>
- Akcil, A., Koldas, S., 2006. Acid Mine Drainage (AMD): causes, treatment and case studies. *J. Clean. Prod.* 14, 1139–1145. <https://doi.org/10.1016/j.jclepro.2004.09.006>
- Akerman, A., Poitrasson, F., Oliva, P., Audry, S., Prunier, J., Braun, J.J., 2014. The isotopic fingerprint of Fe cycling in an equatorial soil-plant-water system: The Nsimi watershed, South Cameroon. *Chem. Geol.* 385, 104–116. <https://doi.org/10.1016/j.chemgeo.2014.07.003>
- Alan A. DiSpirito, Tuovinen, O.H., 1982a. Uranous Ion Oxidation and Carbon Dioxide Fixation by *Thiobacillus ferrooxidans*. *Arch. Microbiol.* 133, 28–32.
- Alan A. DiSpirito, Tuovinen, O.H., 1982b. Kinetics of Uranous Ion and Ferrous Iron Oxidation by *Thiobacillus ferrooxidans*. *Arch. Microbiol.* 133, 33–37.
- Alessi, D.S., Lezama-Pacheco, J.S., Stubbs, J.E., Janousch, M., Bargar, J.R., Persson, P., Bernier-Latmani, R., 2014. The product of microbial uranium reduction includes multiple species with U(IV)-phosphate coordination. *Geochim. Cosmochim. Acta* 131, 115–127. <https://doi.org/10.1016/j.gca.2014.01.005>
- Alessi, D.S., Uster, B., Borca, C.N., Grolimund, D., Bernier-Latmani, R., 2013. Beam-induced oxidation of monomeric U(IV) species. *J. Synchrotron Radiat.* 20, 197–199. <https://doi.org/10.1107/S0909049512041763>
- Alessi, D.S., Uster, B., Veeramani, H., Suvorova, E.I., Lezama-Pacheco, J.S., Stubbs, J.E., Bargar, J.R., Bernier-Latmani, R., 2012. Quantitative separation of monomeric U(IV) from UO<sub>2</sub> in products of U(VI) reduction. *Environ. Sci. Technol.* 46, 6150–6157. <https://doi.org/10.1021/es204123z>
- Andersen, M.B., Matthews, A., Vance, D., Bar-Matthews, M., Archer, C., de Souza, G.F., 2018. A 10-fold decline in the deep Eastern Mediterranean thermohaline overturning circulation during the last interglacial period. *Earth Planet. Sci. Lett.* 503, 58–67. <https://doi.org/https://doi.org/10.1016/j.epsl.2018.09.013>
- Andersen, M.B., Stirling, C.H., Weyer, S., 2017. Uranium Isotope Fractionation. *Rev. Mineral. Geochemistry* 82, 799–850. <https://doi.org/10.2138/rmg.2017.82.19>
- Anderson, R.T., Vrionis, H., Ortiz-Bernad, I., Resch, C.T., Long, P.E., Dayvault, R., Karp, K.,

- Marutzky, S., Metzler, D.R., Peacock, A.D., White, D.C., Lowe, M., Lovley, D.R., 2003. Stimulating the In Situ Activity of *Geobacter* Species To Remove Uranium from the Groundwater of a Uranium-Contaminated Aquifer. *Appl. Environ. Microbiol.* 69, 5884–5891. <https://doi.org/10.1128/AEM.69.10.5884>
- Arnold, G.L., Anbar, A.D., Barling, J., Lyons, T.W., 2004. Molybdenum Isotope Evidence for Widespread Anoxia in Mid-Proterozoic Oceans. *Science* (80-. ). 304, 87–90. <https://doi.org/10.1126/science.1091785>
- Asael, D., Tissot, F.L.H., Reinhard, C.T., Rouxel, O., Dauphas, N., Lyons, T.W., Ponzevera, E., Liorzou, C., Chéron, S., 2013. Coupled molybdenum, iron and uranium stable isotopes as oceanic paleoredox proxies during the Paleoproterozoic Shunga Event. *Chem. Geol.* 362, 193–210. <https://doi.org/10.1016/j.chemgeo.2013.08.003>
- Bacon, J.R., Davidson, C.M., 2008. Is there a future for sequential chemical extraction? *Analyst* 133, 25–46. <https://doi.org/10.1039/b711896a>
- Baker, M.G., Lalonde, S. V., Konhauser, K.O., Foght, J.M., 2010. Role of extracellular polymeric substances in the surface chemical reactivity of *hymenobacter aerophilus*, a psychrotolerant bacterium. *Appl. Environ. Microbiol.* 76, 102–109. <https://doi.org/10.1128/AEM.02006-09>
- Balci, N., Bullen, T.D., Witte-Lien, K., Shanks, W.C., Motelica, M., Mandernack, K.W., 2006a. Iron isotope fractionation during microbially stimulated Fe(II) oxidation and Fe(III) precipitation. *Geochim. Cosmochim. Acta* 70, 622–639. <https://doi.org/10.1016/j.gca.2005.09.025>
- Balci, N., Bullen, T.D., Witte-Lien, K., Shanks, W.C., Motelica, M., Mandernack, K.W., 2006b. Iron isotope fractionation during microbially stimulated Fe(II) oxidation and Fe(III) precipitation. *Geochim. Cosmochim. Acta* 70, 622–639. <https://doi.org/10.1016/j.gca.2005.09.025>
- Balci, N., Mayer, B., Shanks, W.C., Mandernack, K.W., 2012. Oxygen and sulfur isotope systematics of sulfate produced during abiotic and bacterial oxidation of sphalerite and elemental sulfur. *Geochim. Cosmochim. Acta* 77, 335–351. <https://doi.org/10.1016/j.gca.2011.10.022>
- Balistrieri, L.S., Borrok, D.M., Wanty, R.B., Ridley, W.I., 2008. Fractionation of Cu and Zn isotopes during adsorption onto amorphous Fe(III) oxyhydroxide: Experimental mixing of acid rock drainage and ambient river water. *Geochim. Cosmochim. Acta* 72, 311–328. <https://doi.org/10.1016/j.gca.2007.11.013>
- Ballerstedt, H., Pakostova, E., Johnson, D.B., Schippers, A., 2017. Approaches for eliminating bacteria introduced during in situ bioleaching of fractured sulfidic ores in deep subsurface. *Solid State Phenom.* 262 SSP, 70–74. <https://doi.org/10.4028/www.scientific.net/SSP.262.70>
- Bargar, J.R., Williams, K.H., Campbell, K.M., Long, P.E., Stubbs, J.E., Suvorova, E.I., Lezama-Pacheco, J.S., Alessi, D.S., Stylo, M., Webb, S.M., Davis, J.A., Giammar, D.E., Blue, L.Y., Bernier-Latmani, R., 2013. Uranium redox transition pathways in acetate-amended sediments. *Proc. Natl. Acad. Sci.* 110, 4506–4511. <https://doi.org/10.1073/pnas.1219198110>
- Basu, A., Brown, S.T., Christensen, J.N., Depaolo, D.J., Reimus, P.W., Heikoop, J.M.,



- Woldegabriel, G., Simmons, A.M., House, B.M., Hartmann, M., Maher, K., 2015. Isotopic and geochemical tracers for U(VI) reduction and U mobility at an in situ recovery U mine. *Environ. Sci. Technol.* 49, 5939–5947.  
<https://doi.org/10.1021/acs.est.5b00701>
- Basu, A., Sanford, R.A., Johnson, T.M., Lundstrom, C.C., Löffler, F.E., 2014. Uranium isotopic fractionation factors during U(VI) reduction by bacterial isolates. *Geochim. Cosmochim. Acta* 136, 100–113. <https://doi.org/10.1016/j.gca.2014.02.041>
- Bea, S.A., Ayora, C., Carrera, J., Saaltink, M.W., Dold, B., 2010. Geochemical and environmental controls on the genesis of soluble efflorescent salts in Coastal Mine Tailings Deposits: A discussion based on reactive transport modeling. *J. Contam. Hydrol.* 111, 65–82. <https://doi.org/10.1016/j.jconhyd.2009.12.005>
- Beard, B.L., Handler, R.M., Scherer, M.M., Wu, L., Czaja, A.D., Heimann, A., Johnson, C.M., 2010. Iron isotope fractionation between aqueous ferrous iron and goethite. *Earth Planet. Sci. Lett.* 295, 241–250. <https://doi.org/10.1016/j.epsl.2010.04.006>
- Beard, B.L., Johnson, C.M., 2004. Fe Isotope Variations in the Modern Beard, B.L., Johnson, C.M., 2004. Fe Isotope Variations in the Modern and Ancient Earth and Other Planetary Bodies. *Rev. Mineral. Geochemistry* 55, 319 LP – 357. and Ancient Earth and Other Planetary Bodies. *Rev. Mineral. Geochemistry* 55, 319 LP – 357.
- Beard, B.L., Johnson, C.M., 1999. High precision iron isotope measurements of terrestrial and lunar samples. *Geochim. Cosmochim. Acta* 63, 1653–1660.
- Berglund, M., Wieser, M.E., 2011. Isotopic compositions of the elements 2009 (IUPAC technical report). *Pure Appl. Chem.* 83, 397–410. <https://doi.org/10.1351/PAC-REP-10-06-02>
- Bernier-Latmani, R., Veeramani, H., Vecchia, E.D., Junier, P., Lezama-Pacheco, J.S., Suvorova, E.I., Sharp, J.O., Wigginton, N.S., Bargar, J.R., 2010. Non-uraninite products of microbial U (VI) reduction. *Environ. Sci. Technol.* 44, 9456–9462.
- Bhattacharyya, A., Campbell, K.M., Kelly, S.D., Roebbert, Y., Weyer, S., Bernier-Latmani, R., Borch, T., 2017. Biogenic non-crystalline U (IV) revealed as major component in uranium ore deposits. *Nat. Commun.* 8, 1–8. <https://doi.org/10.1038/ncomms15538>
- Bigalke, M., Kersten, M., Weyer, S., Wilcke, W., 2013. Isotopes Trace Biogeochemistry and Sources of Cu and Zn in an intertidal soil. *Soil Sci. Soc. Am. J.* 77, 680–691.  
<https://doi.org/DOI 10.2136/sssaj2012.0225>
- Bigalke, M., Weyer, S., Kobza, J., Wilcke, W., 2010a. Stable Cu and Zn isotope ratios as tracers of sources and transport of Cu and Zn in contaminated soil. *Geochim. Cosmochim. Acta* 74, 6801–6813. <https://doi.org/10.1016/j.gca.2010.08.044>
- Bigalke, M., Weyer, S., Wilcke, W., 2010b. Stable Copper Isotopes: A Novel Tool to Trace Copper Behavior in Hydromorphic Soils. *Soil Sci. Soc. Am. J.* 74, 60.  
<https://doi.org/10.2136/sssaj2008.0377>
- Bigeleisen, J., 1996. Nuclear size and shape effects in chemical reactions. Isotope chemistry of the heavy elements. *J. Am. Chem. Soc.* 118, 3676–3680.  
<https://doi.org/10.1021/ja954076k>
- Boenigk, J., Wodniok, S., Glücksman, E., 2015. Biodiversity and earth history. Springer.
- Bopp, C.J.I., Lundstrom, C.C., Johnson, T.M., Sanford, R.A., Long, P.E., Williams, K.H.,

2010. Uranium  $^{238}\text{U} / ^{235}\text{U}$  Isotope Ratios as Indicators of Reduction : Results from an in situ Biostimulation. *Environ. Sci. Technol.* 44, 5927–5933.
- Borch, T., Kretzschmar, R., Skappler, A., Van Cappellen, P., Ginder-Vogel, M., Voegelin, A., Campbell, K.M., 2010. Biogeochemical redox processes and their impact on contaminant dynamics. *Environ. Sci. Technol.* 44, 15–23. <https://doi.org/10.1021/es9026248>
- Borch, T., Roche, N., Johnson, T.E., 2012. Determination of contaminant levels and remediation efficacy in groundwater at a former in situ recovery uranium mine. *J. Environ. Monit.* 14, 1814. <https://doi.org/10.1039/c2em30077j>
- Borrok, D.M., Wanty, R.B., Ridley, W.I., Wolf, R., Lamothe, P.J., Adams, M., 2007. Separation of copper, iron, and zinc from complex aqueous solutions for isotopic measurement. *Chem. Geol.* 242, 400–414. <https://doi.org/10.1016/j.chemgeo.2007.04.004>
- Boyanov, M.I., Fletcher, K.E., Kwon, M.J., Rui, X., O’Loughlin, E.J., Löffler, F.E., Kemner, K.M., 2011. Solution and microbial controls on the formation of reduced U(IV) species. *Environ. Sci. Technol.* 45, 8336–8344. <https://doi.org/10.1021/es2014049>
- Brantley, S.L., Liermann, L.J., Guynn, R.L., Anbar, A.D., Icopini, G.A., Barling, J., 2004. Fe isotopic fractionation during mineral dissolution with and without bacteria. *Geochim. Cosmochim. Acta* 68, 3189–3204. <https://doi.org/10.1016/j.gca.2004.01.023>
- Brennecka, G.A., Borg, L.E., Hutcheon, I.D., Sharp, M.A., Anbar, A.D., 2010. Natural variations in uranium isotope ratios of uranium ore concentrates: Understanding the  $^{238}\text{U}/^{235}\text{U}$  fractionation mechanism. *Earth Planet. Sci. Lett.* 291, 228–233. <https://doi.org/10.1016/j.epsl.2010.01.023>
- Brennecka, G.A., Herrmann, A.D., Algeo, T.J., Anbar, A.D., 2011a. Rapid expansion of oceanic anoxia immediately before the end-Permian mass extinction. *Proc. Natl. Acad. Sci.* 108, 17631–17634. <https://doi.org/10.1073/pnas.1106039108>
- Brennecka, G.A., Wasylenki, L.E., Weyer, S., Anbar, A.D., 2011b. Uranium isotope fractionation during adsorption to manganese oxides. *Environ. Sci. Technol.* 45, 1370–1375.
- Brierley, C.L., 2008. How will biomining be applied in future? *Trans. Nonferrous Met. Soc. China (English Ed.)* 18, 1302–1310. [https://doi.org/10.1016/S1003-6326\(09\)60002-9](https://doi.org/10.1016/S1003-6326(09)60002-9)
- Brown, S.T., Basu, A., Ding, X., Christensen, J.N., DePaolo, D.J., 2018. Uranium isotope fractionation by abiotic reductive precipitation. *Proc. Natl. Acad. Sci.* 201805234. <https://doi.org/10.1073/pnas.1805234115>
- Brüske, A., Martin, A.N., Rammensee, P., Eroglu, S., Lazarov, M., Albut, G., Schuth, S., Aulbach, S., Schoenberg, R., Beukes, N.J., Hofmann, A., Nägler, T., Weyer, S., 2020a. The onset of oxidative weathering traced by uranium isotopes. *Precambrian Res.* 338, 105583. <https://doi.org/10.1016/j.precamres.2019.105583>
- Brüske, A., Weyer, S., Zhao, M.-Y., Planavsky, N.J., Wegwerth, A., Neubert, N., Dellwig, O., Lau, K. V., Lyons, T.W., 2020b. Correlated molybdenum and uranium isotope signatures in modern anoxic sediments: Implications for their use as paleo-redox proxy. *Geochim. Cosmochim. Acta* 270, 449–474. <https://doi.org/https://doi.org/10.1016/j.gca.2019.11.031>
- Bullen, T.D., White, a F., Childs, C.W., Vivit, D. V, Schultz, M.S., 2001. Demonstration of a

- significant iron isotope fractionation in nature. *Geology* 29, 699–702.  
[https://doi.org/10.1130/0091-7613\(2001\)029<0699:DOSAI>2.0.CO;2](https://doi.org/10.1130/0091-7613(2001)029<0699:DOSAI>2.0.CO;2)
- Bura-Nakić, E., Andersen, M.B., Archer, C., de Souza, G.F., Marguš, M., Vance, D., 2018. Coupled Mo-U abundances and isotopes in a small marine euxinic basin: Constraints on processes in euxinic basins. *Geochim. Cosmochim. Acta* 222, 212–229.  
<https://doi.org/https://doi.org/10.1016/j.gca.2017.10.023>
- Campbell, K.M., Davis, J.A., Bargar, J.R., Giammar, D.E., Bernier-Latmani, R., Kukkadapu, R., Williams, K.H., Veramani, H., Ulrich, K.-U., Stubbs, J.E., Yabusaki, S.B., Figueroa, L., Leshner, E., Wilkins, M.J., Peacock, A.D., Long, P.E., 2011. Composition, stability, and measurement of reduced uranium phases for groundwater bioremediation at Old Rifle, CO. *Appl. Geochemistry* 26, S167–S169.  
<https://doi.org/10.1016/j.apgeochem.2011.03.094>
- Campbell, K.M., Gallegos, T.J., Landa, E.R., 2015. Biogeochemical aspects of uranium mineralization, mining, milling, and remediation. *Appl. Geochemistry* 57, 206–235.  
<https://doi.org/10.1016/j.apgeochem.2014.07.022>
- Cantrell, K.J., Kaplan, D.I., Wietsma, T.W., 1995. Zero-valent iron for the in situ remediation of selected metals in groundwater. *J. Hazard. Mater.* 42, 201–212.  
[https://doi.org/10.1016/0304-3894\(95\)00016-N](https://doi.org/10.1016/0304-3894(95)00016-N)
- Castilla, J.C., 1983. Environmental impact in sandy beaches of copper mine tailings at Chañaral, Chile. *Mar. Pollut. Bull.* 14, 459–464. [https://doi.org/10.1016/0025-326X\(83\)90046-2](https://doi.org/10.1016/0025-326X(83)90046-2)
- Cerrato, J.M., Ashner, M.N., Alessi, D.S., Lezama-Pacheco, J.S., Bernier-Latmani, R., Bargar, J.R., Giammar, D.E., 2013. Relative reactivity of biogenic and chemogenic uraninite and biogenic noncrystalline U(IV). *Environ. Sci. Technol.* 47, 9756–9763.  
<https://doi.org/10.1021/es401663t>
- Chapman, J.B., Weiss, D.J., Shan, Y., Lemburger, M., 2009. Iron isotope fractionation during leaching of granite and basalt by hydrochloric and oxalic acids. *Geochim. Cosmochim. Acta* 73, 1312–1324. <https://doi.org/10.1016/j.gca.2008.11.037>
- Choi, M.S., Cho, K.S., Kim, D.S., Ryu, H.W., 2005. Bioleaching of uranium from low grade black schists by *Acidithiobacillus ferrooxidans*. *World J. Microbiol. Biotechnol.* 21, 377–380. <https://doi.org/10.1007/s11274-004-3627-9>
- Croal, L.R., Johnson, C.M., Beard, B.L., Newman, D.K., 2004. Iron isotope fractionation by Fe(II)-oxidizing photoautotrophic bacteria. *Geochim. Cosmochim. Acta* 68, 1227–1242.  
<https://doi.org/10.1016/j.gca.2003.09.011>
- Crosby, H.A., Johnson, C.M., Roden, E.E., Beard, B.L., 2005. Coupled Fe(II)-Fe(III) electron and atom exchange as a mechanism for Fe isotope fractionation during dissimilatory iron oxide reduction. *Environ. Sci. Technol.* 39, 6698–6704.  
<https://doi.org/10.1021/es0505346>
- Crosby, H.A., Roden, E.E., Johnson, C.M., Beard, B.L., 2007. The mechanisms of iron isotope fractionation produced during dissimilatory Fe(III) reduction by *Shewanella putrefaciens* and *Geobacter sulfurreducens*. *Geobiology* 5, 169–189.  
<https://doi.org/10.1111/j.1472-4669.2007.00103.x>
- Dahlkamp, F.J., 2013. Uranium ore deposits. Springer Science & Business Media.

- Dalai, P., Kaddour, H., Sahai, N., 2016. Incubating Life: Prebiotic Sources of Organics for the Origin of Life. *Elements* 12, 401–406. <https://doi.org/10.2113/gselements.12.6.401>
- Dang, D.H., Novotnik, B., Wang, W., Georg, R.B., Evans, R.D., 2016. Uranium Isotope Fractionation during Adsorption, (Co)precipitation, and Biotic Reduction. *Environ. Sci. Technol.* 50, 12695–12704. <https://doi.org/10.1021/acs.est.6b01459>
- Dauphas, N., John, S.G., Rouxel, O., 2017. Iron isotope systematics. *Non-Traditional Stable Isot.* 82, 415–510. <https://doi.org/10.2138/rmg.2017.82.11>
- Davis, J.A., Curtis, G.P., 2007. Consideration of Geochemical Issues in Groundwater Restoration at Uranium In-Situ Leach Mining Facilities.
- de Pablo, J., Casas, I., Gimenez, J., Molera, M., Torrero, M.E., 1997. Effect of temperature and bicarbonate concentration on the kinetics of UO<sub>2</sub>(s) dissolution under oxidizing conditions, in: *Materials Research Society Symposium - Proceedings*. pp. 535–542. <https://doi.org/10.1557/proc-465-535>
- DiSpirito, A.A., Talnagi, J.W., Tuovinen, O.H., 1983. Accumulation and cellular distribution of uranium in *Thiobacillus ferrooxidans*. *Arch. Microbiol.* 135, 250–253. <https://doi.org/10.1007/BF00413476>
- DiSpirito, A.A., Tuovinen, O.H., 1981. Oxygen uptake coupled with uranous sulfate oxidation by *thiobacillus ferrooxidans* and *T. acidophilus*. *Geomicrobiol. J.* 2, 275–291. <https://doi.org/10.1080/01490458109377767>
- Dold, B., 2017. Acid rock drainage prediction: A critical review. *J. Geochemical Explor.* 172, 120–132. <https://doi.org/10.1016/j.gexplo.2016.09.014>
- Dold, B., 2010. Basic Concepts in Environmental Geochemistry of Sulfidic Mine-Waste Management. *Waste Manag.* 24, 173–198. <https://doi.org/10.1016/j.wasman.2003.09.005>
- Dold, B., 2007. Biogeochemical processes in mine tailings with special focus on marine shore tailings deposits and their remediation. *Biohydrometallurgy From Single Cell to Environ.* 20–21, 177–185. <https://doi.org/10.4028/www.scientific.net/AMR.20-21.177>
- Dold, B., 2006. Element flows associated with marine shore mine tailings deposits. *Environ. Sci. Technol.* 40, 752–758. <https://doi.org/10.1021/es051475z>
- Dold, B., 2003. Speciation of the most soluble phases in a sequential extraction procedure adapted for geochemical studies of copper sulfide mine waste. *J. Geochemical Explor.* 80, 55–68. [https://doi.org/10.1016/S0375-6742\(03\)00182-1](https://doi.org/10.1016/S0375-6742(03)00182-1)
- Dold, B., Fontboté, L., 2001. Element cycling and secondary mineralogy in porphyry copper tailings as a function of climate, primary mineralogy, and mineral processing. *J. Geochemical Explor.* 74, 3–55. [https://doi.org/10.1016/S0375-6742\(01\)00174-1](https://doi.org/10.1016/S0375-6742(01)00174-1)
- Dopson, M., Baker-Austin, C., Koppineedi, P.R., Bond, P.L., 2003. Growth in sulfidic mineral environments: Metal resistance mechanisms in acidophilic micro-organisms. *Microbiology* 149, 1959–1970. <https://doi.org/10.1099/mic.0.26296-0>
- Dreissig, I., Weiss, S., Hennig, C., Bernhard, G., Zänker, H., 2011. Formation of uranium(IV)-silica colloids at near-neutral pH. *Geochim. Cosmochim. Acta* 75, 352–367. <https://doi.org/10.1016/j.gca.2010.10.011>
- Duquène, L., Tack, F., Meers, E., Baeten, J., Wannijn, J., Vandenhove, H., 2008. Effect of biodegradable amendments on uranium solubility in contaminated soils. *Sci. Total Environ.* 391, 26–33. <https://doi.org/10.1016/j.scitotenv.2007.10.042>

- Eccleston, M., Kelly, D.P., 1978. Oxidation kinetics and chemostat growth kinetics of *Thiobacillus ferrooxidans* on tetrathionate and thiosulfate. *J. Bacteriol.* 134, 718–727. <https://doi.org/10.1128/jb.134.3.718-727.1978>
- Ehrlich, S., Butler, I.B., Halicz, L., Rickard, D., Oldroyd, A., Matthews, A., 2004. Experimental study of the copper isotope fractionation between aqueous Cu(II) and covellite, CuS. *Chem. Geol.* 209, 259–269. <https://doi.org/10.1016/j.chemgeo.2004.06.010>
- Fantle, M.S., DePaolo, D.J., 2004. Iron isotopic fractionation during continental weathering. *Earth Planet. Sci. Lett.* 228, 547–562. <https://doi.org/10.1016/j.epsl.2004.10.013>
- Fekiacova, Z., Pichat, S., Cornu, S., Balesdent, J., 2013. Inferences from the vertical distribution of Fe isotopic compositions on pedogenetic processes in soils. *Geoderma* 209–210, 110–118. <https://doi.org/10.1016/j.geoderma.2013.06.007>
- Finneran, K.T., Housewright, M.E., Lovley, D.R., 2002. Multiple influences of nitrate on uranium solubility during bioremediation of uranium-contaminated subsurface sediments. *Environ. Microbiol.* 4, 510–516. <https://doi.org/10.1046/j.1462-2920.2002.00317.x>
- Fletcher, K.E., Boyanov, M.I., Thomas, S.H., Wu, Q., Kemner, K.M., Löffler, F.E., 2010. U(VI) reduction to mononuclear U(IV) by desulfitobacterium species. *Environ. Sci. Technol.* 44, 4705–4709. <https://doi.org/10.1021/es903636c>
- Frazier, S.W., Kretzschmar, R., Kraemer, S.M., 2005. Bacterial siderophores promote dissolution of UO<sub>2</sub> under reducing conditions. *Environ. Sci. Technol.* 39, 5709–5715. <https://doi.org/10.1021/es050270n>
- Fulton, J.L., Hoffmann, M.M., Darab, J.G., Palmer, B.J., Stern, E. a., 2000. Copper(I) and Copper(II) Coordination Structure under Hydrothermal Conditions at 325 °C: An X-ray Absorption Fine Structure and Molecular Dynamics Study. *J. Phys. Chem. A* 104, 11651–11663. <https://doi.org/10.1021/jp001949a>
- Gallegos, T.J., Campbell, K.M., Zielinski, R.A., Reimus, P.W., Clay, J.T., Janot, N., Bargar, J.R., Benzel, W.M., 2015. Persistent U(IV) and U(VI) following in-situ recovery (ISR) mining of a sandstone uranium deposit, Wyoming, USA. *Appl. Geochemistry* 63, 222–234. <https://doi.org/10.1016/j.apgeochem.2015.08.017>
- Gault, A.G., Cooke, D.R., Townsend, A.T., Charnock, J.M., Polya, D.A., 2005. Mechanisms of arsenic attenuation in acid mine drainage from Mount Bischoff, western Tasmania. *Sci. Total Environ.* 345, 219–228. <https://doi.org/10.1016/j.scitotenv.2004.10.030>
- Gavrilescu, M., Pavel, L.V., Cretescu, I., 2009. Characterization and remediation of soils contaminated with uranium. *J. Hazard. Mater.* 163, 475–510. <https://doi.org/10.1016/j.jhazmat.2008.07.103>
- Ginder-Vogel, M., Criddle, C.S., Fendorf, S., 2006. Thermodynamic constraints on the oxidation of biogenic UO<sub>2</sub> by Fe(III) (Hydr)oxides. *Environ. Sci. Technol.* 40, 3544–3550. <https://doi.org/10.1021/es052305p>
- Ginder-Vogel, M., Fendorf, S., 2007. Chapter 11 Biogeochemical Uranium Redox Transformations: Potential Oxidants of Uraninite. *Dev. Earth Environ. Sci.* [https://doi.org/10.1016/S1571-9197\(07\)07011-5](https://doi.org/10.1016/S1571-9197(07)07011-5)
- Ginder-Vogel, M., Stewart, B., Fendorf, S., 2010. Kinetic and mechanistic constraints on the

- oxidation of biogenic uraninite by ferrihydrite. *Environ. Sci. Technol.* 44, 163–169.  
<https://doi.org/10.1021/es902452u>
- Gleyzes, C., Tellier, S., Astruc, M., 2002. Fractionation studies of trace elements in contaminated soils n sediments.pdf. *Trac-Trends Anal. Chem.* 21, 451–467.  
[https://doi.org/10.1016/S0165-9936\(02\)00603-9](https://doi.org/10.1016/S0165-9936(02)00603-9)
- Grenthe, I., Fuger, J., Konings, R.J.M., Lemire, R.J., Muller, A.B., Nguyen-Trung, C., Wanner, H., 2004. Chemical thermodynamics of uranium 1–735.
- Gu, B., Yan, H., Zhou, P., Watson, D.B., Park, M., Istok, J., 2005. Natural humics impact uranium bioreduction and oxidation. *Environ. Sci. Technol.* 39, 5268–5275.  
<https://doi.org/10.1021/es050350r>
- Guelke, M., von Blanckenburg, F., Schoenberg, R., Staubwasser, M., Stuetzel, H., 2010. Determining the stable Fe isotope signature of plant-available iron in soils. *Chem. Geol.* 277, 269–280. <https://doi.org/10.1016/j.chemgeo.2010.08.010>
- Guillaumont, R., Fanghänel, T., Neck, V., Fuger, J., Palmer, D.A., Grenthe, I., Rand, M.H., 2003. Update on the chemical thermodynamics of uranium, neptunium, plutonium, americium and technetium 5, 913.
- Hall, G.E.M., Gauthier, G., Pelchat, J.-C., Pelchat, P., Vaive, J., 1996. Application of a Sequential Extraction Scheme to Ten Geological Certified Reference Materials for the Determination of 20 Elements \* 11.
- Hamidian, H., Rezai, B., Milani, S.A., Vahabzade, F., Shafaie, S.Z., 2009. Microbial leaching of uranium ore. *Asian J. Chem.* 21, 5808–5820. <https://doi.org/10.5772/17941>
- Hayes, S.M., White, S.A., Thompson, T.L., Maier, R.M., Chorover, J., 2009. Changes in lead and zinc lability during weathering-induced acidification of desert mine tailings: Coupling chemical and micro-scale analyses. *Appl. Geochemistry* 24, 2234–2245.  
<https://doi.org/10.1016/j.apgeochem.2009.09.010>
- Hedrich, S., Schippers, A., 2020. Distribution of acidophilic microorganisms in natural and man-made acidic environments. *Curr. Issues Mol. Biol.* 40, 25–48.  
<https://doi.org/10.21775/CIMB.040.025>
- Hedrich, S., Schippers, A., 2017. Metallgewinnung mittels Geobiotechnologie. *Chemie Ing. Tech.* 89, 29–39. <https://doi.org/10.1002/cite.201600080>
- Hedrich, S., Schlömann, M., Barrie Johnson, D., 2011. The iron-oxidizing proteobacteria. *Microbiology* 157, 1551–1564. <https://doi.org/10.1099/mic.0.045344-0>
- Herbert, R.B., Schippers, A., 2008. Iron isotope fractionation by biogeochemical processes in mine tailings. *Environ. Sci. Technol.* 42, 1117–1122.  
<https://doi.org/10.4028/www.scientific.net/AMR.20-21.237>
- Hindersmann, I., Mansfeldt, T., 2014. Trace element solubility in a multimetal-contaminated soil as affected by redox conditions. *Water. Air. Soil Pollut.* 225.  
<https://doi.org/10.1007/s11270-014-2158-8>
- Hoefs, J., 2018. Stable isotope geochemistry, Sixth Edit. ed. Springer Berlin.
- Huang, J.W., Blaylock, M.J., Kapulnik, Y., Ensley, B.D., 1998. Phytoremediation of uranium-contaminated soils: Role of organic acids in triggering uranium hyperaccumulation in plants. *Environ. Sci. Technol.* 32, 2004–2008.  
<https://doi.org/10.1021/es971027u>

- Hudson-Edwards, K.A., Jamieson, H.E., Lottermoser, B.G., 2011. Mine Wastes: Past, Present, Future. *Elements* 7, 375 LP – 380.
- Hummel, W., Anderegg, G., Rao, L., Puigdomènech, I., Tochiyama, O., 2005. Chemical Thermodynamics of Compounds and Complexes of U, Np, Pu, Am, Tc, Se, Ni and Zr with selected Organic Ligands. *Nucl. Energy* 1134. <https://doi.org/10.1017/CBO9781107415324.004>
- Icopini, G.A., Anbar, A.D., Ruebush, S.S., Tien, M., Brantley, S.L., 2004. Iron isotope fractionation during microbial reduction of iron: The importance of adsorption. *Geology* 32, 205–208. <https://doi.org/10.1130/G20184.1>
- Ilton, E.S., Veblen, D., 1988. Copper inclusions in sheet silicates from porphyry Cu deposits. *Nature* 334, 516–518.
- International Atomic Energy Agency, 2018. Uranium Resources, Production and Demand. International Atomic Energy Agency, Agency, O.N.E., 2014. Uranium 2014 : Resources , Production and Demand (The Red Book) 488. <https://doi.org/10.1787/uranium-2014-en>
- Jambor, J.L., 2003. Mine-waste mineralogy and mineralogical perspectives of acid-base accounting. *Environ. Asp. mine wastes* 31, 117–145.
- Jang, J.H., Mathur, R., Liermann, L.J., Ruebush, S., Brantley, S.L., 2008. An iron isotope signature related to electron transfer between aqueous ferrous iron and goethite. *Chem. Geol.* 250, 40–48. <https://doi.org/10.1016/j.chemgeo.2008.02.002>
- Jemison, N.E., Johnson, T.M., Shiel, A.E., Lundstrom, C.C., 2016a. Uranium Isotopic Fractionation Induced by U(VI) Adsorption onto Common Aquifer Minerals. *Environ. Sci. Technol.* 50, 12232–12240. <https://doi.org/10.1021/acs.est.6b03488>
- Jemison, N.E., Johnson, T.M., Shiel, A.E., Lundstrom, C.C., 2016b. Uranium isotopic fractionation induced by U(VI) adsorption onto common aquifer minerals. *Environ. Sci. Technol.* 50, 12232–12240. <https://doi.org/10.1021/acs.est.6b03488>
- Jemison, N.E., Reimus, P.W., Harris, R., Boukhalfa, H., Clay, J., Chamberlain, K., 2020. Reduction and potential remediation of U(VI) by dithionite at an in-situ recovery mine: Insights gained by  $\delta^{238}\text{U}$ . *Appl. Geochemistry* 115. <https://doi.org/10.1016/j.apgeochem.2020.104560>
- Jemison, N.E., Shiel, A.E., Johnson, T.M., Lundstrom, C.C., Long, P.E., Williams, K.H., 2018. Field Application of  $^{238}\text{U}/^{235}\text{U}$  Measurements to Detect Reoxidation and Mobilization of U(IV). *Environ. Sci. Technol.* 52, 3422–3430. <https://doi.org/10.1021/acs.est.7b05162>
- Jesús, Guajardo, Elpidio, M., Francisco, L., Cristina, Q., Martha, C., María-Eugenia, N., Jesús, González, Facundo, R., 2011. A Comparative Study of the Chelating Effect Between Textured Soya Aqueous Extract and EDTA on  $\text{Fe}^{3+}$ ,  $\text{Pb}^{2+}$ ,  $\text{Hg}^{2+}$ ,  $\text{Cd}^{2+}$  and  $\text{Ni}^{2+}$  Ions. *Soybean Physiol. Biochem.* 313–332. <https://doi.org/10.5772/20061>
- Johnson, C., 2020. Advances in Isotope Geochemistry Iron Geochemistry : An Isotopic Perspective. Springer, Cham, Switzerland.
- Johnson, C.M., Beard, B.L., Albarède, F., 2004a. Overview and General Concepts. *Rev. Mineral. Geochemistry* 55, 1–24. <https://doi.org/10.2138/gsrmg.55.1.1>
- Johnson, C.M., Beard, B.L., Roden, E.E., 2008. The Iron Isotope Fingerprints of Redox and Biogeochemical Cycling in Modern and Ancient Earth. *Annu. Rev. Earth Planet. Sci.* 36,

- 457–493. <https://doi.org/10.1146/annurev.earth.36.031207.124139>
- Johnson, C.M., Beard, B.L., Roden, E.E., Newman, D.K., Neelson, K.H., 2004b. Isotopic Constraints on Biogeochemical Cycling of Fe. *Rev. Mineral. Geochemistry* 55, 359 LP – 408.
- Johnson, D.B., 2014. Biomining-biotechnologies for extracting and recovering metals from ores and waste materials. *Curr. Opin. Biotechnol.* 30, 24–31.  
<https://doi.org/10.1016/j.copbio.2014.04.008>
- Kalinowski, B.E., Oskarsson, A., Albinsson, Y., Arlinger, J., Ödegaard-Jensen, A., Andlid, T., Pedersen, K., 2004. Microbial leaching of uranium and other trace elements from shale mine tailings at Ranstad. *Geoderma* 122, 177–194.  
<https://doi.org/10.1016/j.geoderma.2004.01.007>
- Kappler, A., Johnson, C.M., Crosby, H.A., Beard, B.L., Newman, D.K., 2010. Evidence for equilibrium iron isotope fractionation by nitrate-reducing iron(II)-oxidizing bacteria. *Geochim. Cosmochim. Acta* 74, 2826–2842. <https://doi.org/10.1016/j.gca.2010.02.017>
- Kappler, A., Straub, K.L., 2005. Geomicrobiological Cycling of Iron. *Rev. Mineral. Geochemistry* 59, 85 LP – 108.
- Kefeni, K.K., Msagati, T.A.M., Mamba, B.B., 2017. Acid mine drainage: Prevention, treatment options, and resource recovery: A review. *J. Clean. Prod.* 151, 475–493.  
<https://doi.org/10.1016/j.jclepro.2017.03.082>
- Kelly, D.P., Wood, A.P., 2000. Reclassification of some species of *Thiobacillus* to the newly designated genera *Acidithiobacillus* gen. nov., *Halothiobacillus* gen. nov. and *Thermithiobacillus* gen. nov. *Int. J. Syst. Evol. Microbiol.* 50, 511–516.  
<https://doi.org/10.1099/00207713-50-2-511>
- Kelm, U., Helle, S., Matthies, R., Morales, A., 2009. Distribution of trace elements in soils surrounding the El Teniente porphyry copper deposit, Chile: the influence of smelter emissions and a tailings deposit. *Environ. Geol.* 57, 365–376.  
<https://doi.org/10.1007/s00254-008-1305-1>
- Kendall, B., Brennecka, G.A., Weyer, S., Anbar, A.D., 2013. Uranium isotope fractionation suggests oxidative uranium mobilization at 2.50Ga. *Chem. Geol.* 362, 105–114.  
<https://doi.org/10.1016/j.chemgeo.2013.08.010>
- Kimball, B.E., Mathur, R., Dohnalkova, A.C., Wall, A.J., Runkel, R.L., Brantley, S.L., 2009. Copper isotope fractionation in acid mine drainage. *Geochim. Cosmochim. Acta* 73, 1247–1263. <https://doi.org/10.1016/j.gca.2008.11.035>
- Korehi, H., Blöthe, M., Sitnikova, M.A., Dold, B., Schippers, A., 2013. Metal mobilization by iron- and sulfur-oxidizing bacteria in a multiple extreme mine tailings in the Atacama Desert, Chile. *Environ. Sci. Technol.* 47, 2189–2196. <https://doi.org/10.1021/es304056n>
- Kossoff, D., Dubbin, W.E., Alfredsson, M., Edwards, S.J., Macklin, M.G., Hudson-Edwards, K.A., 2014. Mine tailings dams: Characteristics, failure, environmental impacts, and remediation. *Appl. Geochemistry* 51, 229–245.  
<https://doi.org/10.1016/j.apgeochem.2014.09.010>
- Kusonwiriawong, C., Bigalke, M., Abgottsporn, F., Lazarov, M., Wilcke, W., 2016. Response of Cu partitioning to flooding: A  $\delta^{65}\text{Cu}$  approach in a carbonatic alluvial soil. *Chem. Geol.* 420, 69–76. <https://doi.org/10.1016/j.chemgeo.2015.11.005>



- Kusonwiriawong, C., Bigalke, M., Cornu, S., Montagne, D., Fekiacova, Z., Lazarov, M., Wilcke, W., 2017. Response of copper concentrations and stable isotope ratios to artificial drainage in a French Retisol. *Geoderma* 300, 44–54.  
<https://doi.org/10.1016/j.geoderma.2017.04.003>
- Langmuir, D., 1978. Uranium solution-mineral equilibria at low temperatures with applications to sedimentary ore deposits. *Geochim. Cosmochim. Acta* 42, 547–569.  
[https://doi.org/10.1016/0016-7037\(78\)90001-7](https://doi.org/10.1016/0016-7037(78)90001-7)
- Latta, D.E., Boyanov, M.I., Kemner, K.M., O’Loughlin, E.J., Scherer, M.M., 2012a. Abiotic reduction of uranium by Fe(II) in soil. *Appl. Geochemistry* 27, 1512–1524.  
<https://doi.org/10.1016/j.apgeochem.2012.03.003>
- Latta, D.E., Gorski, C.A., Boyanov, M.I., O’Loughlin, E.J., Kemner, K.M., Scherer, M.M., 2012b. Influence of magnetite stoichiometry on U(VI) reduction. *Environ. Sci. Technol.* 46, 778–86. <https://doi.org/10.1021/es2024912>
- Latta, D.E., Mishra, B., Cook, R.E., Kemner, K.M., Boyanov, M.I., 2014. Stable U(IV) Complexes Form at High-Affinity Mineral Surface Sites. *Environ. Sci. Technol.* 48, 1683–1691. <https://doi.org/10.1021/acs.est.5b04281>
- Lau, K. V., Maher, K., Altiner, D., Kelley, B.M., Kump, L.R., Lehrmann, D.J., Silva-Tamayo, J.C., Weaver, K.L., Yu, M., Payne, J.L., 2016. Marine anoxia and delayed Earth system recovery after the end-Permian extinction. *Proc. Natl. Acad. Sci.* 113, 2360–2365.  
<https://doi.org/10.1073/pnas.1515080113>
- Liu, S.A., Teng, F.Z., Li, S., Wei, G.J., Ma, J.L., Li, D., 2014. Copper and iron isotope fractionation during weathering and pedogenesis: Insights from saprolite profiles. *Geochim. Cosmochim. Acta* 146, 59–75. <https://doi.org/10.1016/j.gca.2014.09.040>
- Lloyd, J.R., Macaskie, L.E., 2000. Bioremediation of Radionuclide-Containing Wastewaters, in: Lovley, D.R. (Ed.), *Environmental Microbe-Metal Interactions*. ASM Press, Washington D.C., pp. 277–327.
- Loreggian, L., Sorwat, J., Byrne, J.M., Kappler, A., Bernier-Latmani, R., 2020. Role of Iron Sulfide Phases in the Stability of Noncrystalline Tetravalent Uranium in Sediments. *Environ. Sci. Technol.* 54, 4840–4846. <https://doi.org/10.1021/acs.est.9b07186>
- Lottermoser, B.G., 2010. *Mine Wastes (third edition): Characterization, treatment and environmental impacts, Mine Wastes (Third Edition): Characterization, Treatment and Environmental Impacts*. <https://doi.org/10.1007/978-3-642-12419-8>
- Lovley, D.R., Phillips, E.J.P., Gorby, Y.A., Landa, E.R., 1991. Microbial reduction of uranium. *Nature* 350, 413–416. <https://doi.org/10.1038/350413a0>
- Lozano, J.C., Rodríguez, P.B., Tomé, F.V., Prieto, C., 2011. Enhancing uranium solubilization in soils by citrate, EDTA, and EDDS chelating amendments. *J. Hazard. Mater.* 198, 224–231. <https://doi.org/10.1016/j.jhazmat.2013.02.021>
- Luo, W., Gu, B., 2011. Dissolution of uranium-bearing minerals and mobilization of uranium by organic ligands in a biologically reduced sediment. *Environ. Sci. Technol.* 45, 2994–2999. <https://doi.org/10.1021/es103073u>
- Luo, W., Gu, B., 2009. Dissolution and mobilization of uranium in a reduced sediment by natural humic substances under anaerobic conditions. *Environ. Sci. Technol.* 43, 152–156. <https://doi.org/10.1021/es8013979>

- Mansfeldt, T., Overesch, M., 2013. Arsenic mobility and speciation in a gleysol with petrogleyic properties: a field and laboratory approach. *J. Environ. Qual.* 42, 1130–41. <https://doi.org/10.2134/jeq2012.0225>
- Mansfeldt, T., Schuth, S., Häusler, W., Wagner, F.E., Kaufhold, S., Overesch, M., 2012. Iron oxide mineralogy and stable iron isotope composition in a Gleysol with petrogleyic properties. *J. Soils Sediments* 12, 97–114. <https://doi.org/10.1007/s11368-011-0402-z>
- Markl, G., Lahaye, Y., Schwinn, G., 2006a. Copper isotopes as monitors of redox processes in hydrothermal mineralization. *Geochim. Cosmochim. Acta* 70, 4215–4228. <https://doi.org/10.1016/j.gca.2006.06.1369>
- Markl, G., von Blanckenburg, F., Wagner, T., 2006b. Iron isotope fractionation during hydrothermal ore deposition and alteration. *Geochim. Cosmochim. Acta* 70, 3011–3030. <https://doi.org/10.1016/j.gca.2006.02.028>
- Mathur, R., Fantle, M.S., 2015. Copper isotopic perspectives on supergene processes: Implications for the global Cu cycle. *Elements* 11, 323–329. <https://doi.org/10.2113/gselements.11.5.323>
- Mathur, R., Ruiz, J., Titley, S.R., Liermann, L.J., Buss, H., Brantley, S.L., 2005. Cu isotopic fractionation in the supergene environment with and without bacteria. *Geochim. Cosmochim. Acta* 69, 5233–5246. <https://doi.org/10.1016/j.gca.2005.06.022>
- Mathur, R., Titley, S.R., Barra, F., Brantley, S.L., Wilson, M., Phillips, A., Munizaga, F., Makshev, V., Vervoort, J., Hart, G., 2009. Exploration potential of Cu isotope fractionation in porphyry copper deposits. *J. Geochemical Explor.* 102, 1–6. <https://doi.org/10.1016/j.gexplo.2008.09.004>
- Mattielli, N., Petit, J.C.J., Deboudt, K., Flament, P., Perdrix, E., Taillez, A., Rimetz-Planchon, J., Weis, D., 2009. Zn isotope study of atmospheric emissions and dry depositions within a 5 km radius of a Pb-Zn refinery. *Atmos. Environ.* 43, 1265–1272. <https://doi.org/10.1016/j.atmosenv.2008.11.030>
- Mehra, O.P., Jackson, M.L., 1958. Iron oxide removal from soils and clays by a dithionite-citrate system buffered with sodium bicarbonate, in: *National Conference on Clays and Clays Minerals*. pp. 317–327.
- Merroun, M.L., Selenska-Pobell, S., 2001. Interactions of three eco-types of *Acidithiobacillus ferrooxidans* with U(VI). *BioMetals* 14, 171–179. <https://doi.org/10.1023/A:1016658209397>
- Mikutta, C., Wiederhold, J.G., Cirpka, O.A., Hofstetter, T.B., Bourdon, B., Gunten, U. Von, 2009. Iron isotope fractionation and atom exchange during sorption of ferrous iron to mineral surfaces. *Geochim. Cosmochim. Acta* 73, 1795–1812. <https://doi.org/10.1016/j.gca.2009.01.014>
- Molinas, M., Faizova, R., Brown, A., Galanzew, J., Schacherl, B., Bartova, B., Meibom, K.L., Vitova, T., Mazzanti, M., Bernier-Latmani, R., 2021. Biological Reduction of a U(V)-Organic Ligand Complex. *Environ. Sci. Technol.* 55, 4753–4761. <https://doi.org/10.1021/acs.est.0c06633>
- Montoya-Pino, C., Weyer, S., Anbar, A.D., Pross, J., Oschmann, W., van de Schootbrugge, B., Arz, H.W., 2010. Global enhancement of ocean anoxia during oceanic anoxic event 2: A quantitative approach using U isotopes. *Geology* 38, 315–318.

- <https://doi.org/10.1130/G30652.1>
- Moynier, F., Fujii, T., Brennecka, G.A., Nielsen, S.G., 2013. Nuclear field shift in natural environments. *Comptes Rendus - Geosci.* 345, 150–159.  
<https://doi.org/10.1016/j.crte.2013.01.004>
- Moynier, F., Vance, D., Fujii, T., Savage, P., 2017. The Isotope Geochemistry of Zinc and Copper. *Rev. Mineral. Geochemistry* 82, 543 LP – 600.
- Muñoz, J.A., Blázquez, M.L., Ballester, A., González, F., 1995. A study of the bioleaching of a Spanish uranium ore. Part I: A review of the bacterial leaching in the treatment of uranium ores. *Hydrometallurgy* 38, 39–57. [https://doi.org/10.1016/0304-386X\(94\)00038-5](https://doi.org/10.1016/0304-386X(94)00038-5)
- Murphy, M.J., Stirling, C.H., Kaltenbach, A., Turner, S.P., Schaefer, B.F., 2014. Fractionation of <sup>238</sup>U/<sup>235</sup>U by reduction during low temperature uranium mineralisation processes. *Earth Planet. Sci. Lett.* 388, 306–317.  
<https://doi.org/10.1016/j.epsl.2013.11.034>
- National Research Council, 2000. *Research Needs in Subsurface Science*.
- Navarrete, J.U., Borrok, D.M., Viveros, M., Ellzey, J.T., 2011. Copper isotope fractionation during surface adsorption and intracellular incorporation by bacteria. *Geochim. Cosmochim. Acta* 75, 784–799. <https://doi.org/10.1016/j.gca.2010.11.011>
- Newsome, L., Morris, K., Lloyd, J.R., 2014. The biogeochemistry and bioremediation of uranium and other priority radionuclides. *Chem. Geol.* 363, 164–184.  
<https://doi.org/10.1016/j.chemgeo.2013.10.034>
- Noordmann, J., Weyer, S., Montoya-Pino, C., Dellwig, O., Neubert, N., Eckert, S., Paetzel, M., Böttcher, M.E., 2015. Uranium and molybdenum isotope systematics in modern euxinic basins: Case studies from the central Baltic Sea and the Kyllaren fjord (Norway). *Chem. Geol.* 396, 182–195. <https://doi.org/10.1016/j.chemgeo.2014.12.012>
- Nordstrom, D.K., 2011. Mine Waters: Acidic to Circumneutral. *Elements* 7, 393 LP – 398.
- Oeser, M., Weyer, S., Horn, I., Schuth, S., 2014. High-precision Fe and Mg isotope ratios of silicate reference glasses determined in situ by femtosecond LA-MC-ICP-MS and by solution nebulisation MC-ICP-MS. *Geostand. Geoanalytical Res.* 38, 311–328.  
<https://doi.org/10.1111/j.1751-908X.2014.00288.x>
- Opfergelt, S., Williams, H.M., Cornelis, J.T., Guicharnaud, R.A., Georg, R.B., Siebert, C., Gislason, S.R., Halliday, A.N., Burton, K.W., 2017. Iron and silicon isotope behaviour accompanying weathering in Icelandic soils, and the implications for iron export from peatlands. *Geochim. Cosmochim. Acta* 217, 273–291.  
<https://doi.org/10.1016/j.gca.2017.08.033>
- Osorio, H., Mangold, S., Denis, Y., Nancuqueo, I., Esparza, M., Johnson, D.B., Bonnefoy, V., Dopson, M., Holmesa, D.S., 2013. Anaerobic sulfur metabolism coupled to dissimilatory iron reduction in the extremophile *Acidithiobacillus ferrooxidans*. *Appl. Environ. Microbiol.* 79, 2172–2181. <https://doi.org/10.1128/AEM.03057-12>
- Otto, H.-H., 2000. Über natürliche und synthetische Silicate des Kupfers. *Aufschluss* 51, 47–55.
- Pal, S., Pradhan, D., Das, T., Sukla, L.B., Roy Chaudhury, G., 2010. Bioleaching of low-grade uranium ore using *Acidithiobacillus ferrooxidans*. *Indian J. Microbiol.* 50, 70–75.

- <https://doi.org/10.1007/s12088-010-0015-z>
- Peacock, C.L., Sherman, D.M., 2004. Copper(II) sorption onto goethite, hematite and lepidocrocite: A surface complexation model based on ab initio molecular geometries and EXAFS spectroscopy. *Geochim. Cosmochim. Acta* 68, 2623–2637.  
<https://doi.org/10.1016/j.gca.2003.11.030>
- Pérez Rodríguez, N., Engström, E., Rodushkin, I., Nason, P., Alakangas, L., Öhlander, B., 2013. Copper and iron isotope fractionation in mine tailings at the Laver and Kristineberg mines, northern Sweden. *Appl. Geochemistry* 32, 204–215.  
<https://doi.org/10.1016/j.apgeochem.2012.10.012>
- Poitrasson, F., Freydier, R., 2005. Heavy iron isotope composition of granites determined by high resolution MC-ICP-MS. *Chem. Geol.* 222, 132–147.  
<https://doi.org/10.1016/j.chemgeo.2005.07.005>
- Pokrovsky, O.S., Viers, J., Emnova, E.E., Kompantseva, E.I., Freydier, R., 2008. Copper isotope fractionation during its interaction with soil and aquatic microorganisms and metal oxy(hydr)oxides: Possible structural control. *Geochim. Cosmochim. Acta* 72, 1742–1757. <https://doi.org/10.1016/j.gca.2008.01.018>
- Ramirez, M., Massolo, S., Frache, R., Correa, J.A., 2005. Metal speciation and environmental impact on sandy beaches due to El Salvador copper mine, Chile. *Mar. Pollut. Bull.* 50, 62–72. <https://doi.org/10.1016/j.marpolbul.2004.08.010>
- Richter, S., Eykens, R., Kühn, H., Aregbe, Y., Verbruggen, A., Weyer, S., 2010. New average values for the n(238U)/n(235U) isotope ratios of natural uranium standards. *Int. J. Mass Spectrom.* 295, 94–97. <https://doi.org/10.1016/j.ijms.2010.06.004>
- Riley, R.G., Zachara, J.M., 1992. Chemical contaminants on DOE lands and selection of contaminant mixtures for subsurface science research. <https://doi.org/10.2172/5202264>
- Roberto, F.F., 2017. Commercial heap biooxidation of refractory gold ores – Revisiting Newmont’s successful deployment at Carlin. *Miner. Eng.* 106, 2–6.  
<https://doi.org/10.1016/j.mineng.2016.09.017>
- Rodríguez, N.P., Khoshkhoo, M., Sandström, Å., Rodushkin, I., Alakangas, L., Öhlander, B., 2015. Isotopic signature of Cu and Fe during bioleaching and electrochemical leaching of a chalcopyrite concentrate. *Int. J. Miner. Process.* 134, 58–65.  
<https://doi.org/10.1016/j.minpro.2014.11.010>
- Rosman, K.J.R., Taylor, P.D.P., 1998. Commission on Isotopic Abundances and Atomic Weights - Isotopic Compositions of the Elements 1997 (Technical Report ). *Pure Appl. Chem.* 70, 217–235.
- Rudnick, R.L., Gao, S., 2003. Composition of the continental crust, 1st ed, The crust.
- Russell, W.A., Papanastassiou, D.A., Tombrello, T.A., 1978. Ca Isotope Fractionation on Earth and Other Solar-System Materials. *Geochim. Cosmochim. Acta* 42, 1075–1090.  
[https://doi.org/10.1016/0016-7037\(78\)90105-9](https://doi.org/10.1016/0016-7037(78)90105-9)
- Ryan, B.M., Kirby, J.K., Degryse, F., Scheiderich, K., McLaughlin, M.J., 2014. Copper isotope fractionation during equilibration with natural and synthetic ligands. *Environ. Sci. Technol.* 48, 8620–8626. <https://doi.org/10.1021/es500764x>
- Saad, E.M., Wang, X., Planavsky, N.J., Reinhard, C.T., Tang, Y., 2017. Redox-independent chromium isotope fractionation induced by ligand-promoted dissolution. *Nat. Commun.*

- 8, 1–10. <https://doi.org/10.1038/s41467-017-01694-y>
- Sani, R.K., Peyton, B.M., Dohnalkova, A., Amonette, J.E., 2005. Reoxidation of reduced uranium with iron(III) (Hydr)oxides under sulfate-reducing conditions. *Environ. Sci. Technol.* 39, 2059–2066. <https://doi.org/10.1021/es0494297>
- Satkoski, A.M., Beukes, N.J., Li, W., Beard, B.L., Johnson, C.M., 2015. A redox-stratified ocean 3.2 billion years ago. *Earth Planet. Sci. Lett.* 430, 43–53. <https://doi.org/10.1016/j.epsl.2015.08.007>
- Schauble, E.A., 2006. Equilibrium uranium isotope fractionation by nuclear volume and mass-dependent processes. AGU Fall Meet. Abstr. V21B-0570.
- Schecher, W.D., McAvoy, D.C., 2007. MINEQL+, v 4.6: A chemical equilibrium modeling system. *Environ. Res. Softw.*
- Schilling, K., Johnson, T.M., Mason, P.R.D., 2014. A sequential extraction technique for mass-balanced stable selenium isotope analysis of soil samples. *Chem. Geol.* 381, 125–130. <https://doi.org/10.1016/j.chemgeo.2014.04.014>
- Schippers, A., 1998. Untersuchungen zur Schwefelchemie der biologischen Laugung von Metallsulfiden. Shaker.
- Schippers, A., Breuker, A., Blazejak, A., Bosecker, K., Kock, D., Wright, T.L., 2010. The biogeochemistry and microbiology of sulfidic mine waste and bioleaching dumps and heaps, and novel Fe(II)-oxidizing bacteria. *Hydrometallurgy* 104, 342–350. <https://doi.org/10.1016/j.hydromet.2010.01.012>
- Schippers, A., Hallmann, R., Wentzien, S., Sand, W., 1995. Microbial diversity in uranium mine waste heaps. *Appl. Environ. Microbiol.* 61, 2930–2935. <https://doi.org/10.1128/aem.61.8.2930-2935.1995>
- Schippers, A., Hedrich, S., Vasters, J., Drobe, M., Sand, W., Willscher, S., 2014. Biomining: metal recovery from ores with microorganisms. *Adv. Biochem. Eng. Biotechnol.* 141, 1–47. [https://doi.org/10.1007/10\\_2013\\_216](https://doi.org/10.1007/10_2013_216)
- Schippers, A., Jozsa, P.G., Sand, W., 1996. Sulfur chemistry in bacterial leaching of pyrite. *Appl. Environ. Microbiol.* 62, 3424–3431. <https://doi.org/10.1128/aem.62.9.3424-3431.1996>
- Schofield, E.J., Veeramani, H., Sharp, J.O., Suvorova, E.I., Conradson, S.D., Ilton, E.S., Bargar, J.R., 2008. Structure of biogenic uraninite produced by *Shewanella oneidensis* strain MR-1. *Environ. Sci. Technol.* 42, 7898–7904.
- Schrenk, M.O., Edwards, K.J., Goodman, R.M., Hamers, R.J., Banfield, J.F., 1998. Distribution of *Thiobacillus ferrooxidans* and *Leptospirillum ferrooxidans*: Implications for generation of acid mine drainage. *Science* (80-. ). 279, 1519–1522. <https://doi.org/10.1126/science.279.5356.1519>
- Schuth, S., Hurraß, J., Münker, C., Mansfeldt, T., 2015. Redox-dependent fractionation of iron isotopes in suspensions of a groundwater-influenced soil. *Chem. Geol.* 392, 74–86. <https://doi.org/10.1016/j.chemgeo.2014.11.007>
- Schuth, S., Mansfeldt, T., 2016. Iron isotope composition of aqueous phases of a lowland environment. *Environ. Chem.* 13, 89–101. <https://doi.org/10.1071/EN15073>
- Shahandeh, H., Hossner, L.R., 2002. Enhancement of uranium phytoaccumulation from contaminated soils. *Soil Sci.* 167, 269–280. <https://doi.org/10.1097/00010694->

200204000-00004

- Sharp, J.O., Lezama-Pacheco, J.S., Schofield, E.J., Junier, P., Ulrich, K.-U., Chinni, S., Veeramani, H., Margot-Roquier, C., Webb, S.M., Tebo, B.M., Giammar, D.E., Bargar, J.R., Bernier-Latmani, R., 2011. Uranium speciation and stability after reductive immobilization in aquifer sediments. *Geochim. Cosmochim. Acta* 75, 6497–6510. <https://doi.org/10.1016/j.gca.2011.08.022>
- Sherman, D.M., 2013. Equilibrium isotopic fractionation of copper during oxidation/reduction, aqueous complexation and ore-forming processes: Predictions from hybrid density functional theory. *Geochim. Cosmochim. Acta* 118, 85–97. <https://doi.org/10.1016/j.gca.2013.04.030>
- Shi, L., Richardson, D.J., Wang, Z., Kerisit, S.N., Rosso, K.M., Zachara, J.M., Fredrickson, J.K., 2009. The roles of outer membrane cytochromes of *Shewanella* and *Geobacter* in extracellular electron transfer. *Environ. Microbiol. Rep.* 1, 220–227. <https://doi.org/10.1111/j.1758-2229.2009.00035.x>
- Shields, W.R., Murphy, T.J., Garner, E.L., 1964. Absolute Isotopic Abundance Ratio and the Atomic Weight of a Reference Sample of Copper. *J. Res. Natl. Bur. Stand.* 68A, 589–592. <https://doi.org/10.1021/ja00868a001>
- Siebert, C., Pett-Ridge, J.C., Opfergelt, S., Guicharnaud, R.A., Halliday, A.N., Burton, K.W., 2015. Molybdenum isotope fractionation in soils: Influence of redox conditions, organic matter, and atmospheric inputs. *Geochim. Cosmochim. Acta* 162, 1–24. <https://doi.org/10.1016/j.gca.2015.04.007>
- Sillitoe, R.H., 2010. Porphyry copper systems. *Econ. Geol.* 105, 3–41. <https://doi.org/10.2113/gsecongeo.105.1.3>
- Silveira, M.L., Alleoni, L.R.F., O'Connor, G.A., Chang, A.C., 2006. Heavy metal sequential extraction methods-A modification for tropical soils. *Chemosphere* 64, 1929–1938. <https://doi.org/10.1016/j.chemosphere.2006.01.018>
- Simate, G.S., Ndlovu, S., 2014. Acid mine drainage: Challenges and opportunities. *J. Environ. Chem. Eng.* <https://doi.org/10.1016/j.jece.2014.07.021>
- Singh, K.B., Dhar, B.B., 1997. Sinkhole subsidence due to mining. *Geotech. Geol. Eng.* 15, 327–341.
- Sivry, Y., Riotte, J., Sonke, J.E., Audry, S., Schäfer, J., Viers, J., Blanc, G., Freydier, R., Dupré, B., 2008. Zn isotopes as tracers of anthropogenic pollution from Zn-ore smelters The Riou Mort-Lot River system. *Chem. Geol.* 255, 295–304. <https://doi.org/10.1016/j.chemgeo.2008.06.038>
- Skulan, J.L., Beard, B.L., Johnson, C.M., 2002. Kinetic and equilibrium Fe isotope fractionation between aqueous Fe(III) and hematite. *Geochim. Cosmochim. Acta* 66, 2995–3015. [https://doi.org/10.1016/S0016-7037\(02\)00902-X](https://doi.org/10.1016/S0016-7037(02)00902-X)
- Smuda, J., Dold, B., Spangenberg, J.E., Pfeifer, H.R., 2008. Geochemistry and stable isotope composition of fresh alkaline porphyry copper tailings: Implications on sources and mobility of elements during transport and early stages of deposition. *Chem. Geol.* 256, 62–76. <https://doi.org/10.1016/j.chemgeo.2008.08.001>
- Song, S., Mathur, R., Ruiz, J., Chen, D., Allin, N., Guo, K., Kang, W., 2016. Fingerprinting two metal contaminants in streams with Cu isotopes near the Dexing Mine, China. *Sci.*

- Total Environ. 544, 677–685. <https://doi.org/10.1016/j.scitotenv.2015.11.101>
- Sonter, L.J., Ali, S.H., Watson, J.E.M., 2018. Mining and biodiversity: Key issues and research needs in conservation science. *Proc. R. Soc. B Biol. Sci.* 285. <https://doi.org/10.1098/rspb.2018.1926>
- Sparks, D.L., 2005. Toxic Metals in the Environment: The Role of Surfaces. *Elements* 1, 193–197. <https://doi.org/10.2113/gselements.1.4.193>
- Staubwasser, M., von Blanckenburg, F., Schippers, A., 2007. What controls iron isotope fractionation in an acid mining pile? *Goldschmidt Conference Abstract*.
- Steudel, R., Holdt, G., Göbel, T., Hazeu, W., 1987. Chromatographic Separation of Higher Polythionates. *Angew. Chemie Int. Ed. English* 26, 151–153.
- Stirling, C.H., Andersen, M.B., Warthmann, R., Halliday, A.N., 2015. Isotope fractionation of  $^{238}\text{U}$  and  $^{235}\text{U}$  during biologically-mediated uranium reduction. *Geochim. Cosmochim. Acta* 163, 200–218. <https://doi.org/10.1016/j.gca.2015.03.017>
- Stylo, M., Alessi, D.S., Shao, P.P., Lezama-Pacheco, J.S., Bargar, J.R., Bernier-Latmani, R., 2013a. Biogeochemical controls on the product of microbial U(VI) reduction. *Environ. Sci. Technol.* 47, 12351–12358. <https://doi.org/10.1021/es402631w>
- Stylo, M., Alessi, D.S., Shao, P.P., Lezama-Pacheco, J.S., Bargar, J.R., Bernier-Latmani, R., 2013b. Biogeochemical controls on the product of microbial U ( VI ) reduction. *Environ. Sci. Technol.* 47, 12351–12358.
- Stylo, M., Neubert, N., Roebbert, Y., Weyer, S., Bernier-Latmani, R., 2015a. Mechanism of Uranium Reduction and Immobilization in *Desulfovibrio vulgaris* Biofilms. *Environ. Sci. Technol.* 49, 10553–10561. <https://doi.org/10.1021/acs.est.5b01769>
- Stylo, M., Neubert, N., Wang, Y., Monga, N., Romaniello, S.J., Weyer, S., Bernier-Latmani, R., 2015b. Uranium isotopes fingerprint biotic reduction. *Proc. Natl. Acad. Sci.* 112, 5619–5624. <https://doi.org/10.1073/pnas.1421841112>
- Suzuki, Y., Tanaka, K., Kozai, N., Ohnuki, T., 2010. Effects of Citrate, NTA, and EDTA on the Reduction of U(VI) by *Shewanella putrefaciens*. *Geomicrobiol. J.* 27, 245–250. <https://doi.org/10.1080/01490450903456764>
- Taylor, G., Farrington, V., Woods, P., Ring, R., Molloy, R., 2004. Review of Environmental Impacts of the Acid In-situ Leach Uranium Mining Process. *CSIRO L. Water Client Rep.* 10593–10659.
- Temple, K.L., Colmer, A.R., 1951. The autotrophic oxidation of iron by a new bacterium, *thiobacillus ferrooxidans*. *J. Bacteriol.* 62, 605–611. <https://doi.org/10.1128/JB.62.5.605-611.1951>
- Teutsch, N., von Gunten, U., Porcelli, D., Cirpka, O.A., Halliday, A.N., 2005. Adsorption as a cause for iron isotope fractionation in reduced groundwater. *Geochim. Cosmochim. Acta* 69, 4175–4185. <https://doi.org/10.1016/j.gca.2005.04.007>
- Thapalia, A., Borrok, D.M., Van Metre, P.C., Musgrove, M., Landa, E.R., 2010. Zn and Cu isotopes as tracers of anthropogenic contamination in a sediment core from an Urban Lake. *Environ. Sci. Technol.* 44, 1544–1550. <https://doi.org/10.1021/es902933y>
- Thiemens, M.H., 2006. History and applications of mass-independent isotope effects. *Annu. Rev. Earth Planet. Sci.* 34, 217–262. <https://doi.org/10.1146/annurev.earth.34.031405.125026>

- Thormann, K.M., Saville, R.M., Shukla, S., Pelletier, D.A., Spormann, A.M., 2004. Initial phases of biofilm formation in *Shewanella oneidensis* MR-1. *J. Bacteriol.* 186, 8096–8104. <https://doi.org/10.1128/JB.186.23.8096-8104.2004>
- Torrero, M.E., Baraj, E., De Pablo, J., Giménez, J., Casas, I., 1997. Kinetics of corrosion and dissolution of uranium dioxide as a function of pH. *Int. J. Chem. Kinet.* 29, 261–267. [https://doi.org/10.1002/\(SICI\)1097-4601\(1997\)29:4<261::AID-KIN4>3.0.CO;2-S](https://doi.org/10.1002/(SICI)1097-4601(1997)29:4<261::AID-KIN4>3.0.CO;2-S)
- Tsarev, S., Waite, T.D., Collins, R.N., 2016. Uranium Reduction by Fe(II) in the Presence of Montmorillonite and Nontronite. *Environ. Sci. Technol.* 50, 8223–8230. <https://doi.org/10.1021/acs.est.6b02000>
- Tuovinen, O.H., Bhatti, T.M., 1999. Microbiological leaching of uranium ores. *Miner. Metall. Process.* 16, 51–60. <https://doi.org/10.1007/bf03403234>
- Ulrich, K.-U., Singh, A., Schofield, E.J., Bargar, J.R., Veeramani, H., Sharp, J.O., Bernier-Latmani, R., Giammar, D.E., 2008. Dissolution of Biogenic and Synthetic UO<sub>2</sub> under Varied Reducing Conditions. *Environ. Sci. Technol.* 42, 5600–5606. <https://doi.org/10.1021/es800647u>
- United States Geological Survey (USGS), 2020. Mineral Commodity Summaries 2020, U.S Department OF The Interior, U.S Geological Survey.
- Uvarova, Y.A., Kyser, T.K., Geagea, M.L., Chipley, D., 2014. Variations in the uranium isotopic compositions of uranium ores from different types of uranium deposits. *Geochim. Cosmochim. Acta* 146, 1–17. <https://doi.org/10.1016/j.gca.2014.09.034>
- Valdés, J., Pedroso, I., Quatrini, R., Dodson, R.J., Tettelin, H., Blake, R., Eisen, J.A., Holmes, D.S., 2008. Acidithiobacillus ferrooxidans metabolism: From genome sequence to industrial applications. *BMC Genomics* 9, 1–24. <https://doi.org/10.1186/1471-2164-9-597>
- Valls, M., De Lorenzo, V., 2002. Exploiting the genetic and biochemical capacities of bacteria for the remediation of heavy metal pollution. *FEMS Microbiol. Rev.* 26, 327–338. [https://doi.org/10.1016/S0168-6445\(02\)00114-6](https://doi.org/10.1016/S0168-6445(02)00114-6)
- Vance, D., Archer, C., Bermin, J., Perkins, J., Statham, P.J., Lohan, M.C., Ellwood, M.J., Mills, R.A., 2008. The copper isotope geochemistry of rivers and the oceans. *Earth Planet. Sci. Lett.* 274, 204–213. <https://doi.org/10.1016/j.epsl.2008.07.026>
- Veeramani, H., Alessi, D.S., Suvorova, E.I., Lezama-Pacheco, J.S., Stubbs, J.E., Sharp, J.O., Dippon, U., Kappler, A., Bargar, J.R., Bernier-Latmani, R., 2011. Products of abiotic U(VI) reduction by biogenic magnetite and vivianite. *Geochim. Cosmochim. Acta* 75, 2512–2528. <https://doi.org/10.1016/j.gca.2011.02.024>
- Veeramani, H., Scheinost, A.C., Monsegue, N., Qafoku, N.P., Kukkadapu, R., Newville, M., Lanzirotti, A., Pruden, A., Murayama, M., Hochella, M.F., 2013. Abiotic reductive immobilization of U(VI) by biogenic mackinawite. *Environ. Sci. Technol.* 47, 2361–2369. <https://doi.org/10.1021/es304025x>
- Villa, I.M., Bonardi, M.L., De Bièvre, P., Holden, N.E., Renne, P.R., 2016. IUPAC-IUGS status report on the half-lives of <sup>238</sup>U, <sup>235</sup>U and <sup>234</sup>U. *Geochim. Cosmochim. Acta* 172, 387–392. <https://doi.org/10.1016/j.gca.2015.10.011>
- Wakeman, K., Auvinen, H., Johnson, D.B., 2008. Microbiological and geochemical dynamics in simulated-heap leaching of a polymetallic sulfide ore. *Biotechnol. Bioeng.* 101, 739–



750. <https://doi.org/10.1002/bit.21951>
- Wall, J.D., Krumholz, L.R., 2006. Uranium Reduction. *Annu. Rev. Microbiol.* 60, 149–166. <https://doi.org/10.1146/annurev.micro.59.030804.121357>
- Wan, J., Tokunaga, T.K., Brodie, E., Wang, Z., Zheng, Z., Herman, D., Hazen, T.C., Firestone, M.K., Sutton, S.R., 2005. Reoxidation of bio-reduced uranium under reducing conditions. *Environ. Sci. Technol.* 39, 6162–6169. <https://doi.org/10.1021/es048236g>
- Wang, C., Harbottle, D., Liu, Q., Xu, Z., 2014. Current state of fine mineral tailings treatment: A critical review on theory and practice. *Miner. Eng.* 58, 113–131. <https://doi.org/10.1016/j.mineng.2014.01.018>
- Wang, X., Johnson, T.M., Lundstrom, C.C., 2015a. Isotope fractionation during oxidation of tetravalent uranium by dissolved oxygen. *Geochim. Cosmochim. Acta* 150, 160–170. <https://doi.org/10.1016/j.gca.2014.12.007>
- Wang, X., Johnson, T.M., Lundstrom, C.C., 2015b. Low temperature equilibrium isotope fractionation and isotope exchange kinetics between U(IV) and U(VI). *Geochim. Cosmochim. Acta* 158, 262–275. <https://doi.org/10.1016/j.gca.2015.03.006>
- Wang, X., Planavsky, N.J., Hofmann, A., Saupe, E.E., De Corte, B.P., Philippot, P., LaLonde, S. V., Jemison, N.E., Zou, H., Ossa, F.O., Rybacki, K., Alfimova, N., Larson, M.J., Tsikos, H., Fralick, P.W., Johnson, T.M., Knudsen, A.C., Reinhard, C.T., Konhauser, K.O., 2018. A Mesoarchean shift in uranium isotope systematics. *Geochim. Cosmochim. Acta* 238, 438–452. <https://doi.org/10.1016/j.gca.2018.07.024>
- Wang, Y., Fruttschi, M., Suvorova, E.I., Phrommavanh, V., Descostes, M., Osman, A.A.A., Geipel, G., Bernier-Latmani, R., 2013. Mobile uranium(IV)-bearing colloids in a mining-impacted wetland. *Nat. Commun.* 4, 1–9. <https://doi.org/10.1038/ncomms3942>
- Wasylenki, L.E., 2012. Establishing the Basis for Using Stable Isotope Ratios of Metals as Paleoredox Proxies. *Isot. Anal. Fundam. Appl. Using ICP-MS* 317–350. <https://doi.org/10.1002/9783527650484.ch11>
- Weinstein, C., Moynier, F., Wang, K., Paniello, R., Foriel, J., Catalano, J., Pichat, S., 2011. Isotopic fractionation of Cu in plants. *Chem. Geol.* 286, 266–271. <https://doi.org/10.1016/j.chemgeo.2011.05.010>
- Weyer, S., Anbar, A.D., Brey, G.P., Münker, C., Mezger, K., Woodland, A.B., 2005. Iron isotope fractionation during planetary differentiation. *Earth Planet. Sci. Lett.* 240, 251–264. <https://doi.org/10.1016/j.epsl.2005.09.023>
- Weyer, S., Anbar, A.D., Gerdes, A., Gordon, G.W., Algeo, T.J., Boyle, E.A., 2008. Natural fractionation of  $^{238}\text{U}/^{235}\text{U}$ . *Geochim. Cosmochim. Acta* 72, 345–359. <https://doi.org/10.1016/j.gca.2007.11.012>
- Weyer, S., Schwieters, J.B., 2003. High precision Fe isotope measurements with high mass resolution MC-ICPMS. *Int. J. Mass Spectrom.* 226, 355–368. [https://doi.org/10.1016/S1387-3806\(03\)00078-2](https://doi.org/10.1016/S1387-3806(03)00078-2)
- Wiederhold, J.G., 2015. Metal stable isotope signatures as tracers in environmental geochemistry. *Environ. Sci. Technol.* 49, 2606–2624. <https://doi.org/10.1021/es504683e>
- Wiederhold, J.G., Kraemer, S.M., Teutsch, N., Borer, P.M., Halliday, A.N., Kretzschmar, R., 2006. Iron isotope fractionation during proton-promoted, ligand-controlled, and reductive dissolution of goethite. *Environ. Sci. Technol.* 40, 3787–3793.

- <https://doi.org/10.1021/es052228y>
- Wiederhold, J.G., Skyllberg, U., Drott, A., Jiskra, M., Jonsson, S., Björn, E., Bourdon, B., Kretzschmar, R., 2015. Mercury isotope signatures in contaminated sediments as a tracer for local industrial pollution sources. *Environ. Sci. Technol.* 49, 177–185.  
<https://doi.org/10.1021/es5044358>
- Wiederhold, J.G., Smith, R.S., Siebner, H., Jew, A.D., Brown, G.E., Bourdon, B., Kretzschmar, R., 2013. Mercury isotope signatures as tracers for Hg cycling at the new idria Hg mine. *Environ. Sci. Technol.* 47, 6137–6145. <https://doi.org/10.1021/es305245z>
- Wiederhold, J.G., Teutsch, N., Kraemer, S.M., Halliday, A.N., Kretzschmar, R., 2007a. Iron Isotope Fractionation during Pedogenesis in Redoximorphic Soils. *Soil Sci. Soc. Am. J.* 71, 1840. <https://doi.org/10.2136/sssaj2006.0379>
- Wiederhold, J.G., Teutsch, N., Kraemer, S.M., Halliday, A.N., Kretzschmar, R., 2007b. Iron isotope fractionation in oxic soils by mineral weathering and podzolization. *Geochim. Cosmochim. Acta* 71, 5821–5833. <https://doi.org/10.1016/j.gca.2007.07.023>
- Williams, K.H., Bargar, J.R., Lloyd, J.R., Lovley, D.R., 2013. Bioremediation of uranium-contaminated groundwater: A systems approach to subsurface biogeochemistry. *Curr. Opin. Biotechnol.* 24, 489–497. <https://doi.org/10.1016/j.copbio.2012.10.008>
- WoldeGabriel, G., Boukhalfa, H., Ware, S.D., Cheshire, M., Reimus, P., Heikoop, J., Conradson, S.D., Batuk, O., Havrilla, G., House, B., Simmons, A., Clay, J., Basu, A., Christensen, J.N., Brown, S.T., DePaolo, D.J., 2014. Characterization of cores from an in-situ recovery mined uranium deposit in Wyoming: Implications for post-mining restoration. *Chem. Geol.* 390, 32–45. <https://doi.org/10.1016/j.chemgeo.2014.10.009>
- Wu, L., Beard, B.L., Roden, E.E., Johnson, C.M., 2009. Influence of pH and dissolved Si on Fe isotope fractionation during dissimilatory microbial reduction of hematite. *Geochim. Cosmochim. Acta* 73, 5584–5599. <https://doi.org/10.1016/j.gca.2009.06.026>
- Yan, L., Hu, H., Zhang, S., Chen, P., Wang, W., Li, H., 2017. Arsenic tolerance and bioleaching from realgar based on response surface methodology by *Acidithiobacillus ferrooxidans* isolated from Wudalianchi volcanic lake, northeast China. *Electron. J. Biotechnol.* 25, 50–57. <https://doi.org/10.1016/j.ejbt.2016.11.007>
- Yan, L., Yin, H., Zhang, S., Leng, F., Nan, W., Li, H., 2010. Biosorption of inorganic and organic arsenic from aqueous solution by *Acidithiobacillus ferrooxidans* BY-3. *J. Hazard. Mater.* 178, 209–217. <https://doi.org/10.1016/j.jhazmat.2010.01.065>
- Yesavage, T., Fantle, M.S., Vervoort, J., Mathur, R., Jin, L., Liermann, L.J., Brantley, S.L., 2012. Fe cycling in the Shale Hills Critical Zone Observatory, Pennsylvania: An analysis of biogeochemical weathering and Fe isotope fractionation. *Geochim. Cosmochim. Acta* 99, 18–38. <https://doi.org/10.1016/j.gca.2012.09.029>
- Zammit, C.M., Brugger, J., Southam, G., Reith, F., 2014. In situ recovery of uranium - The microbial influence. *Hydrometallurgy* 150, 236–244.  
<https://doi.org/10.1016/j.hydromet.2014.06.003>
- Zhang, L., Wang, J., Bai, Z., Lv, C., 2015. Effects of vegetation on runoff and soil erosion on reclaimed land in an opencast coal-mine dump in a loess area. *Catena* 128, 44–53.  
<https://doi.org/10.1016/j.catena.2015.01.016>
- Zhang, R., Hedrich, S., Römer, F., Goldmann, D., Schippers, A., 2020. Bioleaching of cobalt

- from Cu/Co-rich sulfidic mine tailings from the polymetallic Rammelsberg mine, Germany. *Hydrometallurgy* 197, 105443.  
<https://doi.org/10.1016/j.hydromet.2020.105443>
- Zhang, S., Yan, L., Xing, W., Chen, P., Zhang, Y., Wang, W., 2018. *Acidithiobacillus ferrooxidans* and its potential application. *Extremophiles* 22, 563–579.  
<https://doi.org/10.1007/s00792-018-1024-9>
- Zhu, X.K., Guo, Y., Williams, R.J.P., O’Nions, R.K., Matthews, A., Belshaw, N.S., Canters, G.W., de Waal, E.C., Weser, U., Burgess, B.K., Salvato, B., 2002. Mass fractionation processes of transition metal isotopes. *Earth Planet. Sci. Lett.* 200, 47–62.  
[https://doi.org/10.1016/S0012-821X\(02\)00615-5](https://doi.org/10.1016/S0012-821X(02)00615-5)

## Curriculum Vitae

# Yvonne Röbbert

---

Date and place of birth: 22.01.1991 in Gehrden  
Nationality: German  
Email: y.roebbert@mineralogie.uni-hannover.de

## Education

---

- 10/2010 – 12/2015      **Master of Science, Geosciences**  
Leibniz Universität Hannover
- Specialization: Mineralogy-Geochemistry
  - Niedersachsen-Stipendium 2014 (scholarship)
  - Master thesis: Biotic and abiotic  $^{238}\text{U}/^{235}\text{U}$  fractionation – applications to bioremediation and U ore roll-front deposits
  - final grade (1.0)
- 09/2003 – 06/2010      **A-Levels**  
Hannah-Arendt-Gymnasium Barsinghausen
- final grade (1.4)

## Work experience

---

- since 08/2016      **PhD student**  
Institute for Mineralogy Hannover, Mobilization and isotope fractionation of uranium, copper and iron in the environment – implications for (bio)remediation of contaminated sites and mine tailings
- 01/2018 - 03/2020      **Experiments in the microbiology laboratory**  
Federal Institute for Geosciences and Natural Resources
- 04/2013 - 02/2016      **Student research assistant (geochemistry)**  
Institute for Mineralogy Hannover
- 02/2013 – 03/2013      **Internship (soil science)**  
German Environment Agency Dessau
- 06/2011 – 05/2012      **Student research assistant (geophysics)**  
LIAG Hannover

## Engagements/additional activities

---

04/2017-04/2019 & since 04/2021	executive board of the institute, representative for scientific staff
since 02/2017	secretary to the board of the association: "Freunde der Geowissenschaften Hannover e.V."
general	engagements in the institute, e.g. organization of lab outings and Christmas parties
03/2017	tutor of a student excursion to East Africa (Kenya and Tanzania)
2018	supervision of a bachelor thesis: "Isotopenfraktionierung von $^{238}\text{U}/^{235}\text{U}$ bei der Mobilisierung von nicht-kristallinen U(IV) durch organische Liganden"
2020	supervision of a master thesis

## Additional skills

---

Languages:	German – first language English – fluent French (DELF A1, A2, B1, B2)
Software:	MS PowerPoint, MS Word, MS Excel – excellent knowledge Adobe Illustrator - good knowledge
workshops:	third-party funds short course, Leibniz Universität Hannover (12/2017) "Tools in Biogeochemistry", Universität Tübingen (08/2019) "Advances in (bio-)hydrometallurgy and application" BGR Hannover (05/2019) "Geomicrobiology" workshop, TU Kaiserslautern (10/2019)

## International experience

---

02/2015 – 03/2015	École polytechnique fédérale de Lausanne (EPFL)
11/2016 – 12/2016	Environmental Microbiology Laboratory
11/2019	
2016 - 2019	Several international conferences (Goldschmidt and AGU)

## Publications

---

2021

- **Roebbert, Y.**, Rosendahl, C. D., Brown, A., Schippers, A., Bernier-Latmani, R. & Weyer, S. (2021). Uranium Isotope Fractionation during Anoxic Mobilization of Noncrystalline U(IV) by Ligand Complexation. *Environmental Science & Technology*.

2020

- Hueter, A., Huck, S., Heimhofer, U., Bodin, S., Weyer, S., Jochum, K. P., **Roebbert, Y.** & Immenhauser, A. (2020). Evaluating the role of coastal hypoxia on the transient expansion of microencruster intervals during the early Aptian. *Lethaia*.

2018

- **Roebbert, Y.**, Rabe, K., Lazarov, M., Schuth, S., Schippers, A., Dold, B., & Weyer, S. (2018): Fractionation of Fe and Cu isotopes in acid mine tailings: Modification and application of a sequential extraction method, *Chemical Geology*

2017

- Bhattacharyya, A., Campbell, K. M., Kelly, S. D., **Roebbert, Y.**, Weyer, S., Bernier-Latmani, R., & Borch, T. (2017): Biogenic non-crystalline U (IV) revealed as major component in uranium ore deposits, *Nature Communications*, 8.

2015

- Stylo M., Neubert N., **Roebbert Y.**, Weyer S., & Bernier-Latmani R. (2015). Mechanism of uranium reduction and immobilization in *Desulfovibrio vulgaris* biofilms. *Environmental Science & Technology*, 49(17), 10553-10561.

## Conference abstracts

---

07/2021

### Goldschmidt-Conference 2021

- **Roebbert, Y.**, Rosendahl, C., Brown, A., Schippers, A., Bernier-Latmani, R., Weyer, S. (2018): Isotopic signature of tetravalent uranium mobilization by complexation or oxidation. Virtual Goldschmidt-Conference 2021.

08/2019

### Goldschmidt-Conference 2019

- **Roebbert, Y.**, Schippers, A., Bernier-Latmani, R., Weyer, S. (2018): Mobilization of non-crystalline U(IV) by complexation with organic ligands generates U isotope fractionation. Goldschmidt-Conference 2019, Barcelona, Spain.

12/2018

### AGU fall meeting 2018 (Washington, D.C., USA)

- **Roebbert, Y.**, Schippers, A., Bernier-Latmani, R., Weyer, S. (2018): Isotope fractionation of  $^{238}\text{U}/^{235}\text{U}$  during mobilization of non-crystalline U(IV) by complexation with organic ligands

10/2018

### Uranium biogeochemistry conference 2018 (Ascona, Switzerland)

- **Roebbert, Y.**, Schippers, A., Bernier-Latmani, R., Weyer, S. (2018): U isotope fractionation during mobilization of non-crystalline U(IV) by complexation with organic ligands
- Borch, T., Bhattacharyya, A., **Roebbert, Y.**, Stone, J. J., Weyer, S., Clay, J., Bernier-Latmani, R., Campbell, K. (2018): Biogeochemical characterization of sediment and groundwater before and after in-situ recovery (ISR) mining of uranium in Wyoming, USA.
- Pan, Z., **Roebbert, Y.**, Beck, A., Vitova, T., Weyer, S., Bernier-Latmani, R. (2018). U(VI) Isotopic Fractionation during its Abiotic Reduction by Magnetite

- 09/2018      **GeoBonn 2018**
- **Roebbert, Y.**, Schippers, A., Bernier-Latmani, R., Weyer, S. (2018): Isotopic signature of non-crystalline U(IV) complexation with organic ligands
- 06/2018      **DMG section meeting (Göttingen)**
- **Roebbert, Y.**, Schippers, A., Weyer, S. (2018): Uranium isotope fractionation related to non-crystalline U(IV)
- 09/2017      **Jahrestagung der Arbeitsgemeinschaft Stabile Isotope e.V.**
- **Roebbert, Y.**, Rabe, K., Lazarov, M., Schippers, A., Dold, B. & Weyer, S. (2017): Acidic mine tailings and Fe / Cu isotope fractionation: modification and application of a sequential extraction method, ASI 2017, Hannover
- 09/2017      **GeoBremen 2017**
- **Roebbert, Y.**, Rabe, K., Lazarov, M., Schippers, A., Dold, B. & Weyer, S. (2017): Fractionation of Fe and Cu isotopes in acidic mine tailings: modification and application of a sequential extraction method, GeoBremen 2017, Bremen
- 08/2017      **Goldschmidt-Conference 2017**
- **Roebbert, Y.**, Rabe, K., Lazarov, M., Schippers, A., Dold, B. & Weyer, S. (2017): Fe and Cu Isotope Fractionation in Acidic Mine Tailings: Modification and Application of a Sequential Extraction Method, Goldschmidt-Conference 2017, Paris, France
- 11/2016      **14th Swiss Geoscience Meeting, Geneva**
- Loreggian, L., **Roebbert, Y.**, Neubert, N., Weyer, S. & Bernier-Latmani, R. (2016): Uranium isotope fractionation during abiotic reduction by magnetite, 14th Swiss Geoscience Meeting, Genf, Switzerland
- 06/2016      **Goldschmidt- Conference 2016**
- Loreggian, L., **Roebbert, Y.**, Weyer, S. & Bernier-Latmani, R. (2016).  $^{238}\text{U}/^{235}\text{U}$  Fractionation during U(VI) Reduction by Synthetic Magnetite. Goldschmidt-conference 2016, Yokohama, Japan (Poster).
- 10/2015      **GeoBerlin**
- **Röbbert, Y.**, Bhattacharyya, A., Loreggian, L., Borch, T., Pierau, N., Bernier-Latmani, R. & Weyer, S. (2015). Biotic and abiotic  $^{238}\text{U}/^{235}\text{U}$  fractionation – applications to bioremediation and U ore roll-front deposits. GeoBerlin 2015. Berlin.
- 08/2015      **Goldschmidt-Conference 2015**
- Loreggian, L., **Roebbert, Y.**, Bernier-Latmani, R. & Weyer, S. (2015).  $^{238}\text{U}/^{235}\text{U}$  Fractionation during U(VI) Reduction by Synthetic Magnetite. Goldschmidt-Conference 2015, Prague, Czech Republic (Poster).
  - Bhattacharyya, A., Campbell, K., **Roebbert, Y.**, Weyer, S., Bernier-Latmani, R. & Borch, T. (2015). Elucidating the Role of Non-Crystalline U(IV) in Uranium Roll-Front Formation. Goldschmidt-Conference 2015, Prague, Czech Republic (Poster).
  - Stylo M., Neubert N., **Roebbert Y.**, Weyer S. & Bernier-Latmani R. (2015). Mechanism of Uranium Reduction and Immobilization in *Desulfovibrio vulgaris* Biofilms. Goldschmidt-Conference 2015, Prague, Czech Republic.
- 06/2015      **DMG- section meeting 2015**
- **Röbbert, Y.**, Bhattacharyya, A., Loreggian, L., Borch, T., Pierau, N., Bernier-Latmani, R., Weyer, S. (2015). Biotic and abiotic U isotope fractionation – applications to bioremediation and U ore roll-front deposits. DMG-section meeting 2015, Potsdam.